

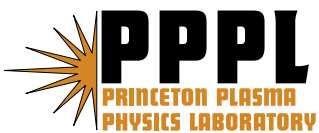
PPPL-4270

PPPL-4270

## Neutral Particle Analyzer Vertically Scanning Measurements of MHD-induced Energetic Ion Redistribution or Loss in the National Spherical Torus Experiment

S.S. Medley, R. Andre, R.E. Bell, D.S. Darrow, C.W. Domier, E.D. Fredrickson,  
N.N. Gorelenkov, S.M. Kaye, B.P. LeBlanc, K.C. Lee, F.M. Levinton, D. Liu,  
N.C. Luhmann, Jr., J.E. Menard, H. Park, D. Stutman, A.L. Roquemore,  
K. Tritz, H. Yuh and the NSTX Team

November 2007



# Princeton Plasma Physics Laboratory

## Report Disclaimers

---

### Full Legal Disclaimer

This report was prepared as an account of work sponsored by an agency of the United States Government. Neither the United States Government nor any agency thereof, nor any of their employees, nor any of their contractors, subcontractors or their employees, makes any warranty, express or implied, or assumes any legal liability or responsibility for the accuracy, completeness, or any third party's use or the results of such use of any information, apparatus, product, or process disclosed, or represents that its use would not infringe privately owned rights. Reference herein to any specific commercial product, process, or service by trade name, trademark, manufacturer, or otherwise, does not necessarily constitute or imply its endorsement, recommendation, or favoring by the United States Government or any agency thereof or its contractors or subcontractors. The views and opinions of authors expressed herein do not necessarily state or reflect those of the United States Government or any agency thereof.

### Trademark Disclaimer

Reference herein to any specific commercial product, process, or service by trade name, trademark, manufacturer, or otherwise, does not necessarily constitute or imply its endorsement, recommendation, or favoring by the United States Government or any agency thereof or its contractors or subcontractors.

---

## PPPL Report Availability

### Princeton Plasma Physics Laboratory:

<http://www.pppl.gov/techreports.cfm>

### Office of Scientific and Technical Information (OSTI):

<http://www.osti.gov/bridge>

---

### Related Links:

[U.S. Department of Energy](#)

[Office of Scientific and Technical Information](#)

[Fusion Links](#)

# Neutral Particle Analyzer Vertically Scanning Measurements of MHD-induced Energetic Ion Redistribution or Loss in the National Spherical Torus Experiment

S. S. Medley<sup>1</sup>, R. Andre<sup>1</sup>, R. E. Bell<sup>1</sup>, D. S. Darrow<sup>1</sup>, C. W. Domier<sup>2</sup>, E. D. Fredrickson<sup>1</sup>, N. N. Gorelenkov<sup>1</sup>, S. M. Kaye<sup>1</sup>, B. P. LeBlanc<sup>1</sup>, K. C. Lee<sup>2</sup>, F. M. Levinton<sup>3</sup>, D. Liu<sup>4</sup>, N. C. Luhmann, Jr.<sup>2</sup>, J. E. Menard<sup>1</sup>, H. Park<sup>1</sup>, D. Stutman<sup>5</sup>, A. L. Roquemore<sup>1</sup>, K. Tritz<sup>5</sup>, H. Yuh<sup>3</sup> and the NSTX Team

<sup>1</sup>*Princeton Plasma Physics Laboratory, Princeton, NJ 08543*

<sup>2</sup>*University of California at Davis, Davis, CA 95616*

<sup>3</sup>*Nova Photonics, Inc., Princeton, NJ 08543*

<sup>4</sup>*University of California at Irvine, Irvine, CA 92697*

<sup>5</sup>*Johns Hopkins University, Baltimore, Maryland 21218*

Email: [medley@pppl.gov](mailto:medley@pppl.gov)

## Abstract

Observations of magneto-hydro-dynamic (MHD) induced redistribution or loss of energetic ions measured using the vertically scanning capability of the Neutral Particle Analyzer diagnostic on the National Spherical Torus Experiment (NSTX) are presented along with TRANSP and ORBIT code analysis of the results. Although redistribution or loss of energetic ions due to bursting fishbone-like and low-frequency ( $f \sim 10$  kHz) kink-type MHD activity has been reported previously, the primary goal of this work is to study redistribution or loss due to continuous Alfvénic ( $f \sim 20 - 150$  kHz) modes, a topic that heretofore has not been investigated in detail for NSTX plasmas. Initial indications are that the former drive energetic ion loss whereas the continuous Alfvénic modes only cause redistribution and the energetic ions remain confined.

## 1.0 Introduction

The National Spherical Torus Experiment (NSTX) [1] is a midsize low aspect ratio fusion research facility with auxiliary heating from Neutral Beam Injection (NBI) and High Harmonic Fast Wave (HHFW) launch. Typical NSTX parameters are major radius  $R_0 = 0.85 - 0.9$  m, minor radius  $a = 0.67$  m resulting in an aspect ratio of  $A = R_0/a \sim 1.3$ , plasma

current  $I_p = 0.3 - 1.5$  MA and toroidal field  $B_T = 3 - 6$  kG. Three co-directed deuterium neutral beam sources have injected power up to  $P_{NB} = 7$  MW at full neutral energies up to  $E_b = 100$  keV. HHFW heating at 30 MHz has delivered up to  $P_{RF} = 1.6$  MW to deuterium and helium plasmas.

Determining the attractiveness of the spherical torus concept [2] in the areas of high- $\beta$  stability, confinement, non-inductive current drive and divertor physics for pulse lengths much longer than the energy confinement time is the mission of the NSTX device. The performance milestones that were achieved to date in NSTX have been reported elsewhere [3-5]. H-modes triggered by NBI heating are routinely obtained in NSTX and have become a standard operational scenario [6]. L-mode to H-mode transitions triggered by NBI heating have been obtained over a wide parameter range in  $I_p \leq 1.2$  MA,  $B_T \leq 5.5$  kG, and  $n_e \leq 8 \times 10^{13}$  cm<sup>-3</sup> in either lower-single-null or double-null diverted discharges with elongation  $\Delta \leq 3.0$ , triangularity  $\Delta \leq 0.85$  and plasma pulse length exceeding 1.5 s. To date NSTX has achieved, non-simultaneously, stored energies up to 0.39 MJ, energy confinement times  $\tau_E \leq 0.12$  s and  $\tau_T \leq 40\%$  where  $\tau_T = \langle p \rangle / (B_0^2 / 2\mu_0)$ ,  $\langle p \rangle$  is the volume averaged total pressure and  $B_0$  is the vacuum magnetic field at  $R_0$ .

On NSTX, the amplitude and structure of Alfvén modes are measured using a suite of diagnostics, including Mirnov magnetic coils attached to first wall structures, Ultra Soft X-Ray (USXR) arrays, a far-infrared tangentially viewing interferometer/polarimeter (FIReTIP) and radially-viewing reflectometry diagnostics. Neutron yield data supported by Neutral Particle Analyzer (NPA) and scintillator Fast Lost Ion Probe (sFLIP) diagnostics are used to assess fast-ion redistribution or loss due to MHD-induced effects.

The neutron production in NSTX is predominantly from beam-target reactions. Thus the neutron rate is a robust measure of the energetic ion population and serves as the primary diagnostic for identification of MHD-induced ion redistribution or loss. In the 2002-2004 run periods, a change in the response of the neutron detectors on NSTX occurred due to inexplicable changes in the detector biases. This situation was corrected [7] and all neutron rates cited in this report were derived from the fission chamber neutron detector using the legacy calibration factor of  $9.0 \times 10^{13}$  neutrons/volt.

The energetic ion distributions are measured using the Neutral Particle Analyzer diagnostic [8]. This diagnostic utilizes a PPPL-designed EIIB spectrometer [9] which measures the mass-resolved energy spectra of H and D neutrals simultaneously with a time resolution of  $\sim 0.1$  ms set by signal-to-noise levels. The calibrated energy range is  $E = 0.5 - 150$  keV and the energy resolution varies from  $\Delta E/E = 3 - 7\%$  from high to low energy. The NPA measures Maxwellian spectra of residual  $H^+$  to obtain ion temperatures [10] and  $D^+$  energetic ion spectra produced by injection of neutral beams into deuterium plasma [11, 12]. As shown in Fig. 1, the NPA views across the co-injection paths of the three NBI lines on NSTX that inject at major radii  $R_{NB} = 69.4$  cm (Source A),  $R_{NB} = 59.2$  cm (Source B) and  $R_{NB} = 48.7$  cm (Source C) and the NPA can be scanned horizontally over a wide range of tangency radii (as well as vertically) on a shot-to-shot basis. In NSTX, by convention the neutral beam tangency radii are positive for *injection* in the co-direction. On the other hand, the convention adopted for the NPA is that positive sightline tangency radii correspond to *viewing* co-directed ions.

Spatial localization of the charge exchange neutral efflux that is measured by the NPA arises from the intersection of the diagnostic sightline with the NBI sources as reported in [13] and documented in Fig. 2. As shown in panel (a), the source of the charge exchange efflux (blue curve) is spatially localized around the footprint of the NB primary neutrals (red curve) that also leads to localization in pitch angle (black curve). As shown in panel (b), the maximum elevation minor radius accessible with vertical scanning (referenced to the major radius corresponding to the intersection of the NPA sightline with the beam neutral footprint) is a function of the selected horizontal tangency radius of the NPA sightline. For the horizontal tangency radius of  $R_{tan} = 80$  cm chosen for the vertical scan data presented in this report, the elevation minor radius as a function of vertical scan angle is shown in panel (c). From TRANSP calculations, the pitch angle associated with the measurements (blue curve) is localized to passing particles ( $v_{||}/v \sim 0.7 - 0.8$ ). For vertical scan angles beyond  $\sim 20$  degrees, the NPA sightline misses the NB neutral footprint and localization of the measurement is lost.

Both the volume-integrated neutron and the line-integrated NPA diagnostics show signal depletion due to fast-ion driven instabilities but cannot distinguish between fast-ion redistribution and loss. Two recently implemented diagnostics on NSTX, the Motional Stark Effect (MSE) and scintillator Fast Lost Ion Probe (sFLIP), facilitate separation of redistribution and loss effects. In particular, sFLIP measures the pitch and energy of fast ions that are ejected from the plasma and intercept the wall-mounted probe thus discriminating fast-ion loss versus redistribution. For certain H-mode discharges where NPA measurements of the NBI energetic ion spectra exhibit MHD-induced fast-ion depletion, the sFLIP data confirm the existence of an ion loss that occurs primarily for passing particles near the NBI full injection energy.

Diagnostics for spatial localization of MHD activity in NSTX H-mode discharges are limited. Reflectometry is ineffectual because of density cutoff in the plasma periphery that precludes access to the core region where some of the most virulent MHD modes tend to be localized. Horizontal mid-plane interferometry, though line-integrated with sparse spatial coverage, is often helpful to identify core-localized electron density fluctuations. The most effective localization during H-modes is provided by multiple USXR arrays.

Although redistribution or loss of energetic ions due to bursting and kink-type MHD activity has been reported previously [14-18], in this work the primary goal is to study redistribution or loss due to continuous Energetic Particle Modes (EPM) and Toroidal Alfvén Eigenmode (TAE) Alfvénic activity, a topic that heretofore has not been investigated in detail for NSTX plasmas. TRANSP [19,20] simulations using space, time and energy dependent anomalous fast ion diffusion and MSE-constrained q-profiles [21] to assess fast-ion redistribution effects are reported. In Section 2.0, measurements of the MHD-induced spatial redistribution of energetic ions obtained by vertical scanning of the NPA diagnostic are presented. TRANSP simulations of these results are presented in Section 3.0 and ORBIT modeling that supports and extends the foregoing TRANSP analysis is presented in Section 4.0. First observations of MHD-induced energetic ion redistribution in Helium L-mode plasmas are presented in Section 5.0. Evidence for ascribing either redistribution or loss of energetic ions to specific types of MHD activity is presented in

Section 6.0. Discussion of the reported experimental observations and numerical simulations is given in Section 7.0 and the paper concludes with a summary in Section 8.0.

## **2.0 NPA Vertically Scanning Measurements of Energetic Ion Redistribution or Loss**

In quiescent or MHD-benign NSTX discharges, NPA measurements of the energetic beam ion distribution are consistent with classical behavior [22]. The appearance of strong, bursting or continuous MHD activity can have significant effects on energetic ( $E \sim 10 - 100$  keV) deuterium ion populations in NSTX; namely, after H-mode onset, the NPA charge exchange spectrum usually exhibits a significant depletion of energetic ions usually only for  $E > E_b/2$  where  $E_b$  is the beam injection energy, though in some cases the depletion was observed to extend down to  $E_b/3$ . More direct (i.e. with minimal variation in pitch angle compared with a horizontal scan) information on MHD-induced radial redistribution of energetic ions is possible using the NPA vertical scanning capability.

### **2.1 Discharge Characteristics and Reproducibility**

A NPA vertical scan was performed for a series of reproducible discharges having the characteristics shown in Fig. 3. Evolution contour plots of the Multi-Point Thompson Scattering (MPTS) electron temperature and density are shown in Fig. 4 and corresponding plots of the CHarge Exchange Recombination Spectroscopy (CHERS) toroidal velocity and  $Z_{\text{eff}}$  are shown in Fig. 5. Obtaining reliable measurements of energetic ion redistribution during a vertical scan depends critically on the characteristics and reproducibility of the plasma conditions. Variations in plasma parameters and profiles can result in ‘faux’ depletion signatures on the NPA signal [13] as well as excursions in the measured neutron yield. One such parameter, the outer gap width, was very stable during the scan run at  $\Delta_{\text{gap}} \sim 10$  cm. Otherwise, for the vertically scanning data set a transition in the discharge behavior occurred at  $t \sim 0.55$  s due to the onset of sawtooth activity. Tables I – IV summarize the behavior of the plasma parameters  $Z_{\text{eff}}$ ,  $v_{\square}$ ,  $n_e$ , and  $T_e$  that are all referenced to the Shafranov-shifted major radius of  $R_{\text{maj}} = 110$  cm.

Mirnov spectrograms for the low frequency range ( $f = 0 - 100$  kHz) and high frequency range ( $f = 200 - 2000$  kHz) MHD activity (without Doppler correction) are shown in Fig. 6. Bursting activity appears on panel (b) between  $t \sim 0.6 - 0.8$  s that is characteristic of all discharges in the NPA vertical scan data set. The transition in high frequency activity after  $t \sim 0.55$  s is due to collapse of the toroidal rotation velocity.

A Mirnov spectrogram for SN122631 providing more MHD mode detail in the low frequency ( $f = 0 - 150$  kHz) range is shown in Fig. 7. The spectrogram shows magnetic fluctuations measured with a Mirnov coil located on the outboard mid-plane wall of the vacuum vessel color-coded according to the toroidal mode number where black, red, green, blue, cyan and magenta correspond to  $n = 1$  through 6, respectively.

A family of TAE modes is seen in the time period  $t = 0.1 - 0.2$  s with toroidal mode numbers from  $n = 1$  to  $n = 4$ . From  $t \approx 0.2$  s to  $t \approx 0.4$  s, a commonly observed  $n = 1$  mode is seen. Typically this mode is core localized with a predominantly kink structure and the onset of the mode is marked by a rapid, downward frequency chirp in a manner associated with energetic particle modes (EPM). As  $q_{\min}$  is typically greater than unity at this time, the chirping mode is not a true fishbone, but could be one of several possible related EPMS such as an infernal fishbone which would be an  $n = 1$  infernal mode excited by the fast ions. The saturated state of this EPM is accompanied by  $n = 2$  and  $n = 3$  harmonics. While these harmonics might originally represent non-linear distortion of the  $n = 1$  mode, their persistence after the  $n = 1$  component disappears suggests that they may also be independent modes.

Starting after  $t \sim 0.35$  s, several families of higher frequency modes appear. The lowest frequency of these families appears at about  $t = 0.38$  s between 15 kHz and 30 kHz. The family consists of an  $n = 3$  (green) and  $n = 4$  (blue) mode. After  $t = 0.4$  s, the mode frequency falls rapidly, mirroring the behavior of the kink-like modes.

The second family appears nearly concurrently and consists of  $n = 2$  (red),  $n = 3$  (green),  $n = 4$  (blue),  $n = 5$  (cyan) and  $n = 6$  (magenta) modes with frequencies spanning 40 kHz up to  $\approx 100$  kHz. The third family shows up at about  $t = 0.4$ s with  $n = 3$ ,  $n = 4$ ,  $n = 5$  and  $n = 6$  modes at frequencies ranging from 80 kHz up to about 120 kHz. The fourth

**Table I Core  $Z_{\text{eff}}$  Discharge Reproducibility**

Shot	$Z_{\text{eff}} - \text{initial}$	$t_{\text{initial}}(\text{ms})$	$Z_{\text{eff}} - \text{maximum}$	$t_{\text{maximum}}(\text{ms})$
122626	1.2	200	1.6	700
122627	1.1	200	1.5	600
122629	1.2	200	1.5	550
122630	1.2	200	1.5	600
122631	1.1	200	1.6	600
122632	1.2	200	1.5	600
122634	1.2	200	1.7	650
122635	1.2	200	1.5	550
122636	1.1	200	1.7	700
122639	1.2	200	1.8	700
122641	1.2	200	1.7	800
122642	1.2	200	1.7	700
122643	1.2	200	1.7	700
122644	1.2	200	1.7	700
122645	1.2	200	1.6	750

Following an initial rise to  $Z_{\text{eff}} \sim 1.1 - 1.2$  around  $t = 200$  ms, it can be seen in Table I that the core  $Z_{\text{eff}}$  increases gradually to a maximum of  $Z_{\text{eff}} \sim 1.5 - 1.8$  near the end of the discharge. Although the edge accumulation of impurities collapses with onset of the toroidal rotation collapse (see Fig. 5), for most discharges the core  $Z_{\text{eff}}$  is not affected by collapse of the toroidal rotation velocity. The increase in core  $Z_{\text{eff}}$  during the discharge flattop is modest and the effect on neutron yield and charge exchange neutral efflux is expected to be minimal.

**Table II Core Toroidal Rotation Velocity Discharge Reproducibility**

Shot	$V_{\square}$ - maximum $V_{\square}(\text{kms}^{-1})$	$t_{\text{Maximum}}(\text{ms})$	$V_{\square}$ - transition $V_{\square}(\text{kms}^{-1})$	$t_{\text{transition}}(\text{ms})$
122626	250	550	150	650
122627	250	500	150	570
122629	250	520	150	550
122630	250	520	150	600
122631	250	500	150	650
122632	250	500	150	600
122634	250	500	100	650
122635	250	500	125	650
122636	250	500	150	650
122639	225	550	150	700
122641	250	600	125	700
122642	250	550	100	650
122643	250	500	150	650
122644	250	500	100	700
122645	225	550	150	650

In Table II, it can be seen that the toroidal rotation velocity collapses after  $t \sim 580 \pm 60$  ms by  $\sim 100 \text{ kms}^{-1}$  and the toroidal velocity continues to decline for the duration of the discharge. This collapse in toroidal rotation velocity appears to be the driver for other changes in plasma parameter profiles, including the nature of the MHD activity. The inherent effect on the NPA signal (which depends on the relative velocity between energetic ions and beam primary neutrals) and neutron yield (which depends on beam target reactions with thermal neutrals) is expected to be negligible.

Except for SN122626, the discharges also had an earlier transient decrease in toroidal rotation of  $\sim 50 - 100 \text{ kms}^{-1}$  around  $t = 200 - 250$  ms, but the toroidal rotation subsequently recovered. This early drop does not appear to affect plasma profiles.

**Table III Core Electron Density Discharge Reproducibility**

Shot	$n_e$ – maximum $n_e(x10^{13} \text{ cm}^{-3})$	$t_{\text{Maximum}}(\text{ms})$	$n_e$ - transition $n_e(x10^{13} \text{ cm}^{-3})$	$t_{\text{transition}} (\text{ms})$
122626	9.0	630	6.5	750
122627	8.5	550	7.5	700
122629	8.0	550	7.0	700
122630	8.0	550	6.0	650
122631	8.5	600	7.0	800
122632	8.0	600	6.0	750
122634	9.0	630	7.0	700
122635	8.0	600	6.5	700
122636	9.0	620	7.0	700
122639	9.5	750	7.0	800
122641	9.0	700	7.0	800
122642	9.0	630	6.5	750
122643	9.0	630	7.0	700
122644	9.0	600	6.0	800
122645	9.0	630	7.0	750

The electron density rises smoothly until  $t \sim 620 \pm 70$  ms and then collapses as shown in Table III. The electron density collapse thus appears to lag the toroidal velocity collapse (see Table II) by  $\sim 40$  ms. This drop will contribute to an decrease in the neutron yield due to an decrease in the plasma target ion density for the primary neutron source of beam-plasma interactions. The density drop should reduce depletion of the NPA signal due to attenuation of the charge exchange neutral flux.

**Table IV Core Electron Temperature Discharge Reproducibility**

Shot	$T_e$ – ramp-up $T_e$ (keV)	$t_{\text{ramp-up}}$ (ms)	$T_e$ - maximum $T_e$ (keV)	$t_{\text{maximum}}$ (ms)
122626	0.7	200	1.0	700
122627	0.7	200	1.1	700
122629	0.7	200	1.2	700
122630	0.8	200	1.2	650
122631	0.8	200	1.1	800
122632	1.0	200	1.2	700
122634	0.9	200	1.1	700
122635	0.8	200	1.2	700
122636	0.8	200	1.0	700
122639	0.8	200	1.0	800
122641	0.9	200	1.1	600
122642	0.8	200	1.1	600
122643	0.9	200	1.1	600
122644	0.8	200	1.1	750
122645	0.8	200	1.1	600

Following an initial rise to  $T_e \sim 0.8 - 1.0$  keV around  $t = 200$  ms, it can be seen in Table IV that the core  $T_e$  increases gradually to a maximum of  $T_e \sim 1.0 - 1.2$  keV near the end of the discharge and is not affected by collapse of the toroidal rotation velocity. The increase in core  $T_e$  during the discharge flattop is modest and the effect on neutron yield is expected to be minimal.

family starts a little later with frequencies of 130 kHz to 140 kHz and just an  $n = 5$  and  $n = 6$  mode.

Identification of these mode families requires careful modeling. However, it is reasonable to infer that the first family represents Beta-induced Alfvén Acoustic Eigenmode (BAAE) [23], the second family may live in the Beta-induced Alfvén Eigenmode (BAE) [24, 25] gap, the third family would then be Toroidal Alfvén Eigenmodes (TAE) [18] and the fourth family, although less certain, might inhabit the Ellipticity-induced Alfvén Eigenmode (EAE) [26] gap.

Following  $t \sim 0.6$  s, the plasma becomes infested with bursting, chirping  $n = 1$  fishbone-like modes and their harmonics, together with a continuous  $n = 2$  mode.

A plot of the Mirnov root-mean-square (rms) magnetic field fluctuation amplitude in low frequency range ( $f = 0 - 100$  kHz) for all of the shots in the vertical scan data set is shown in Fig. 8 using 15-point smoothing. A transition from relatively low amplitude activity ( $\Delta B \sim 10^{-2}$  Gauss) to increased amplitude ( $\Delta B \sim 10^{-1}$  Gauss) coincides with the transition of the discharge from L-Mode to H-Mode at  $t \sim 0.2$  s. The mode amplitude subsequently subsides until an increase that is driven by the onset of sawtooth activity around  $t \sim 0.6$  s.

The root-mean-square amplitude of the high frequency activity ( $f = 200 - 2000$  kHz) shown in Fig. 9 is remarkably constant for most of the discharge duration at an amplitude that is 1 – 2 orders of magnitude below the low frequency amplitude. Due to this reduced amplitude, the high frequency activity is assumed to play a minor role, if any, in redistribution or loss of energetic ions since MHD-driven diffusion of energetic ions scales as  $(\Delta B/B)^2$ .

## **2.2 NPA Vertically Scanning Deuterium Energetic Ion Spectra**

NPA vertically scanning results are shown in Fig. 10 where the vertical minor radius axis is the distance along a vertical line centered at the intersection of the NPA sightline with the NB footprint (see Fig. 1). Several features of the NPA spectra in Fig. 10 should

be noted. The NPA flux is displayed on a linear z-axis and the larger efflux at lower energy is the E/2 component of the neutral beam. The measurements in the top panel corresponding to a MHD-quiescent period ( $\Delta B \sim 10^{-2}$  Gauss) show a monotonically decreasing energetic ion distribution from the core outwards. By contrast, during strong MHD activity ( $\Delta B \sim 10^{-1}$  Gauss) the energetic ion distribution in the core region is depleted and the core ions are redistributed radially outwards to form a ‘shoulder’ on the measured distribution as evident in the bottom panel. The criterion for ‘quiescent’ is that the low frequency mode amplitude,  $\Delta B$ , according to the Mirnov spectrogram is reduced by an order of magnitude or more relative to the ‘active’ phase. Since MHD-driven diffusion of energetic ions scales as  $(\Delta B/B)^2$ , redistribution should be reduced by a factor of  $\sim 10^{-2}$  or more.

In a separate experiment, a vertical scan was taken during NBI into a gas-filled torus with toroidal magnetic fields only in the range  $B_T = 3.5 - 4.5$  kG and with Source A only at  $E_b = 90$  keV that were run for the purpose of MSE calibration as shown in Fig. 11 (note the linear NPA flux scale). The NPA spatial resolution is  $\sim 2.5$  cm. An abrupt drop in flux occurs at  $R_{\text{Minor}} \sim 35$  cm when the NPA sightline passes below the footprint of the beam primary neutrals. This agrees reasonably with the footprint expected from the geometry of the NB ion source that has a height of 40 cm centered on the NSTX mid-plane and provides an independent calibration of the vertical scan radius. (See also Fig. 31 to be discussed in Section 4.0.) The NPA-measured NBI particle fractions derived from the data in Fig. 11 are  $E_b/3:E_b/2:E_b = 0.42:0.42:0.16$  that compare favorably with the NBI calibration values of  $E_b/3:E_b/2:E_b = 0.44:0.39:0.17$  for 100 keV extraction energy.

Returning to the NPA vertical scan during H-mode plasmas, while Fig. 10 provides a convenient global view of the data, better detail can be seen in selected slices of the scanning profile as shown in Fig. 12. The energetic ion distributions (note the linear flux scale) versus vertical minor radius are plotted at times  $t = 100$  and  $200$  ms for an energy of  $E_D = 80$  keV. The energetic ion depletion in the core and the outward redistribution is clearly evident. As shown in Fig. 13, following the initial redistribution between  $t = 100$  and  $200$  ms the NPA spectra continue to exhibit depletion as seen for the  $t = 300$  and  $600$  ms

plots. This depletion is due in part to attenuation of the charge exchange neutral efflux with increasing plasma density (see Fig. 3a) and, as advocated in this report, in part to MHD-induced energetic ion redistribution.

Figures 14(a) and 14(b) show NPA energetic ion spectra at selected radii on the measured vertical profile at  $t = 50$  ms (L-mode) and  $t = 100$  ms (onset of H-mode), respectively, during injection of NB Sources A and B. In the energy range  $E_b/2 < E < E_b$ , the magnitude of the core efflux (black curve) is  $\ln(\text{NPA Flux}/\text{Energy}^{1/2}) \sim 18 \pm 0.2$ . Figure 14(c) corresponds to  $t = 200$  ms when NB Sources A, B and C were injecting. In the energy range  $E_b/2 < E < E_b$ , the magnitude of the core efflux (black curve) is  $\ln(\text{NPA Flux}/\text{Energy}^{1/2}) \sim 19.5 \pm 0.3$ . This core efflux is lower than for  $t = 100$  ms in Fig. 14(b) in spite of the addition of NB Source C due in part to neutral particle attenuation (incoming and outgoing) driven by increased electron density and in part to MHD-induced redistribution. Although the profile is core-peaked, it no longer falls off smoothly with increasing vertical minor radius but remains flat at  $\sim 40\%$  of the core-peak value, a behavior attributed to MHD-induced energetic ion redistribution. Figure 14(d) shows the continuing, strong depletion of the NPA energetic ion flux.

The solid state Neutral Particle Analyzer (ssNPA) array [27,28] on NSTX consists of four chords with tangency radii  $R_{\text{tan}} = 90, 100$  and  $120$  cm that view across the three co-injection neutral beam lines as shown in the top panel of Fig. 15. Each chord utilizes a silicon photodiode to measure the energy distribution of charge exchange fast neutral particles (30~100 keV) with energy resolution  $\Delta E = 10$  keV and time resolution  $\Delta t = 2$  ms. The measurements of three inner chords (i.e. Chords 1-3) are spatially localized with major radii of  $R_{\text{int}} = 66, 92$  and  $118$  cm by charge exchange production on NBI neutrals where the ssNPA sightlines intersect the beam footprint. Chord 4 is less well localized because of the contribution of edge neutrals to the measured charge exchange efflux and will be omitted from the analysis to follow. The bottom panel of Fig. 15 shows typical temporal evolutions of neutral flux measured by Chords 1-3 of the ssNPA. An overlay of two discharges, SN122631 (red) and SN122645 (black), indicate good reproducibility of the ssNPA measurements during the NPA vertically scanning shot sequence.

Figure 16 shows the energetic neutral particle efflux derived from the measurements of Chords 1-3 of the ssNPA at three selected time slices (100 ms, 200 ms and 500 ms) for SN122645. Chord 1 and Chord 2 are spatially localized on the inboard side of the Shafranov-shifted magnetic axis, while Chord 3 is localized near the magnetic axis. At  $t = 100$  ms, NB sources A and B were injecting at  $E_b = 90$  keV and the discharge was in L-mode. During this MHD ‘quiescent’ period, the energetic ion efflux monotonically decreases by a modest amount from Chord 3 to Chord 1 as shown in Fig. 16(a). The changes in the amplitude and shape of the energy spectra from Chord 3 to Chord 1 can be attributed to incoming NB attenuation and fast ion slowing down effects. At  $t = 200$  ms, all NB sources were injecting and H-Mode was established attended by strong low-frequency MHD activity (see Fig. 3). At this time, Fig. 16(b) shows that the energetic ion efflux decreases significantly from Chord 3 to Chord 1 at  $t = 200$  ms and Fig. 16(c) shows continuation of the strong depletion at  $t = 500$  ms. In Fig. 16(c), the ssNPA energy spectrum for Chord 2 at  $t = 500$  ms also exhibits a significant depletion of fast ions in the range  $E_b/2 < E < E_b$ . Figure 17 shows the corresponding global view of the data shown in Fig. 16. The above observations agree with the NPA measurements shown in Figs. 13-14. It is noted that a tail above the injected beam energy occurs on the ssNPA energy spectra. Since neutron-induced noise has been subtracted, this tail is mainly caused by pulse pile-up.

### 3.0 TRANSP Code Analysis of Energetic Ion Redistribution or Loss

It is well documented that numerous types of MHD activity can have various effects on ion behavior in both conventional [29,30] and spherical [13,15,31] tokamaks and in particular MHD activity can induce energetic ion loss. To palliate the lack of a physics-based model for MHD-induced loss of energetic ions in TRANSP, an existing capability to modify the energetic ion diffusion in a manner that mocks up MHD redistribution or loss is invoked. Note that energetic ion diffusion is generally small in conventional tokamaks [29] and there is no evidence so far that this is not the case in spherical tokamaks as well. So the use of enhanced energetic ion diffusion as a tool to emulate the observed MHD ion

loss must not be construed as implying that elevated energetic ion diffusion is a feature of spherical tokamaks.

In the TRANSP code, anomalous fast ion diffusion (AFID) can be enhanced over a specified region of physical space in the discharge corresponding to localization of the MHD activity as well as over a specified ion energy range to accommodate the energy-selective depletion observed in the NPA measurements. The time dependence of the fast ion diffusion can also be specified. A two-fold criteria was employed for specifying the fast ion diffusion parameters: the first was to obtain agreement between the measured neutron rate and that generated by the kinetically based TRANSP simulation, and the second was to simultaneously obtain agreement with the NPA energetic ion measurements. An additional criterion was to simultaneously obtain a good match between the calculated and MSE-measured toroidal current profiles.

The anomalous fast ion diffusion model effecting this goal, shown in Fig. 18, is as follows: (1) in time, the diffusivity was ramped up from a small value at the start of beam injection to  $\Gamma_i^{\text{Fast}} = 70 \text{ m}^2/\text{s}$  at the end of the discharge in steps that closely correlated with changes in the MHD activity; (2) the radial profile of the diffusivity was chosen to be core-peaked which is consistent with the USXR measurements of the radial distribution of MHD activity shown in Fig. 19; (3) in energy, the diffusivity multiplier was increased from zero at  $E = 10 \text{ keV}$  to 0.5 at  $E_b/3 = 50 \text{ keV}$  followed by a dip then an increase to 0.7 at  $E_b/2$ . Thereafter it was ramped up to  $\sim 1.0$  near the beam full injection energy. The selected energy behavior corresponds to the measured NPA ion distribution shown in Figs. 13a and 13b. TRANSP results obtained by applying this anomalous fast ion diffusion model to SN122631 are presented in Sections 3.1 and 3.2 below.

Figure 20 shows FReTIP measurements of the line-averaged electron density (upper panels) and the electron density fluctuations (lower panels) from the four sightlines currently in operation. In conjunction with Fig. 7 and Fig. 8, it would appear that significant density fluctuations only occur during periods of the discharge that exhibit bursting or low-f MHD activity and are absent during the phase  $t \sim 0.35 - 0.55 \text{ s}$  that is dominated by TAE-like activity. Unfortunately, sFLIP energetic ion loss measurements were not available for the vertically scanning shot sequence, but in a surrogate discharge to be discussed in

Section 6.0 it will be demonstrated that the FIRETIP electron density fluctuations are closely correlated with energetic ion losses observed by the sFLIP diagnostic. It will be inferred from this observation that bursting-type and low-f kink-like MHD activity drive energetic ion loss whereas TAE-type activity only causes redistribution and the energetic ions remain confined.

Figures 21a and 21b show detail of the FIRETIP electron density fluctuations in the time interval  $t = 300 - 302$  ms and  $t = 710 - 712$  ms (marked by the red and blue lines, respectively, in Fig. 20). The frequency of the  $\Delta n_e/n_e$  oscillations is  $\sim 8$  kHz which is in reasonable agreement with the low-f Mirnov data during this time interval as seen in Fig. 6. As clearly demonstrated in Fig. 21d, the electron density oscillations are core localized in agreement with USXR data shown in Fig. 19.

### 3.1 Energetic Particle Analysis

Figure 22a provides a comparison of the measured neutron yield (black curve) against the TRANSP-calculated neutron yield with (122631M11-red curve) and without (122631M09-blue curve) anomalous fast ion diffusion. In some TRANSP analyses, such as presented herein for SN122631, the calculated neutron rate significantly exceeds the neutron measurement. This commonly occurs in H-mode discharges characterized by strong MHD activity [7]. The absolute error in the measured neutron rate is estimated to be 25% so the disparity significantly exceeds the measurement error. Since neutrons are produced primarily by beam-target reactions, it is not surprising that the fast ion diffusion had to be raised to a value that led to the  $\sim 60$  % loss of the energetic beam ions as seen later in Fig. 25. In Fig. 22a, an excellent match exists between the measured neutron yield and the TRANSP simulation that employs anomalous fast ion diffusion.

The effect on the NPA signal evolution for  $E_D = 70$  keV is shown in Fig. 22b using the same curve color designations as for the neutrons. Likewise, the energetic ion distribution at  $t = 700$  ms (when the ion loss has nearly saturated) is shown in Fig. 22c. As can be seen, an excellent match exists between the measured energetic ion distribution measurements and the TRANSP simulations with anomalous fast ion diffusion, normalized

at  $E \sim 30$  keV. However, the TRANSP-simulated NPA signal evolution with AFID improves the match with measurement by only  $\sim 50\%$  and the shortfall is attributed to inadequate treatment of beam halo neutrals as will be discussed later.

The TRANSP-simulated NPA vertical scan radial distributions are shown in Fig. 23 for selected times during the discharge that correspond to various stages of MHD activity. As the discharge progresses, the initially monotonic ( $t = 200$  ms) energetic ion distribution flattens in the core region ( $t = 300$  ms) and subsequently becomes hollow ( $t = 400$  ms) and develops a pronounced shoulder around  $r/a \sim 0.5$  ( $t = 700$  ms).

The effect of MHD-induced energetic ion redistribution on the plasma current density profiles is assessed by comparing MSE-measured profiles with calculated current profiles. Unfortunately, this analysis was not available for the reference vertical scan discharge SN112631 used in this report, so the process is illustrated using a surrogate discharge [13] as shown in Fig. 24. An equilibrium code is used to compute the inductive (orange) and bootstrap (red) current profile components as described in [16]. The Neutral Beam Injection Current Driven (NBICD) component (blue) from TRANSP calculation and the summation of the aforementioned components yields the calculated total (black) toroidal current profile. The measured current profile (gray) is derived from an MSE-constrained reconstruction that uses the CHERS radial electric field profile from carbon impurity force balance to correct the MSE pitch angle data.

In Fig. 24(a), it can be seen that the calculated total current density exceeds the MSE-reconstruction value by  $\sim 25\%$  in the core region. However, as shown in Fig. 24(b), the TRANSP-calculated redistribution of fast ions using the AFID model reduces the NBICD component and hence the calculated total current density in the core to essentially the same value as the MSE reconstruction. The bands on the  $q$  profiles represent variations in the input parameters to the modeling.

### **3.2 Power Balance and Transport Analysis**

As shown in the upper panel of Fig. 25, invoking anomalous fast ion diffusion diminishes the neutral beam power input to the electrons by  $\sim 10\%$  and ions by  $\sim 25\%$ .

The NB fast ion orbit loss to the first wall structures (lower panel) increases by  $\sim 0.25$  MW as a result of the imposed AFID. In the next few figures, it will be seen that the diminished power input to ions and electrons causes TRANSP to reduce the appropriate diffusivities (hence increase the confinement times) in order to match the measured ion and electron temperatures used as input to the calculation.

The impact of this ion loss on transport and other parameters of interest is shown in Figs. 26 – 29. The volume-integrated ion power balance at  $t = 700$  ms is shown in Fig. 26 without (blue curves) and with (red curves) AFID. (Normalized radius,  $r/a$ , is square root of toroidal magnetic flux normalized to total flux.) In general, the power densities for ion conduction and ion heating are lower with anomalous fast ion diffusion than without. As reported elsewhere [32], a power balance puzzle sometimes arises in TRANSP analysis of some NSTX discharges wherein the ion loss power sometimes exceeds classical ion heating. However, this is not the case for the cited discharge SN122631. Complementary results for the electron power balance with and without fast ion diffusion are given in Fig. 27.

Figure 28 shows profiles of the flux surface average thermal diffusivities extracted from TRANSP power and momentum balance analysis plotted against normalized minor radius for the time of interest. In these calculations, heating source and loss terms are evaluated, and the unaccounted for “balance” is assumed to be diffusive and assigned a local diffusivity. Including energetic ion loss reduces the electron and ion diffusivities. A neoclassical prediction of the ion diffusivity,  $\chi_i^{NC}$ , obtained from the NCLASS code [33] is unchanged with the inclusion of fast ion diffusion. This is partially due to the fact that  $\chi_i^{NC}$  is computed using the neoclassical ion thermal flux from NCLASS and the measured local gradient and density, ignoring energetic ions. In the core region,  $\chi_0 \ll \chi_i \approx \chi_e \ll \chi_i^{NC} \ll \chi_i^{Fast}$  with and without fast ion diffusion. Near the mid-radius region,  $\chi_0 \approx \chi_i^{NC} \ll \chi_i \sim \chi_e \ll \chi_i^{Fast}$  both with and without the fast ion diffusion model. It can be seen that fast ion diffusion reduces  $\chi_e$ ,  $\chi_i$ , and  $\chi_0$ .

In most NSTX discharges, the electron thermal confinement is characteristically poor relative to the ion thermal confinement [34]. This does not appear to be the case here since  $\tau_e \sim \tau_i$  for  $r/a < 0.6$ .

Figure 29a shows the total energy confinement time,  $\tau_E$ , and Fig. 29b the toroidal beta,  $\beta_T$ , with and without AFID. Of note is that the confinement time with AFID (red curve) is larger than without AFID (blue curve). This is understandable, since loss of neutral beam heating power as a result of MHD-induced energetic ion loss naturally requires improved energy confinement to realize the measured input values for  $T_e$  and  $T_i$ . On the other hand, toroidal beta decreases with the inclusion of fast ion diffusion. This is due to the fact that fast ion diffusion reduces both the parallel and perpendicular energetic ion betas by  $\sim 8\%$  due to a reduction in the energetic ion pressure profile. (Note that non-thermal ions usually contribute  $\sim 25 - 30\%$  to the stored energy and toroidal beta in NSTX.)

#### 4.0 ORBIT Code Analysis

The energetic ion signal for the NPA diagnostic consists of a complex line-integrated measurement along a manifold through a multi-dimensional space consisting of physical coordinates, energy and pitch angle. For ‘passive’ measurements the source of neutrals for charge exchange reactions is a gas mantle surrounding the plasma whose density attenuates strongly with distance into the plasma. For effectiveness, neutral beam and other sources of auxiliary heating are configured so that the energetic ion distribution peaks in the plasma core region in order for the particles to be confined. The energy resolution and the trajectory of the NPA sightline through the plasma define other dimensionalities such as pitch angle. As a result, for passive NPA measurements the manifold through this multi-dimensional space is very broad. On the other hand, for ‘active’ NPA diagnostics using either heating neutral beams or a dedicated diagnostic NB, this manifold becomes significantly narrower. In the case of NSTX, the line-integrated NPA measurement actually becomes strongly localized in both space and pitch angle to a region defined by the intersection of the diagnostic sightline with the footprint of the beam neutrals. Even so, the ‘thickness’ of this reduced manifold varies with the trajectory of the

NPA sightline through the plasma.

ORBIT [35,36] code modeling can provide valuable insight into several characteristics of the NPA measurements of energetic ion distributions. The ORBIT code, which can handle highly non-circular geometries as well as non-axisymmetric magnetic perturbations, follows beam ion guiding center orbits and calculates the effect that MHD modes have on the energetic ion distribution. Figure 30 gives selected confined guiding center passing particle orbits (solid lines) for  $E = 65$  keV deuterium ions calculated with the ORBIT code using a magnetic equilibrium derived at  $t = 700$  ms from a typical H-mode discharge similar to SN122631. The orbits correspond to values of  $R_{\text{maj}}$  and  $v_{\parallel}/v$  for representative NPA tangency radius used in the vertical scan. The dashed line shows the lost particle orbit just inside of the confinement boundary for passing particles. Note that the presented ORBIT calculations do not include finite Larmor radius effects, which may change the confinement region. The electric field due to toroidal plasma rotation was included in the calculation, but had a negligible effect on the passing particle orbits. Overlaid in blue is a scaled facsimile of the beam neutral footprint shown in Fig. 31 (to be discussed momentarily) that is positioned at a major radius corresponding to the intersection of the NPA sightline with the NB for a horizontal tangency radius of  $R_{\text{tan}} = 80$  cm.

Based on Fig. 30, the NPA efflux redistribution measured along the scanned vertical minor radius shown in Fig. 10 are interpreted as caused by an MHD-induced radial outward redistribution of the energetic ions. Clearly, ions displaced to outboard orbits are simultaneously displaced vertically since their guiding-center orbits ‘track’ the more vertically extended flux surfaces.

Figure 31 shows the beam neutral footprint for Source A in a poloidal plane passing through the NB tangency radius of  $R_{\text{NB}} = 69.4$  cm that was calculated using a stand-alone neutral beam calibration code [37]. The full NSTX NB geometry is used to compute the footprint that includes the full, one-half and one-third energy primary beam neutrals. Beam halo neutrals, however, are not included. The halo neutrals enlarge the overall neutral footprint in the entire poloidal plane by a significant amount, perhaps 25%, albeit with a density of order one-half that of the primary neutrals. Thus the vertical half-height of the

NB footprint extends to  $\sim 40$  cm which is consistent with the energetic ion profiles shown in Fig. 10 and Fig. 11 that were obtained by NPA vertical scanning.

Figure 32 is a contour plot of the neutral beam distribution function at  $E = 65$  keV as a function of major radius and field pitch,  $v_{||}/v$ , taken at the low field side in the mid-plane outside of the magnetic axis. The contours correspond to equally spaced values of the beam ion distribution function. The red circles correspond to the three confined orbits shown in Fig. 30. Since the variation of  $v_{||}/v$  is modest on an orbit trajectory of passing ions, it can be expected that the TRANSP-calculated variation in pitch during the NPA vertical scan is modest. This is verified in Fig. 33 which shows the TRANSP calculated field pitch,  $v_{||}/v$ , versus elevation minor radius that is centered on the intersection of the NPA sightline with the NB footprint. The black curve is the pitch at the peak of the change exchange emissivity measured along the NPA sightline. The red (blue) curves are the maximum (minimum) pitch determined by the width of the emissivity profile that in effect is determined by the horizontal width of the beam primary neutral profile. Beyond an elevation minor radius of  $\sim 50$  cm the curves are discontinued because the NPA sightline passes below the footprint of the beam primary neutrals.

## 5.0 MHD-induced Energetic Ion Redistribution in Helium L-mode Plasmas

MHD-induced energetic ion redistribution is almost always observed in deuterium H-mode discharges but seldom in L-mode plasmas unless the electron density is unusually high and the profile is broad [15]. Recently, however, MHD-induced redistribution was observed in low-density Helium L-mode plasmas. Reference discharge characteristics are shown in Fig. 34 for SN124524. In panel (a), NB Sources A @ 90 keV, and B @ 60 keV were injected in the sequence A-C-A during the  $I_p = 0.8$  MA,  $B_T = 4.5$  kG discharge with source A injecting during the time-of-interest ( $t = 0.3 - 0.4$  s). Panel (d) shows that robust MHD activity with  $f < 30$  kHz and  $n = 1$  occurs during the time-of-interest and panel (c) shows that the amplitude of this activity was  $\sim 10^3$  times greater than the CAE/GAE activity at  $f > 200$  kHz. Note the discontinuity in the y-axis marked by the red  $\sim$  symbol. The low frequency MHD activity after  $t \sim 0.3$  s corresponds initially to bursting

EPM-type activity followed by internal kink-type modes with TAE activity being minimal or absent. The trace in panel (e) exhibits fast ion loss during the time-of-interest corresponding to a pitch angle of  $v_{||}/v \sim 0.8$  (i.e. passing ions). The signal was obtained from one of ten Faraday strips that are built into the sFLIP diagnostic. A contour plot of the NPA flux is shown in panel (f).

Figure 35 shows the NPA vertical scan plots for three selected times (note the linear NPA flux scale). The time  $t = 310$  ms corresponds to 10 ms after start of the combined injection of NB Sources A and C as well as the growth phase of the low-f MHD activity. The NPA energetic ion flux is peaked near the plasma core, but at  $t = 320$  ms redistribution begins and at  $t = 360$  ms the profile is strongly flattened. As seen Fig. 31b, the electron density is relatively constant during the time-of-interest which rules out charge exchange neutral particle attenuation effects as a cause of the observed energetic ion spectra redistribution. This represents the first measurement of energetic ion redistribution when only one type of MHD activity exists and corroborates previous assertions regarding the energetic ion redistribution effects of low frequency MHD activity [15, 16]. TRANSP analysis of these measurements is deferred because the He:D ratio is unknown. Figure 36 shows energy spectra on a natural logarithmic flux scale for  $t = 310$  and  $t = 360$  ms that are displayed in triplets corresponding to vertical minor radii of approximately 0, 10, and 20 cm. The energetic ion redistribution with increasing time is evident.

While the 3D spectra shown in Fig. 35 provide a convenient global view of the redistribution evolution, clearer detail can be seen in Fig. 37 where the energetic ion distributions versus vertical minor radius are plotted at times  $t = 310, 320$  and  $350$  ms for an energy of  $E_D = 75$  keV. The flattening in the core of the energetic ion profile is clearly evident.

## **6.0 Correlation of sFLIP Energetic Ion Loss and FIREtIP $\Delta n_e/n_e$ Fluctuations with MHD Activity**

As mentioned in Section 3.0, sFLIP data was not available in the NPA vertically scanning data set to directly corroborate a correlation between FIREtIP  $\Delta n_e/n_e$  fluctuations and energetic ion loss evidenced by the sFLIP diagnostic. Data from a ‘surrogate’

discharge SN125332 taken in the latter part of the NSTX 2007 run when all relevant diagnostics were online is shown in Fig. 38 to corroborate this inference. The discharge parameters are similar to SN122631 except for modulation of Source B during the pulse. This modulation drives variations in the neutron yield but does not appear to influence any other waveforms in Fig. 38. The sFLIP energetic ion loss bursts beginning around  $t \sim 0.3$  s and  $t \sim 0.9$  s in panel (c) correlate with the FReTIP  $\Delta n_e/n_e$  core fluctuations in panel (f). No  $\Delta n_e/n_e$  fluctuations exist in the higher frequency range ( $f \sim 50 - 200$  kHz) of the FReTIP measurements. The initial sFLIP loss burst at  $t \sim 0.1$  s is due to prompt energetic ion loss that usually attends early neutral beam injection during the current ramp-up phase [38]. The MHD activity from the Mirnov coils shown in panels (d) and (e) is reasonably similar in evolution to that for SN122631 seen in Figs. 6 - 8, including the mode amplitude of the  $\Delta B$  fluctuations. Note that the sFLIP and FReTIP signal activities correlate with the Mirnov coil continuous low frequency ( $f < 20$  kHz) MHD activity (along with sporadic bursting fishbone-like activity). SFLIP energetic ion loss and FReTIP  $\Delta n_e/n_e$  core fluctuations are conspicuously absent during higher-frequency continuous TAE and CAE/GAE activity in the time interval  $t \sim 0.43 - 0.9$  s except possibly for MHD bursting activity at  $t \sim 0.78$  s and  $t \sim 0.83$  s. This leads to the conclusion that both bursting fishbone-like and low-f kink-type MHD modes drive energetic ion loss whereas continuous TAE-like Alfvénic modes only cause redistribution and the energetic ions remain confined.

## 7.0 Discussion

It is well documented in the literature [39, 40] that anomalous transport of energetic ions can be caused by two classes of instabilities: (1) low frequency MHD type instabilities, such as the fishbone, internal kink and ballooning modes, associated with the resonance between the mode frequency and the fast ion toroidal precession frequency, and (2) higher frequency instabilities, such as the shear Alfvén gap modes, associated with the resonance at the fast particle poloidal transit/bounce frequency. Though qualitatively understood, much less data exists for strongly unstable scenarios characterized by *nonlinear* interaction of energetic ions with the kink and tearing modes. The results

presented in this report extend the database supporting energetic ion redistribution or loss associated with nonlinear interaction with low frequency MHD modes.

In NSTX discharges from 2002 - 2007, it is commonplace in discharges with robust MHD activity for the TRANSP-calculated neutron rates to exceed the neutron measurements [7]. In L-mode discharges, the calculated excess is modest with  $(S_{n,TRANSP} - S_{n,Measured}) / S_{n,Measured} \sim 10 \pm 5 \%$ . This is within the 25% uncertainty in the calibration of the fission chamber detector. However, in H-mode discharges the excess can be large with  $(S_{n,TRANSP} - S_{n,Measured}) / S_{n,Measured} \sim 50 \pm 20 \%$ .

As mention earlier, the NSTX neutron detectors have been subject to sometimes inexplicable changes in response [7] during the course of the NSTX experimental campaigns. As a precaution, the responses of the neutron detectors were rechecked prior to issuing this report. As shown in Fig. 39, this check revealed that the responses of the fission chamber (FC) and ZnS detectors were constant over the period 2005-2007 but the response of the 2FG scintillator detector dropped by a factor of  $\sim 2/3$  after 2005 and the correction for the raw signal voltage offset decreased by a factor of four. This does not affect the results of this report since the highly stable fission detector was used throughout for the neutron measurements. For reference, the valid neutron detector calibration factors for the 2006-2007 period are: (1) fission chamber neutron rate = (Raw volts - 0.04) $9.0 \times 10^{13}$  cps/volt, (2) ZnS (1DE) detector neutron rate = (Raw volts - 0.095) $8.35 \times 10^{13}$  cps/volt and 2FG scintillator neutron rate = (Raw volts - 0.015) $11.5 \times 10^{13}$  cps/volt. The appropriate calibrations factors prior to 2006 are documented in [7].

Application of the AFID model in TRANSP to create an acceptable match between the measured and calculated neutron rates as well as the NPA effluxes involves selection of multiple parameters: namely, the space, time and energy dependence of the magnitude of the anomalous fast ion diffusion to be applied. In most cases, multiple combinations of these parameters can achieve similar results: i.e. no unique AFID model exists.

Simulation of the NPA signal using TRANSP is compromised by inadequate treatment of the beam halo neutrals. When a primary beam neutral is deposited via charge exchange on a thermal ion, the thermal ion in turn becomes a neutral known as a halo neutral. As the term implies, halo neutrals remain relatively localized around the

footprint of the beam primary neutrals. However, in the TRANSP code these halo neutrals are volume averaged both poloidally and toroidally. Since the densities of the primary and halo neutrals can be comparable, this situation can significantly affect the TRANSP calculation of the NPA charge exchange production that is localized to the intersection of the NPA sightline with the NB primary and halo footprint.

In many NSTX discharges, the electron density evolves strongly during the first half of the discharge and then flattops or evolves slowly thereafter. During the ‘flattop’ period, the halo neutral effect can be removed by appropriate normalization of the measured and TRANSP-calculated quantities as was done previously in [15,16]. The dominant MHD activity during this period is typically kink-type modes. In this report, however, interest is focused on continuous EPM/TAE Alfvénic eigenmodes that tend to dominate during the period when the electron density (and presumably the halo neutral density) are evolving significantly with time. Therefore, using the TRANSP simulation of the NPA efflux to correct the measured efflux leaving a residual signal that can be ascribed to MHD-induced redistribution effects is a questionable process. As long as the effect of the computational treatment of the halo neutrals in TRANSP remains in doubt, closure of the primary goal of this study cannot be made.

If this compromised treatment of halo neutrals affects only the amplitude of the charge exchange flux, the analysis of MHD-induced redistribution or loss effects presented in this report would not be significantly affected since the calculated and measured fluxes could be normalized. However, the primary and halo neutrals are expected to have different spatial and temporal characteristics: for example, the primary neutral population decreases with penetration distance into the plasma whereas the halo population increases and these processes vary in time with the evolution of the electron density. In an attempt to resolve this dilemma, the effect of halo neutrals on the NPA signals is being investigated using the LOCUST code developed by R. Akers at MAST. The 3D Monte Carlo LOCUST code properly preserves the halo neutral density around the footprint of the beam primary neutrals.

## 8.0 Summary

Although redistribution or loss of energetic ions due to bursting fishbone-like and low-frequency ( $f \sim 10$  kHz) kink-type MHD activity has been reported previously, the primary goal of this work was to study redistribution or loss due to continuous EPM or TAE Alfvénic modes, a topic that heretofore had not been investigated in detail for NSTX plasmas. Initial indications are that the former drive energetic ion loss whereas the continuous EPM or TAE Alfvénic modes only cause redistribution and the energetic ions remain confined. So far, the role regarding energetic ion redistribution or loss of higher-frequency ( $f \sim 200 - 2000$  kHz) CAE/GAE activity that is omnipresent during NSTX H-mode discharges cannot be separated from the lower-frequency activity ( $f \sim 0 - 100$  kHz) that has been the focus of this report. Ignoring the higher frequency activity on the grounds that typical amplitudes of the magnetic fluctuations are 1 – 2 orders of magnitude below those for the lower frequency fluctuations remains to be verified.

TRANSP analysis using anomalous fast ion diffusion can model the MHD-induced energetic ion redistribution or loss effects to yield good agreement between the calculated and measured neutron yields as well as reasonable agreement between the NPA efflux evolution and energy spectra provided steady-state plasma conditions exist. Closure on modeling of the NPA measurements during continuous EPM/TAE-induced redistribution or loss of energetic ions that arise primarily in non-steady-state plasma conditions awaits either an upgrade of the treatment of beam halo neutrals in TRANSP or an independent demonstration that the halo neutral issue is irrelevant.

## Acknowledgements

This work was supported by U.S. DOE Contract DE-AC02-76CH03073, U.S. DOE Grant DE-FG02-99ER54523 (JHU), U.S. DOE Grant DE-FG02-99ER54520 (Nova Photonics) and U.S. DOE Grant DE-FG03-02ER54681 (UC Irvine).

## References

- [1] M. Ono, *et al.*, "Overview of the Initial NSTX Experimental Results," Nucl. Fusion **41**, (2001) 1435
- [2] Y.-K. M. Peng and D. J. Strickler, Nucl. Fusion **26**, (1986) 769
- [3] J. E. Menard, *et al.*, "β-Limiting MHD Instabilities in Improved-performance NSTX Spherical Torus Plasmas," Nucl. Fusion **43**, (2003) 330
- [4] J. E. Menard, *et al.*, "Overview of Recent Physics Results from the National Spherical Torus Experiment (NSTX)," Nucl. Fusion **47**, (2007) S645
- [5] D. A. Gates, *et al.*, "Progress Towards Steady State on NSTX," Nucl. Fusion **46**, (2006) S22 - S28
- [6] S. M. Kaye, *et al.*, "Progress Towards High Performance Plasmas in the National Spherical Torus Experiment (NSTX)." Nucl. Fusion **45**, (2005) S168 – S180
- [7] S. S. Medley, D. S. Darrow and A. L. Roquemore, "Reconciliation of Measured and TRANSP-Calculated Neutron Emission Rates in the National Spherical Torus Experiment: Circa 2002-2005," Princeton Plasma Physics Laboratory Report, PPPL-4080 (2005)
- [8] S. S. Medley and A. L. Roquemore, "Neutral Particle Analyzer Diagnostic on the National Spherical Torus Experiment," Rev. Sci. Instrum. **75**, (2004) 3625
- [9] S. S. Medley and A. L. Roquemore, "Construction and Operation of Parallel Electric and Magnetic Field Spectrometers for Mass/Energy Resolved Multi-Ion Charge Exchange Diagnostics on the Tokamak Fusion Test Reactor," Rev. Sci. Instrum. **69**, (1998) 2651
- [10] S. S. Medley, *et al.*, "Initial Neutral Particle Analyzer Measurements of Ion Temperature in the National Spherical Torus Experiment," Rev. Sci. Instrum. **74**, (2003) 1896
- [11] S. S. Medley, R. E. Bell, E. D. Fredrickson, and A. L. Roquemore, "Energetic Ion Behavior in the National Spherical Torus Experiment," Proc. 30<sup>th</sup> EPS Conference on Controlled Fusion and Plasma Physics, St Petersburg, Russia, 7 - 11 July 2003,

Europhysics Conference Abstracts Vol. 27A, P-4.96. Also Princeton Plasma Physics Laboratory Report, PPPL-3827 (2003)

- [12] S. S. Medley, *et al.*, "Investigation of Collective Fast Ion Instability-induced Redistribution or Loss in the National Spherical Torus Experiment," 21<sup>st</sup> IAEA Fusion Energy Conference, 16 – 21 October, Chengdu, China, CD-ROM EX/P6-13
- [13] S. S. Medley, *et al.*, "Status of Recent Experimental and Analytical Investigation of MHD-Induced Energetic Ion Redistribution or Loss in the National Spherical Torus Experiment," Princeton Plasma Physics Laboratory Report, PPPL-4235 (2007)
- [14] E. D. Fredrickson, N. N. Gorelenkov, D. Darrow, *et al.*, "Wave Driven Fast Ion Loss in the National Spherical Torus Experiment," *Phys. of Plasmas* **10**, (2003) 2852
- [15] S. S. Medley, *et al.*, "MHD-Induced Energetic Ion Loss during H-mode Discharge in the National Spherical Torus Experiment," *Nucl. Fusion* **44**, (2004) 1158
- [16] J. E. Menard, *et al.*, "Observation of Instability-induced Current Redistribution in a Spherical Torus Plasma," *Phys. Rev. Lett.* **97**, (2006) 095022
- [17] E. D. Fredrickson, L. Chen and R. B. White, "Bounce Precession Fishbones in the National Spherical Torus Experiment," *Nucl. Fusion* **43**, (2003) 1258
- [18] E. D. Fredrickson, *et al.*, "Fast Ion Loss in a 'Sea-of-TAE'," *Nucl. Fusion* **46**, (2006) S926 – S931
- [19] R. J. Goldston, D. C. McCune, H. H. Towner, *et al.*, "New Techniques for Calculating Heat and Particle Source Rates due to Neutral Beam Injection in Axisymmetric Tokamaks," *J. Comput. Phys.* **43**, (1981) 61
- [20] J. Onega, M. Evrard, D. McCune, "Numerical Transport Codes," *Transactions of Fusion Technology* **33**, (1998) 181
- [21] F. M. Levinton, *et al.*, "Transport with Reversed Shear in the National Spherical Torus Experiment," *Phys. of Plasmas* **14**, (2007) 056199
- [22] W. W. Heidbrink, M. Miah, D. Darrow, B. LeBlanc, S. S. Medley, A. L. Roquemore and F. E. Cecil, "The Confinement of Dilute Populations of Beam Ions in the National Spherical Torus Experiment," *Nucl. Fusion* **43**, (2003) 883
- [23] N. N. Gorelenkov, H. L. Berk, E. Fredrickson and S. E. Sharapov, "Predictions and Observations of Low-Shear Beta-Induced Shear Alfvén-Acoustic Eigenmodes

- in Toroidal Plasmas,” *Physics Lett. A* **10** (2007) 1016
- [24] W. W. Heidbrink, *et al.*, “What is the “Beta-induced Alfvén Eigenmode”?”, *Phys. Plasmas* **6**, (1999) 1147
- [25] N. N. Gorelenkov and W. W. Heidbrink, “Energetic Particle Effects As an Explanation for the Low Frequencies of Alfvén Modes in the DIII-D Tokamak,” *Nucl. Fusion* **42**, (2002) 150
- [26] E. D. Fredrickson, *et al.*, “Collective Fast Ion Instability-induced Losses in the National Spherical Torus Experiment,” *Phys. Plasmas* **13**, (2006) 056109
- [27] K. Shinohara, *et al.*, “Solid State Neutral Particle Analyzer Array on the National Spherical Torus Experiment,” *Rev. Sci. Instrum.* **75**, (2004) 3640
- [28] D. Liu, *et al.*, “Performance of the Solid State Neutral Particle Analyzer Array on the National Spherical Torus Experiment,” *Rev. Sci. Instrum.* **77**, (2006) 10F113
- [29] W. W. Heidbrink and G. J. Sadler, “The Behavior of Fast Ions in Tokamak Experiments,” *Nucl. Fusion* **34**, (1994) 535
- [30] S. J. Zweben, D. S. Darrow, E. D. Fredrickson, G. Taylor, S. von Goeler and R. B. White, “MHD Induced Alpha Particle Loss in TFTR,” *Nucl. Fusion* **39**, (1999) 1097
- [31] E. D. Fredrickson, *et al.*, “Wave Driven Fast Ion Loss in the National Spherical Torus Experiment,” *Phys. Plasmas* **10**, (2003) 2852
- [32] D. A. Gates, N. N. Gorelenkov, and R. B. White, “Ion Heating by Fast-Particle-Induced Alfvén Turbulence,” *Phys. Rev. Lett.* **87**, (2001) 205003
- [33] W. A. Houlberg, *et al.*, “Bootstrap Current and Neoclassical Transport in Tokamaks of Arbitrary Collisionality and Aspect Ratio,” *Phys. Plasmas* **4**, (1997) 3230
- [34] B. P. LeBlanc, *et al.*, “Confinement Studies of Auxiliary Heated NSTX Plasmas,” *Nucl. Fusion* **44**, (2004) 513
- [35] R. B. White and M. S. Chance, “Hamiltonian Guiding Center Drift Orbit Calculation for Plasmas of Arbitrary Cross Section,” *Phys. Fluids* **27**, (1984) 2455
- [36] R. B. White, “Canonical Hamiltonian Guiding Center Variables,” *Phys. Fluids B* **2**, (1990) 845
- [37] R. E. Bell, “Carbon Ion Plume Emission Produced by Charge Exchange with Neutral

- Beams on NSTX,” Princeton Plasma Physics Laboratory Report, PPPL-4167 (2006)
- [38] S. S. Medley, *et al.*, “Prompt Loss of Energetic Ions during Early Neutral Beam Injection in the National Spherical Torus Experiment,” Princeton Plasma Physics Laboratory Report, PPPL-4060 (2005)
- [39] “ITER Physics Basis,” Nucl. Fusion **39**, (1999) 2137-2664
- [40] R. Ikeda, “Progress in the ITER Physics Basis,” Nucl. Fusion **47**, (2007) S1-S414
- See “Chapter 5: Physics of Energetic Ions,” S264-S284

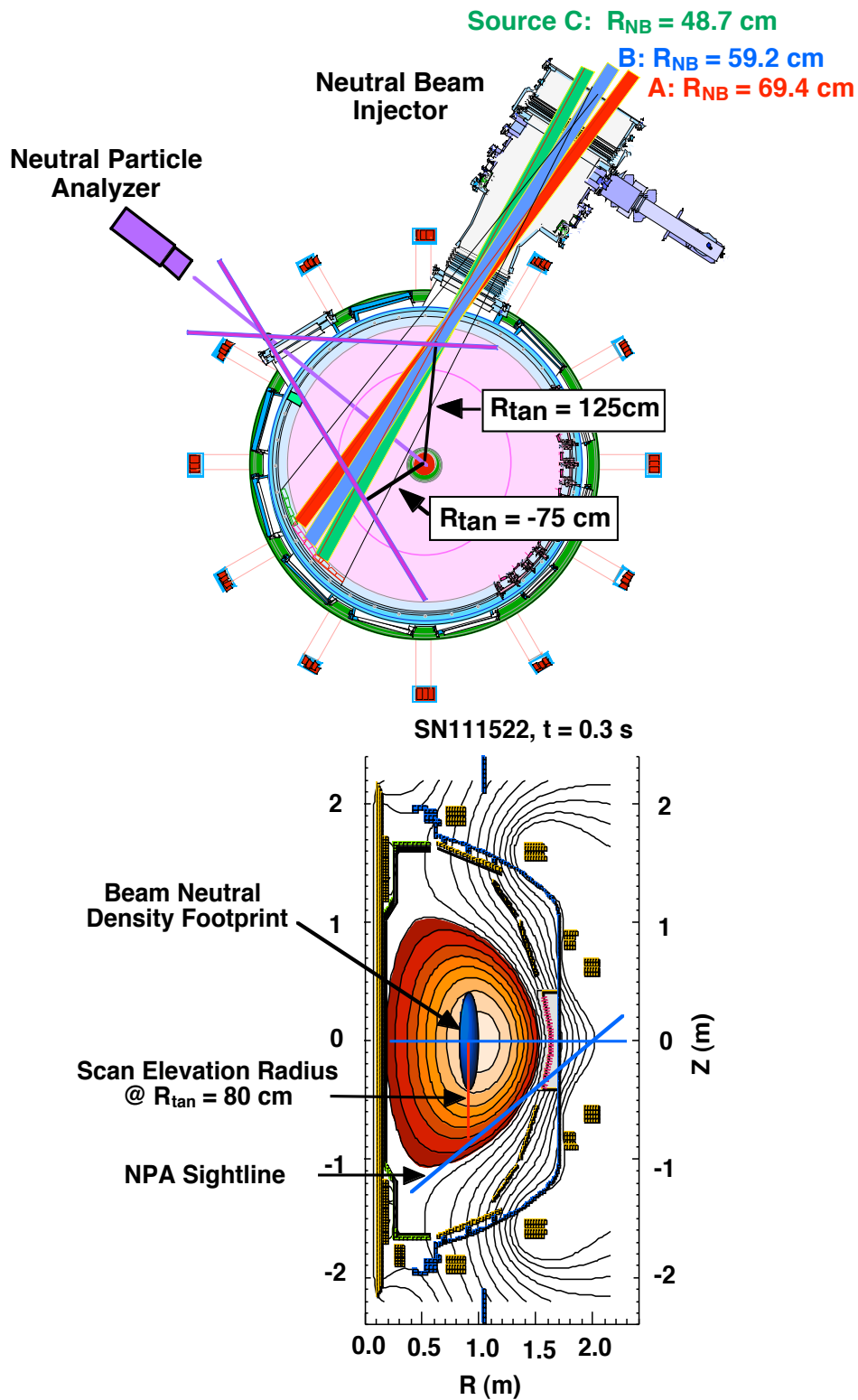


Fig. 1. The Neutral Particle Analyzer (NPA) on NSTX views across the three neutral beam injection sources and can be scanned horizontally (top) over a wide range of sightline tangency radii,  $R_{tan}$ , as well as vertically (bottom) on a shot-to-shot basis.  $R_{tan}$  is the perpendicular distance between the machine center and the NPA sightline.

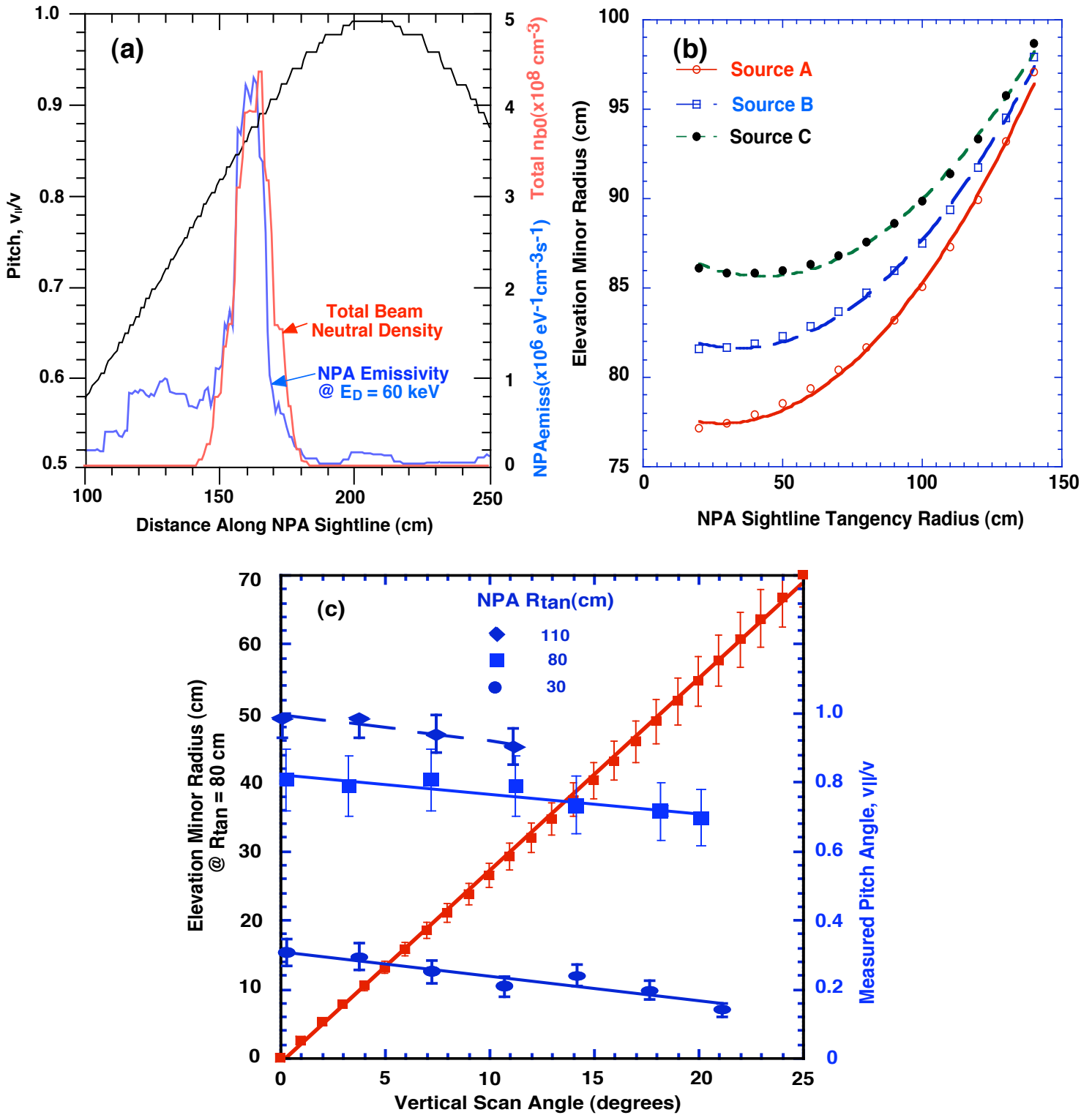


Fig. 2. Pitch angle and spatial localization of the NPA flux arises (panel (a)) from the intersection of the diagnostic sightline with the NB sources. The maximum elevation minor radius accessible for vertical scanning depends on the choice of horizontal tangency radius (panel (b)). Panel (c) shows the elevation minor radius for the vertical scan at  $R_{tan} = 80$  cm. The pitch angle data terminates when the elevated NPA sightline misses the NB footprint.

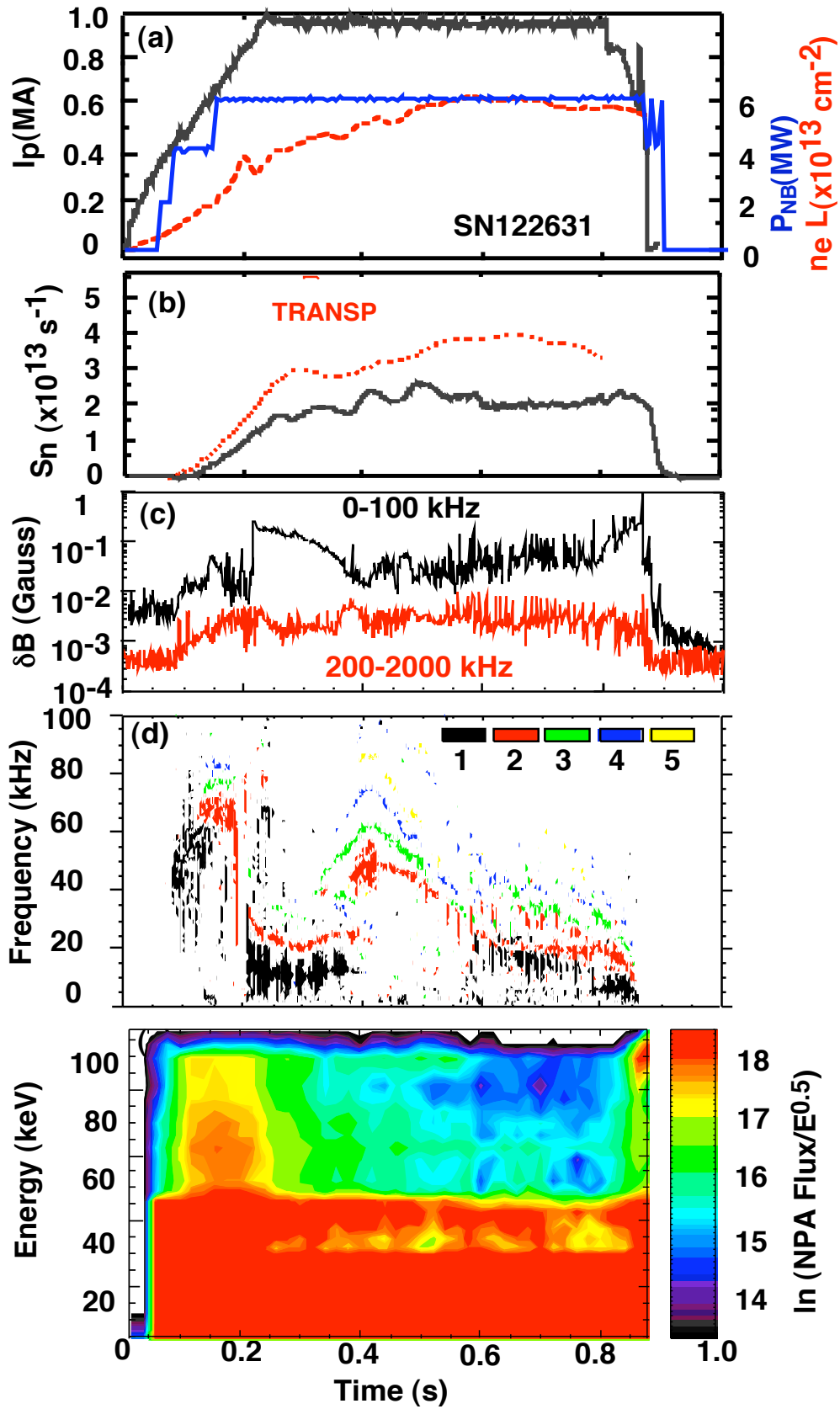
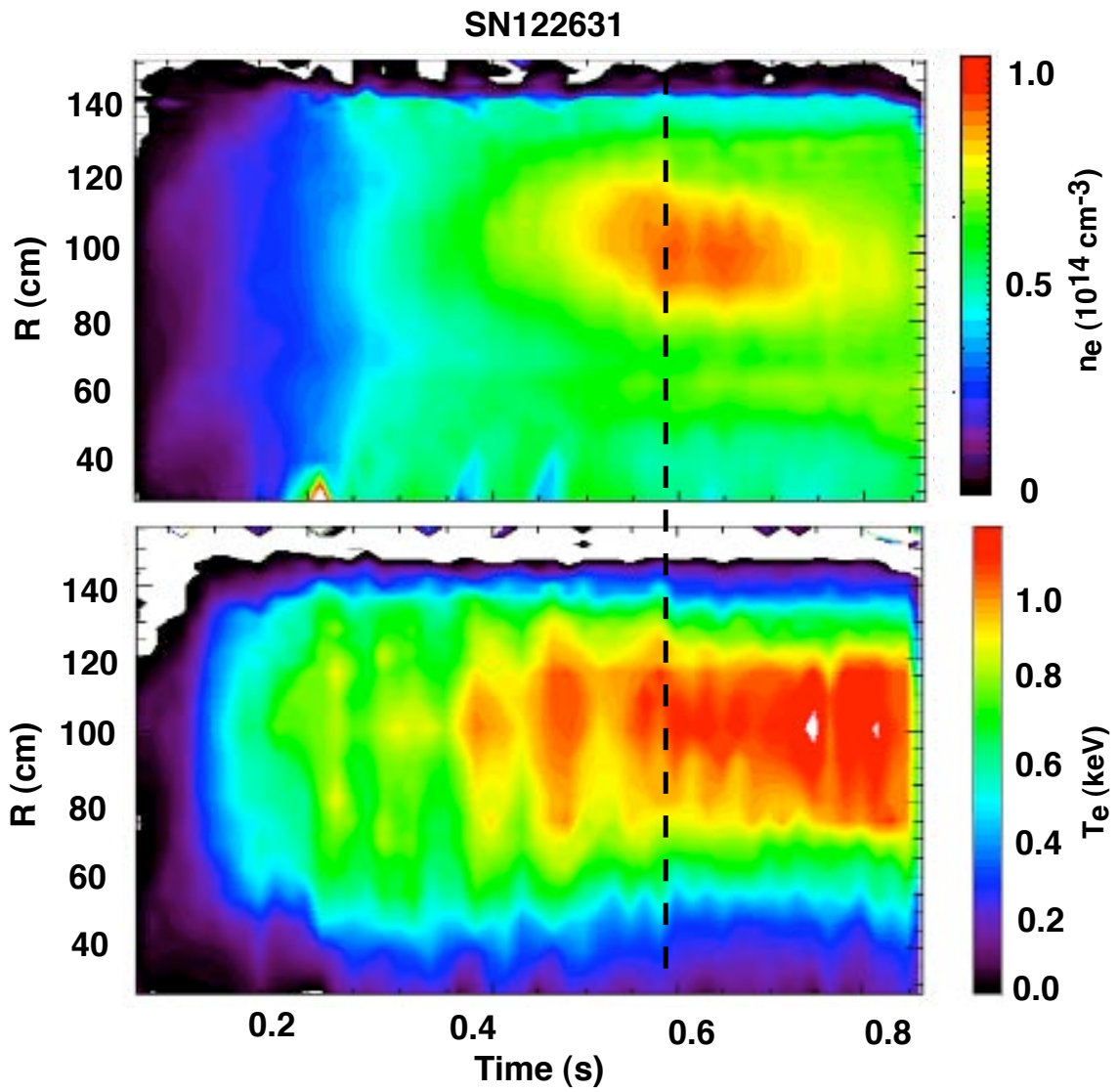


Fig. 3. Discharge characteristics for the NPA vertical scan.



*Fig. 4. MPTS contour plots show that for SN122631 a reconnection event at  $t \sim 0.6$  s leads to a collapse in the core electron density (top panel) and an increase in the core electron temperature (bottom panel).*

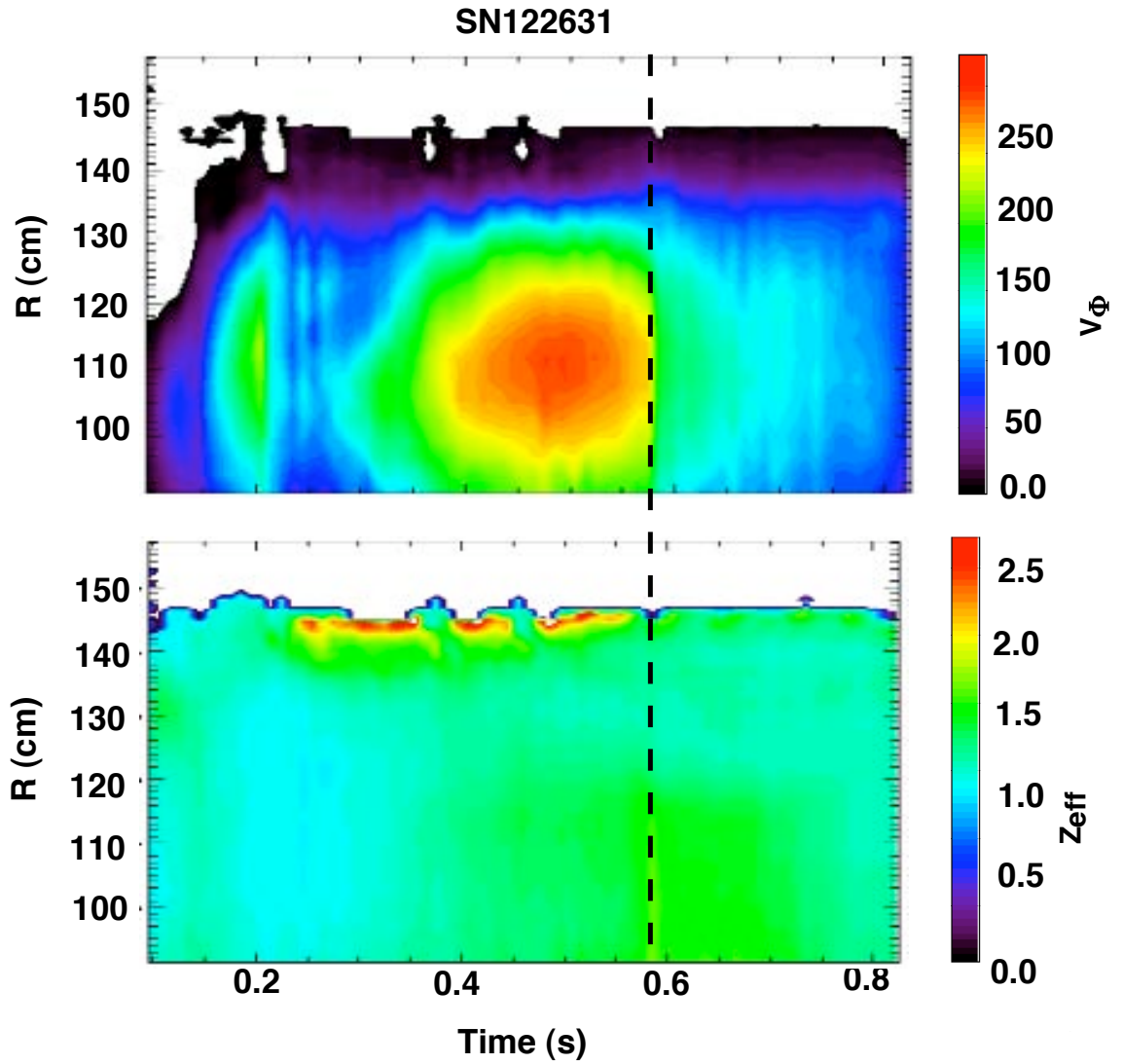


Fig. 5. *CHERS* contour plots show that for SN122631 a reconnection event at  $t \sim 0.6$  s leads to a collapse in the core toroidal rotation velocity,  $v_\phi$  (km/s), (top panel) and an increase in the core  $Z_{\text{eff}}$  (bottom panel).

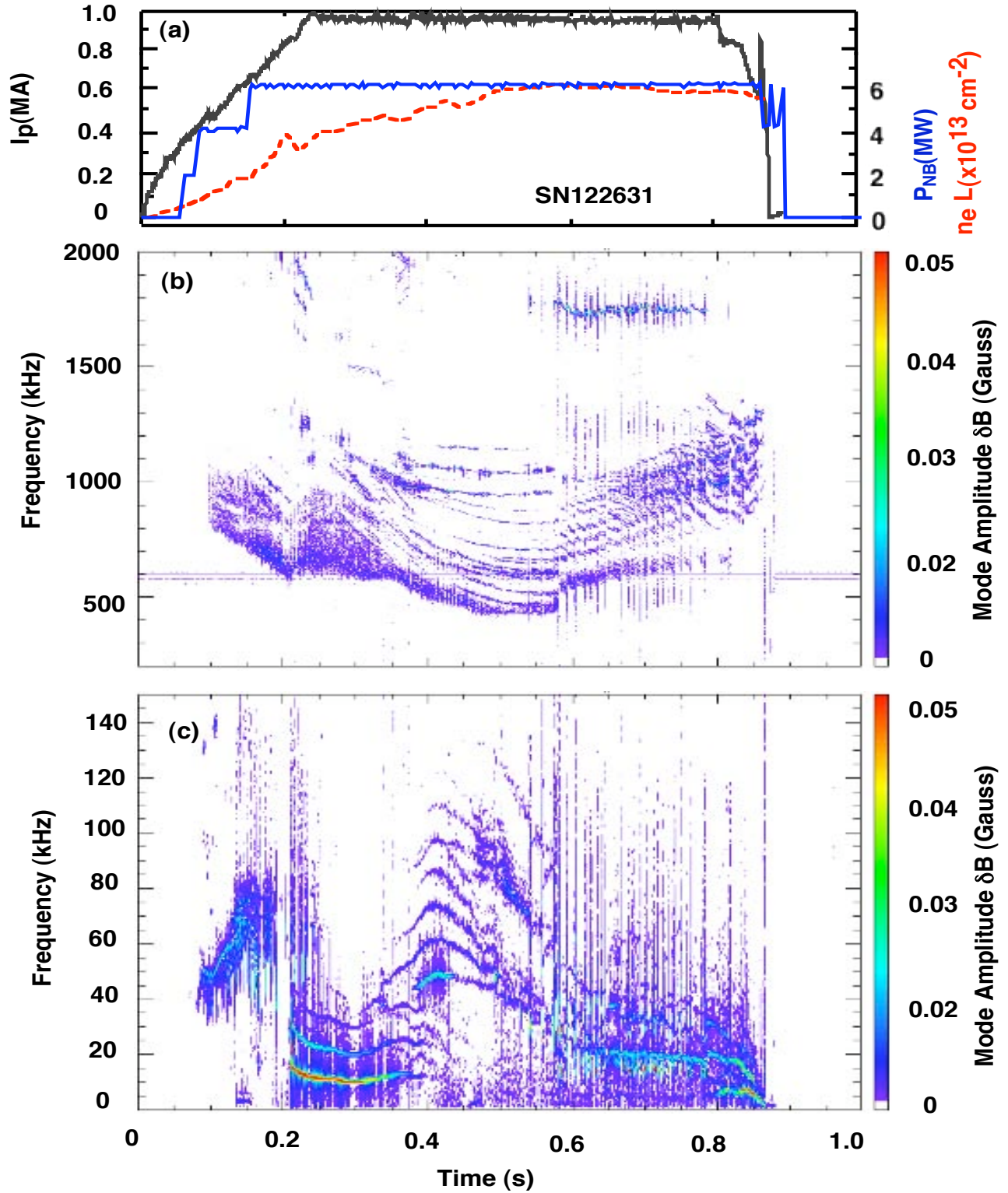


Fig. 6. Mirnov spectrograms for SN122631 covering the high ( $f = 200$ - $2000$  kHz) and low frequency ( $f = 0$ - $100$  kHz) ranges.



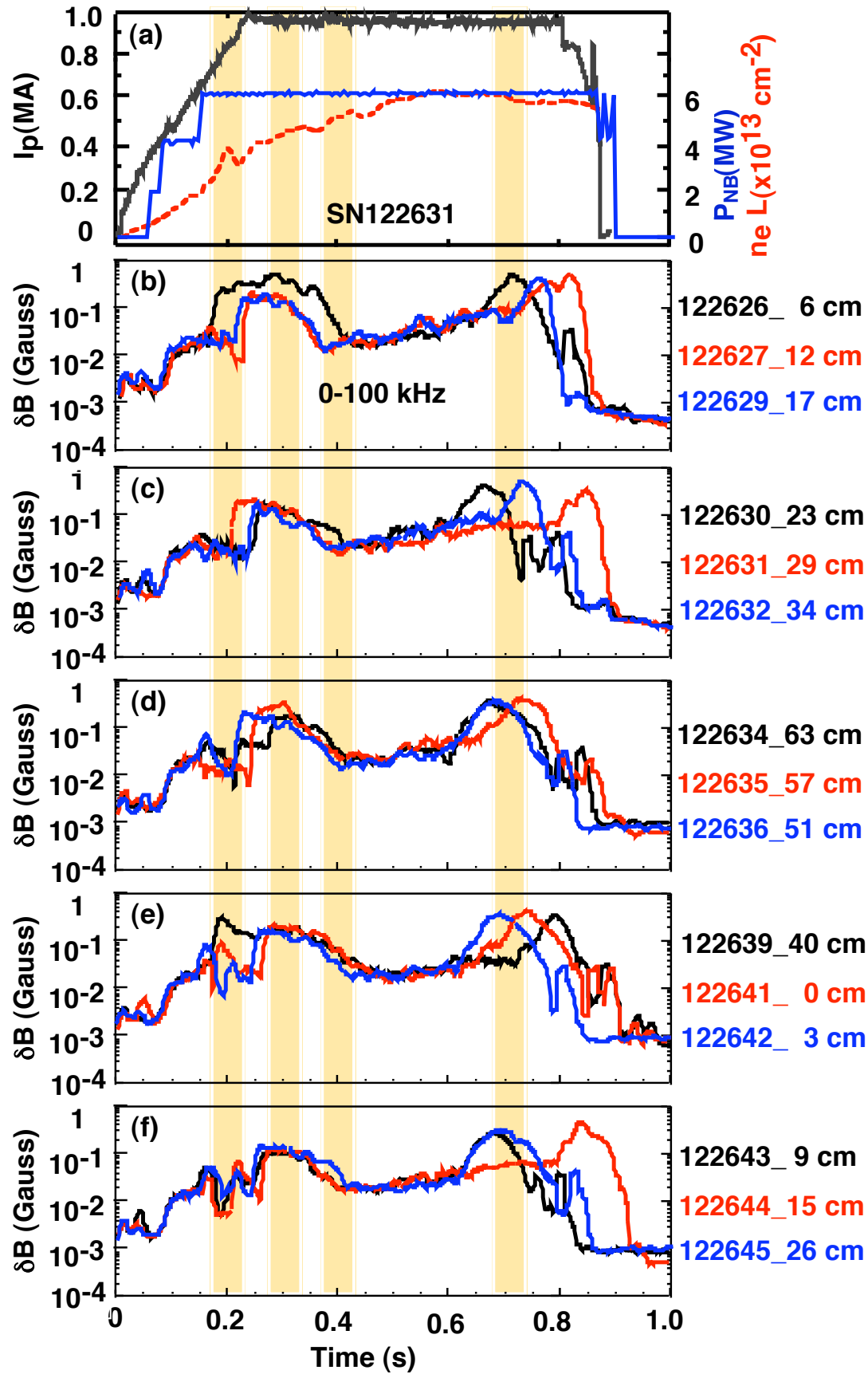


Fig. 8. Total magnetic field fluctuation (rms) in the frequency range  $f = 0-100$  kHz.

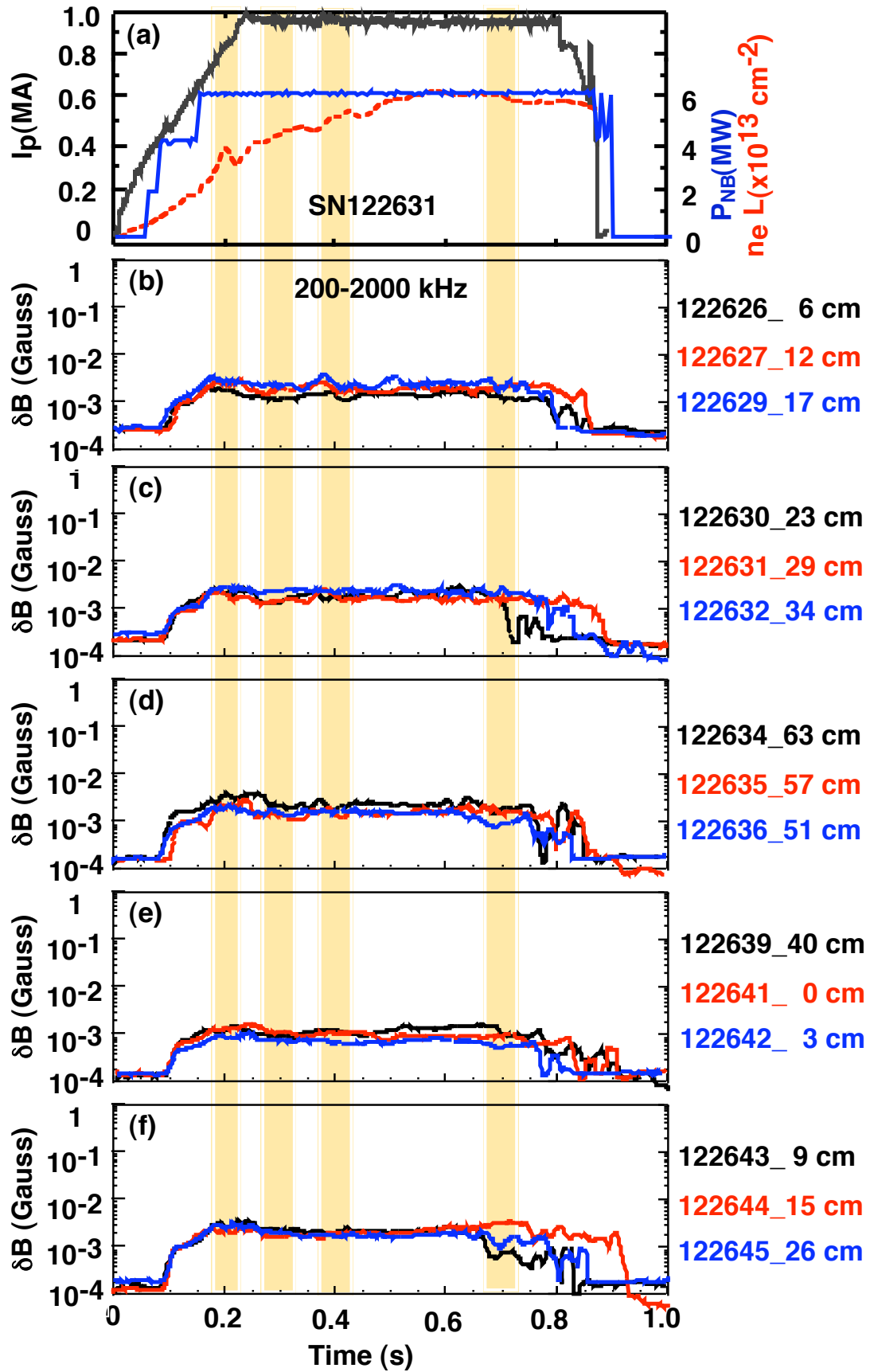


Fig. 9. Total magnetic field fluctuation (rms) in the frequency range  $f = 200\text{-}2000\text{kHz}$ .

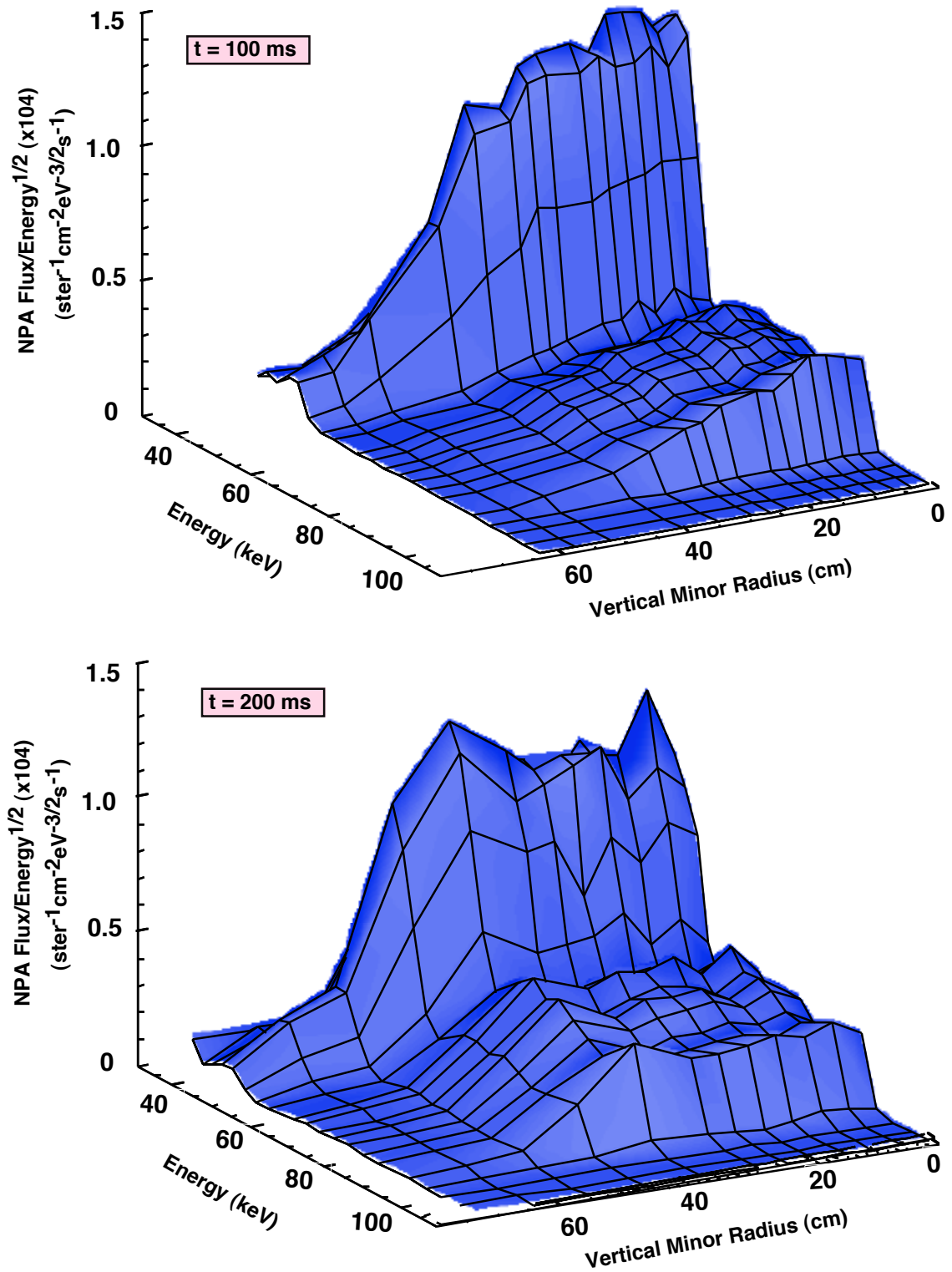


Fig. 10. NPA vertical scan during MHD-quiescent (top panel) and MHD-active (bottom panel) discharge periods (time binning  $\Delta t = 20 \text{ ms}$ ).

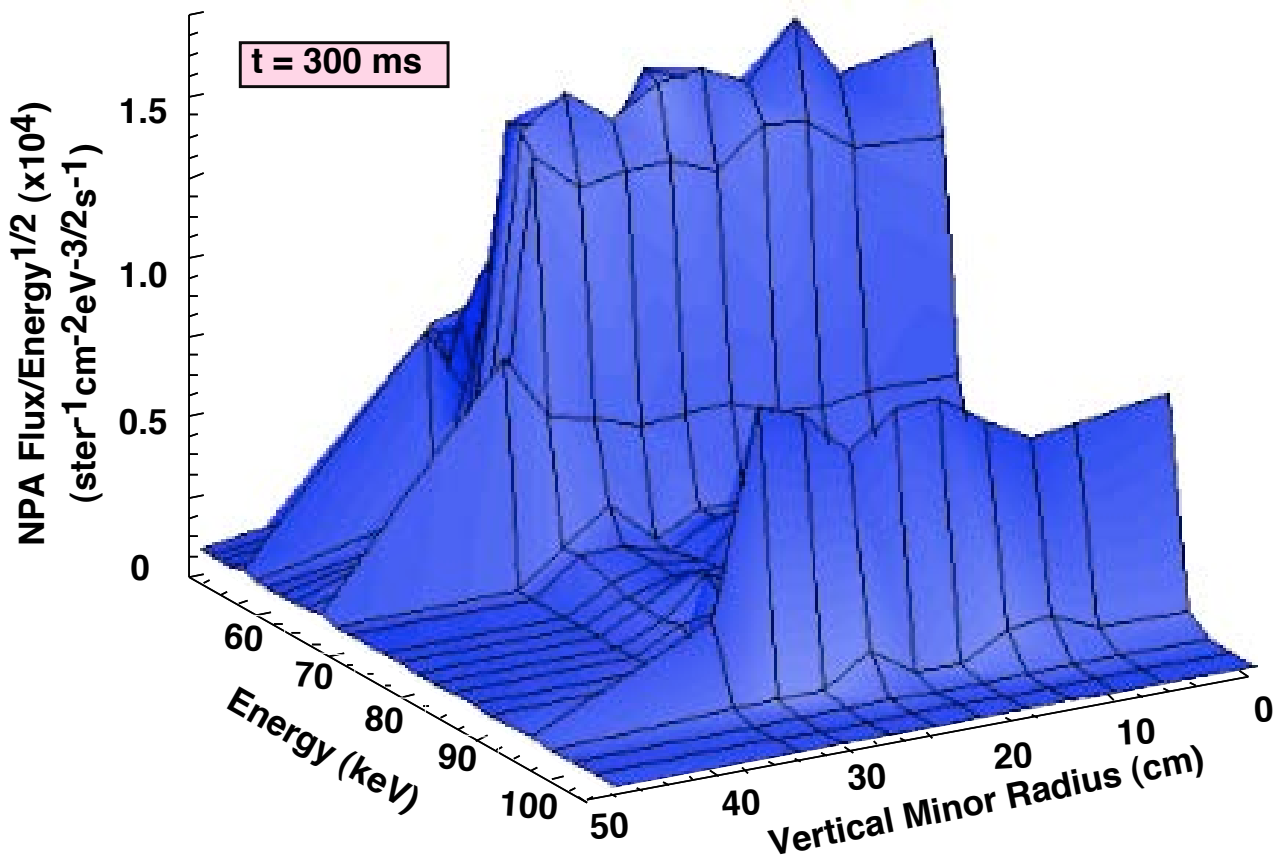


Fig. 11. NPA vertical scan during NBI into a Helium gas-filled torus with toroidal fields only ( $B_T = 3.5 - 5.5$  kG), a condition used for calibration of the MSE diagnostic. The profile shows the beam primary neutral footprint only and not the profile extending halo neutrals that would exist in a plasma discharge. The variations in peak amplitude of the flux are due to changes in the toroidal field: high toroidal fields produce higher peaks corresponding to energetic ions being better 'confined'.

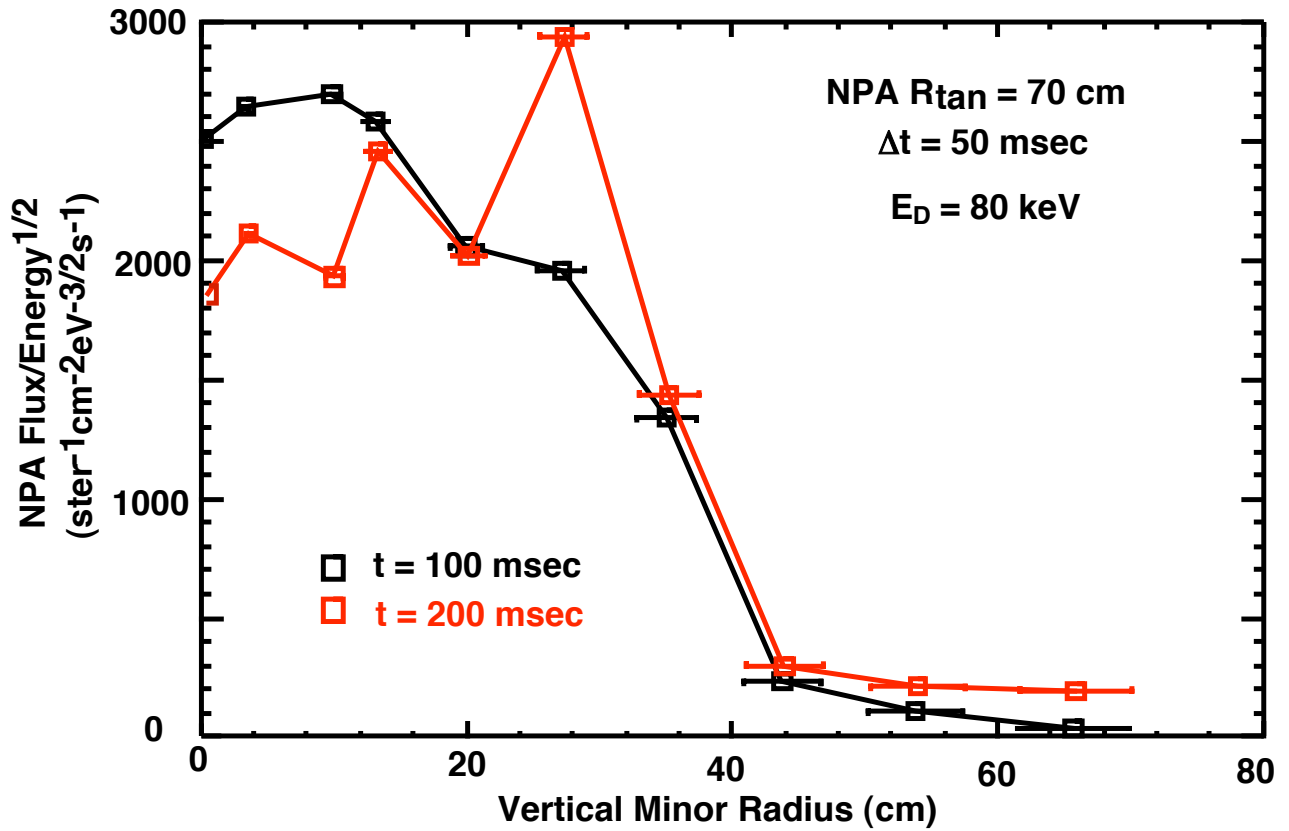


Fig. 12. The energetic ion flux on a linear scale versus vertical minor radius are plotted at times  $t = 100$  and  $200 \text{ ms}$  for an energy of  $E_D = 80 \text{ keV}$ . The depletion in the core and outward redistribution of the energetic ion profile to form a shoulder is clearly evident.

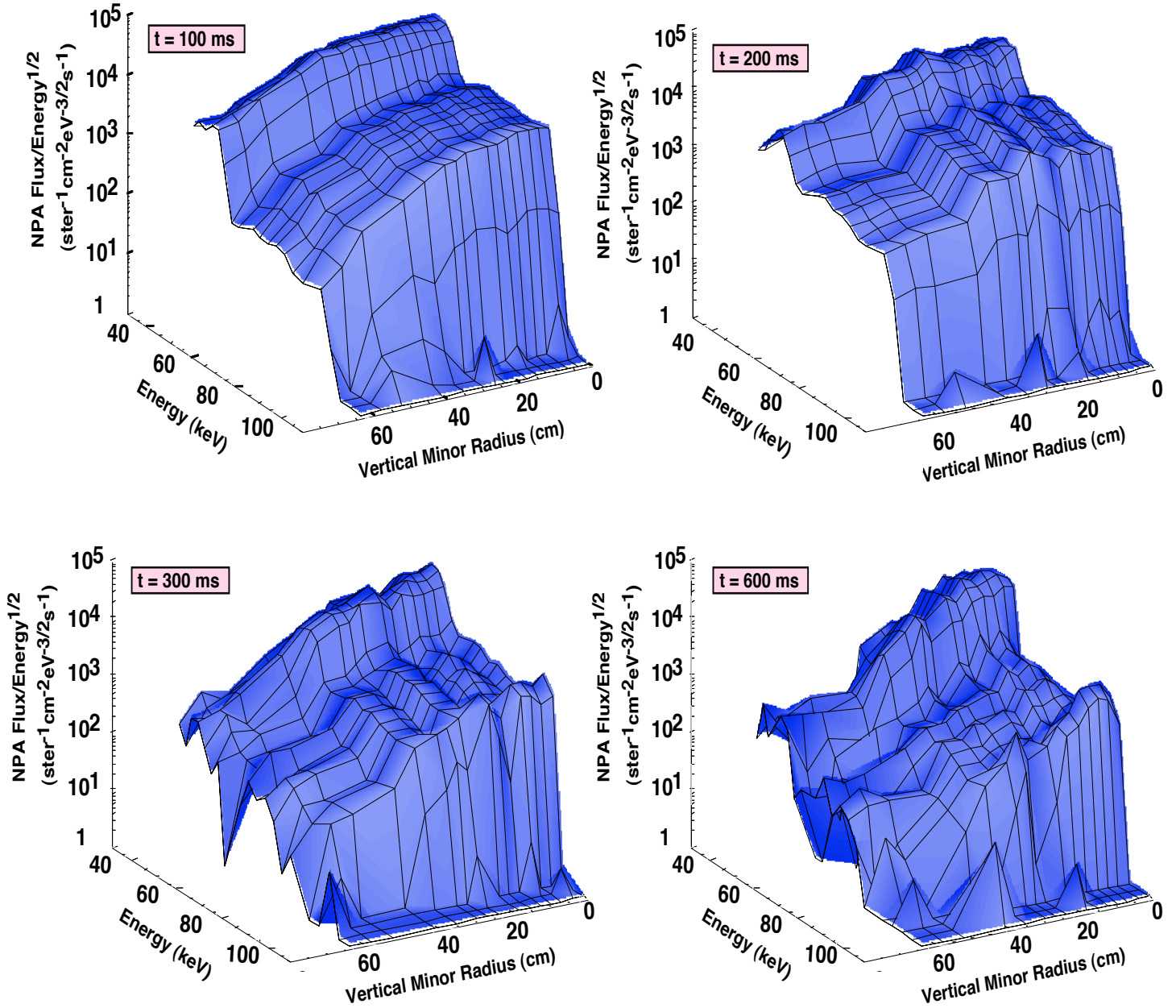


Fig. 13. NPA vertical scan spectra are shown on a logarithmic scale. At  $t = 100 \text{ ms}$  the spectrum is core-peaked then at  $t = 200 \text{ ms}$  becomes redistributed to form a shoulder around a vertical minor radius of 40 cm. Depletion of the spectra occurs at later times.

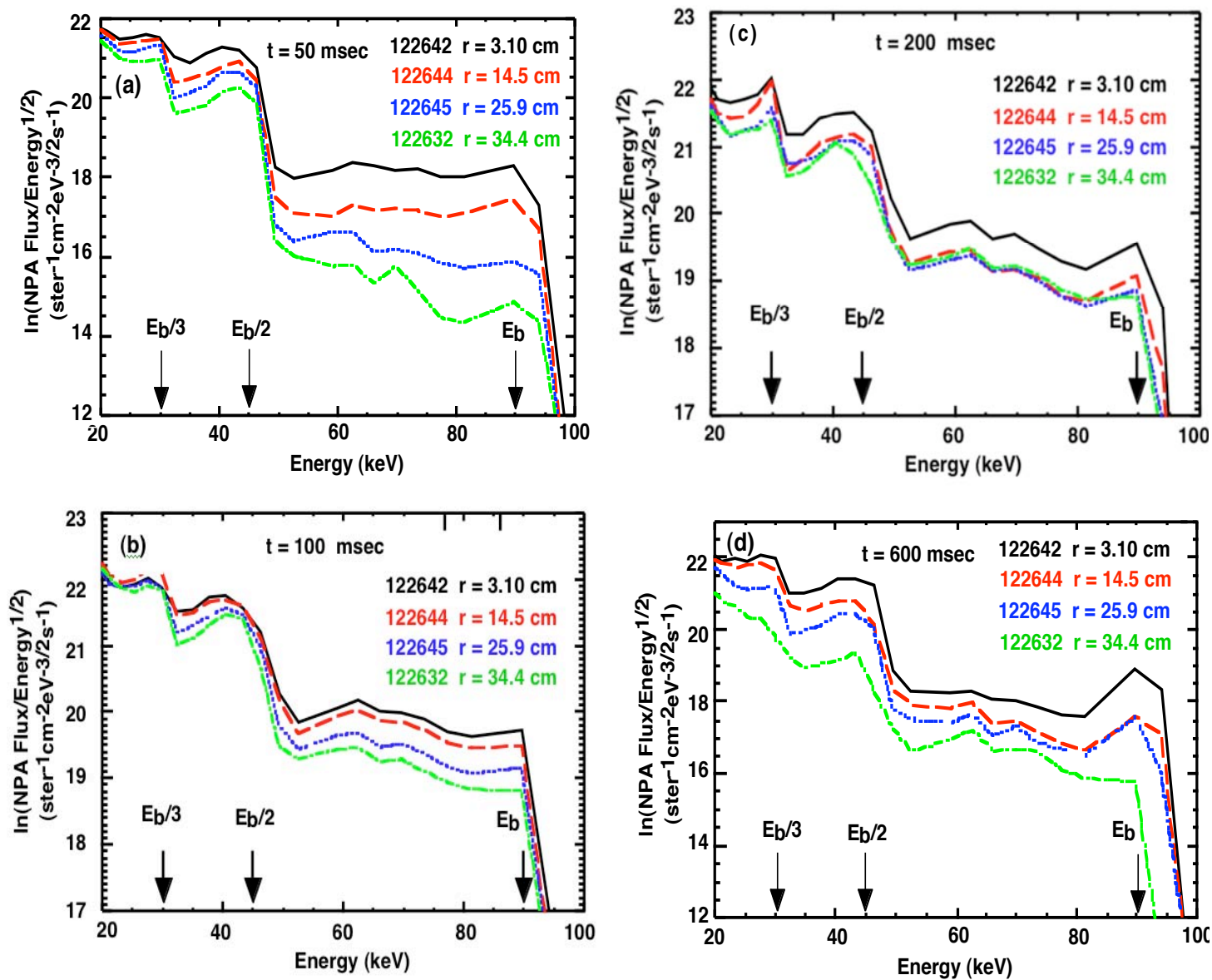


Fig. 14. Energetic ion spectra on a natural logarithmic scale from the NPA vertical scan profiles (Fig. 13) for selected radii at  $t = 50, 100, 200$  and  $600$  ms.

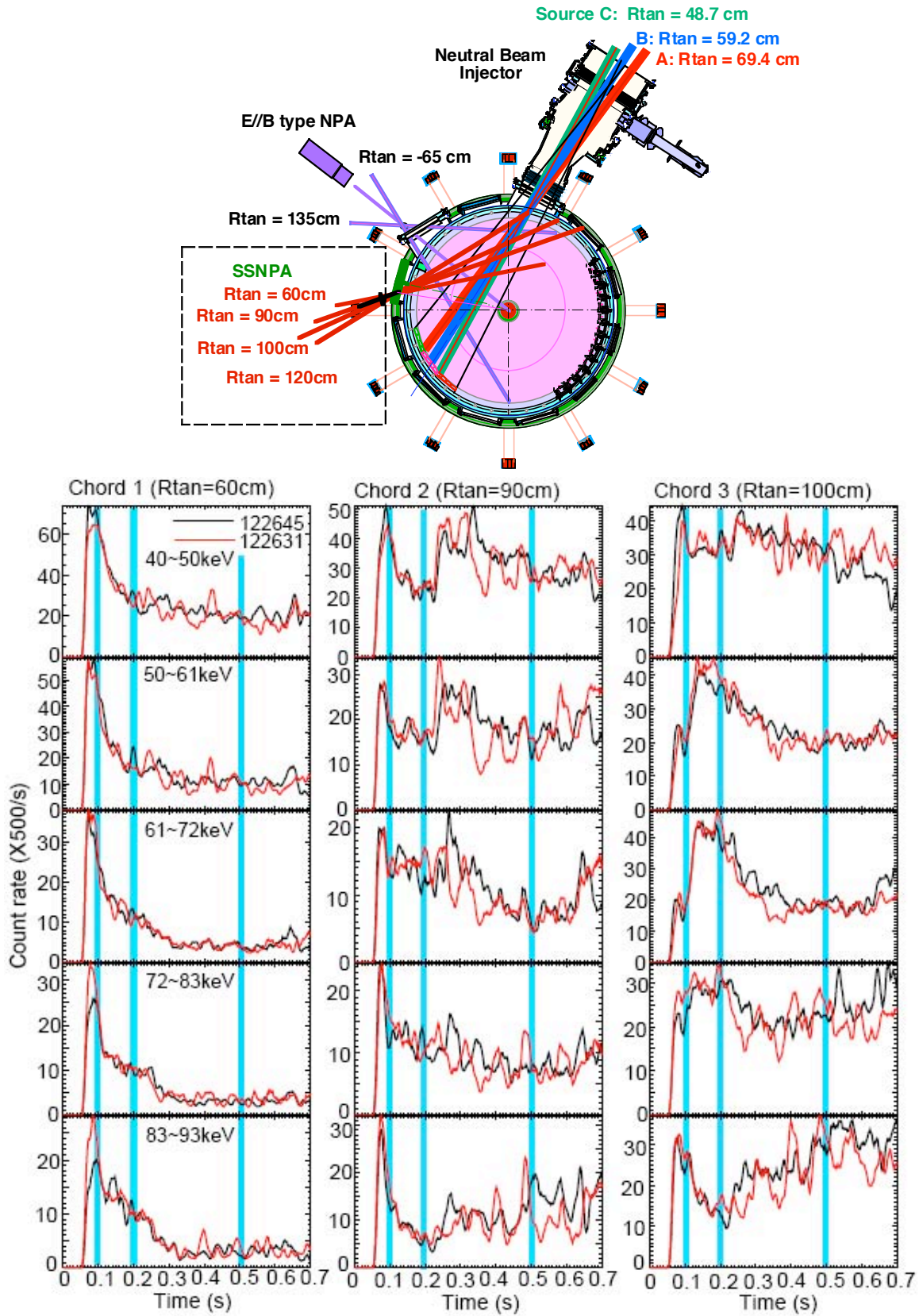


Fig. 15. Temporal evolution of three selected ssNPA chords ( $R_{tan} = 60\text{ cm}$ ,  $R_{tan} = 90\text{ cm}$  and  $R_{tan} = 100\text{ cm}$ ) for SN122645 and SN122631.

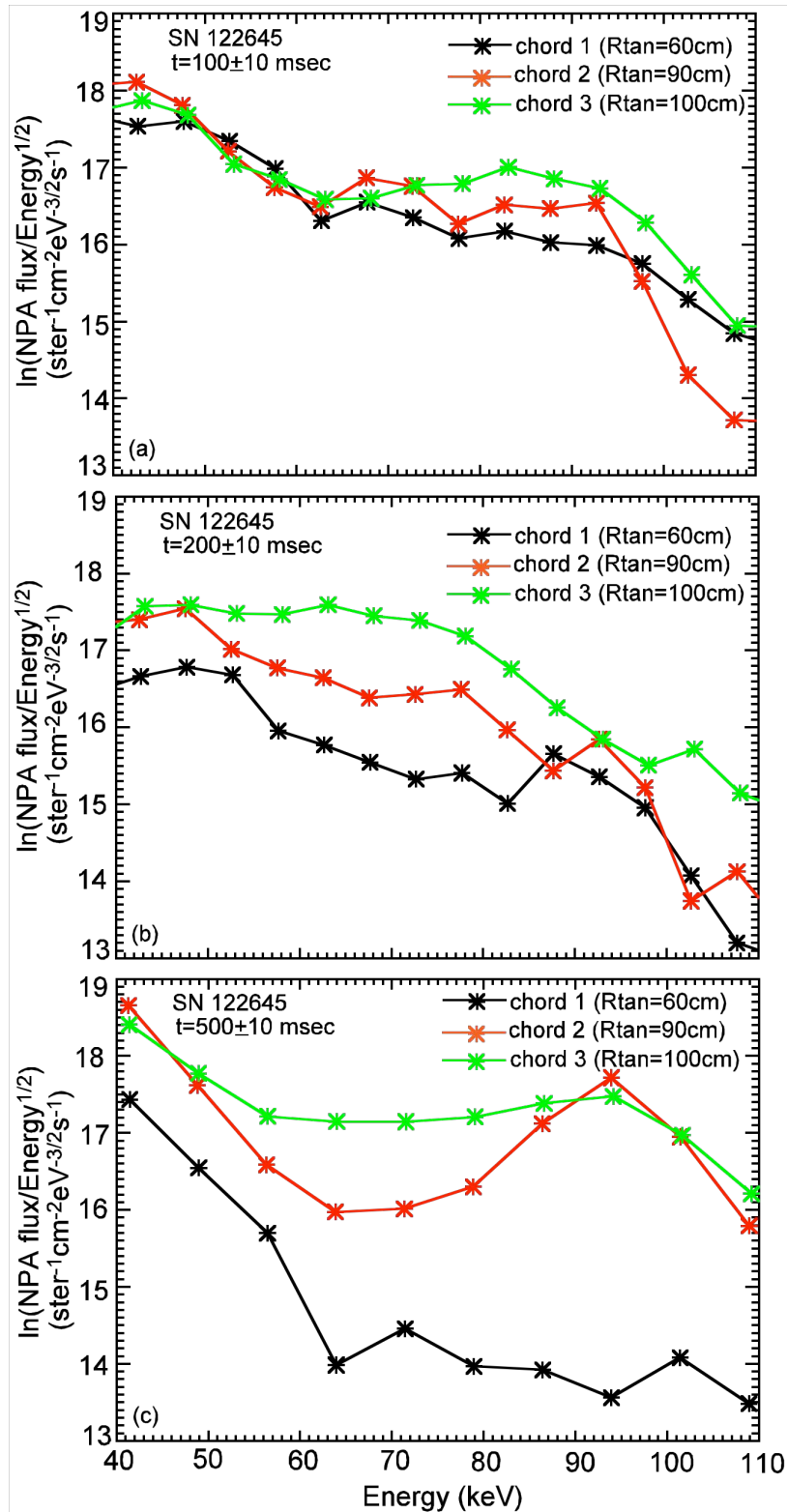


Fig. 16. Energy spectra of three selected ssNPA chords ( $R_{\text{tan}} = 60$  cm,  $R_{\text{tan}} = 90$  cm and  $R_{\text{tan}} = 100$  cm) at  $t = 100$ ,  $200$  and  $500$  ms. The tail above the injected energy (90 keV) is caused by pile up. (The neutron-induced noise has been subtracted.)

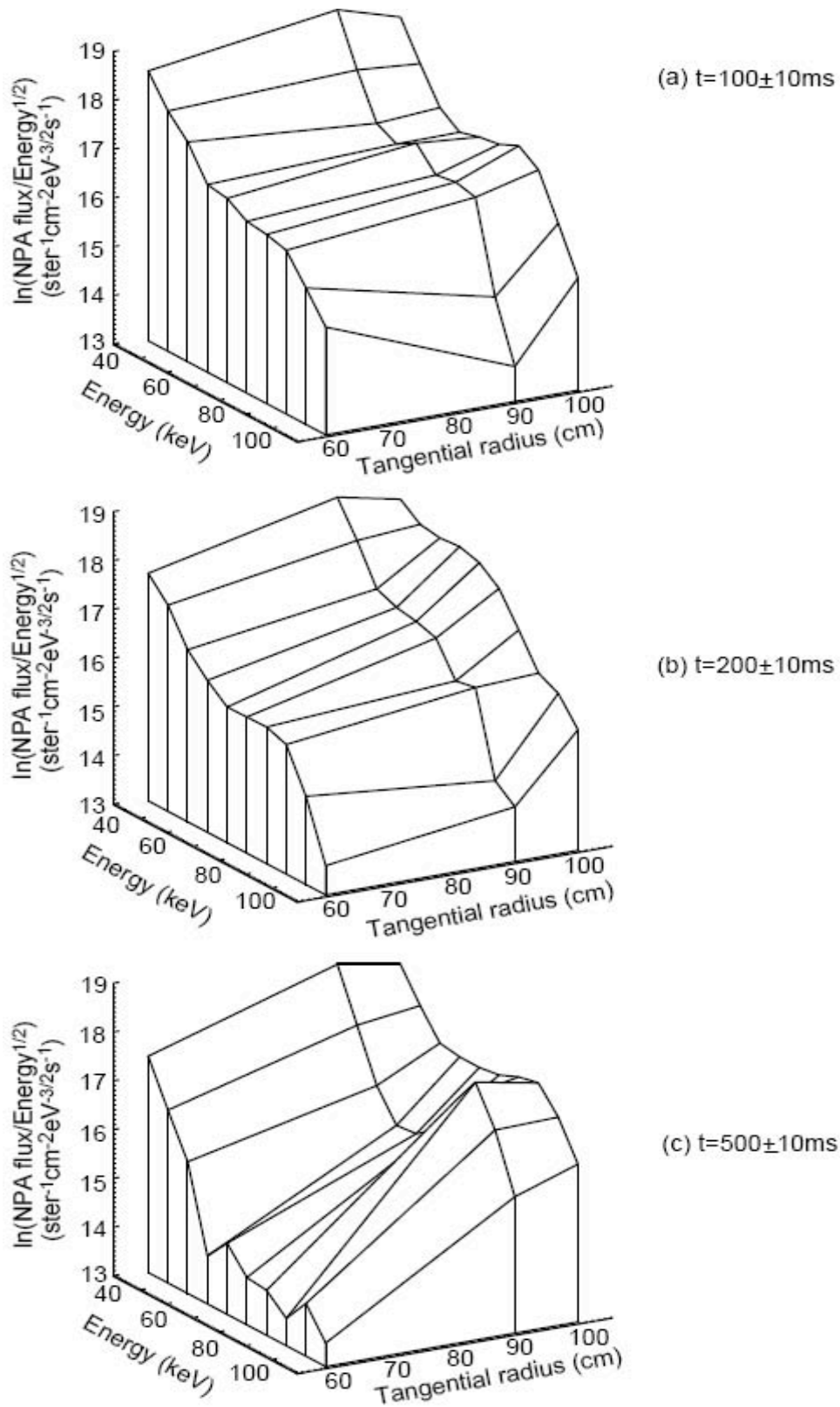


Fig. 17. Global 3D view of the energy spectra of three selected ssNPA chords ( $R_{\text{tan}} = 60\text{ cm}$ ,  $R_{\text{tan}} = 90\text{ cm}$  and  $R_{\text{tan}} = 100\text{ cm}$ ) at  $t = 100, 200$  and  $500\text{ ms}$ .

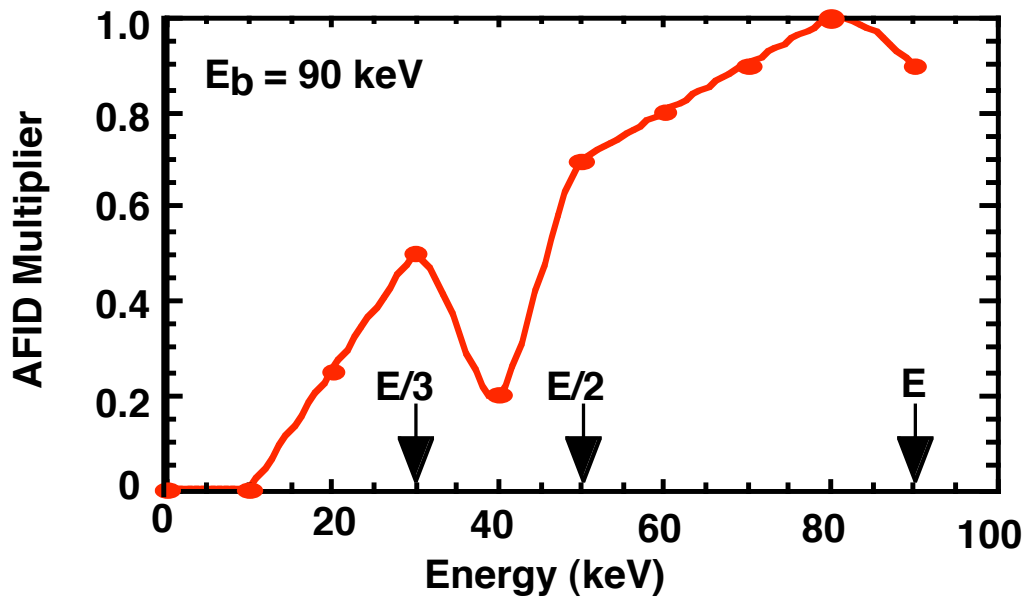
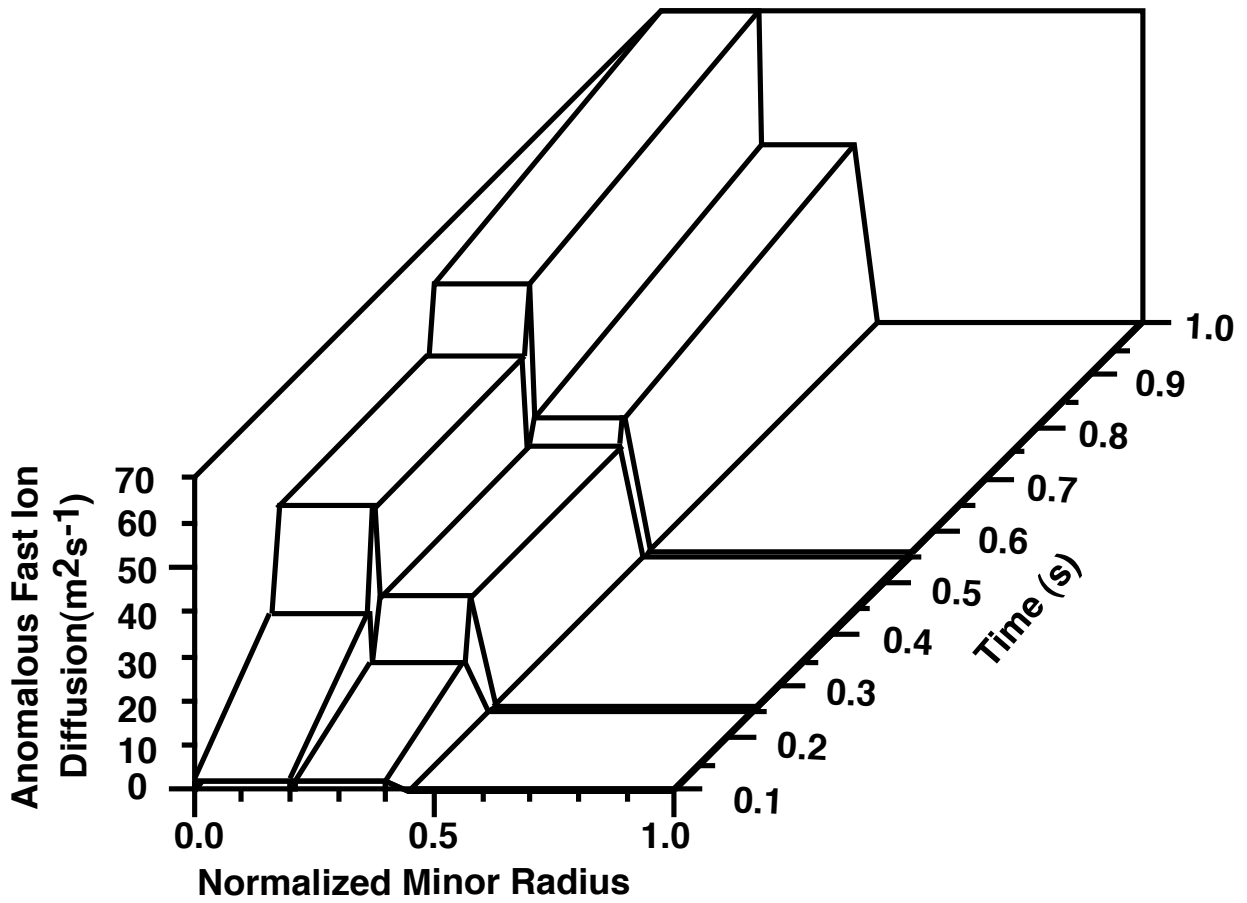


Fig. 18. Illustration of the TRANSP anomalous fast ion diffusion parameters (AFID file G122631.D2F) utilized in TRANSP for SN122631M11.

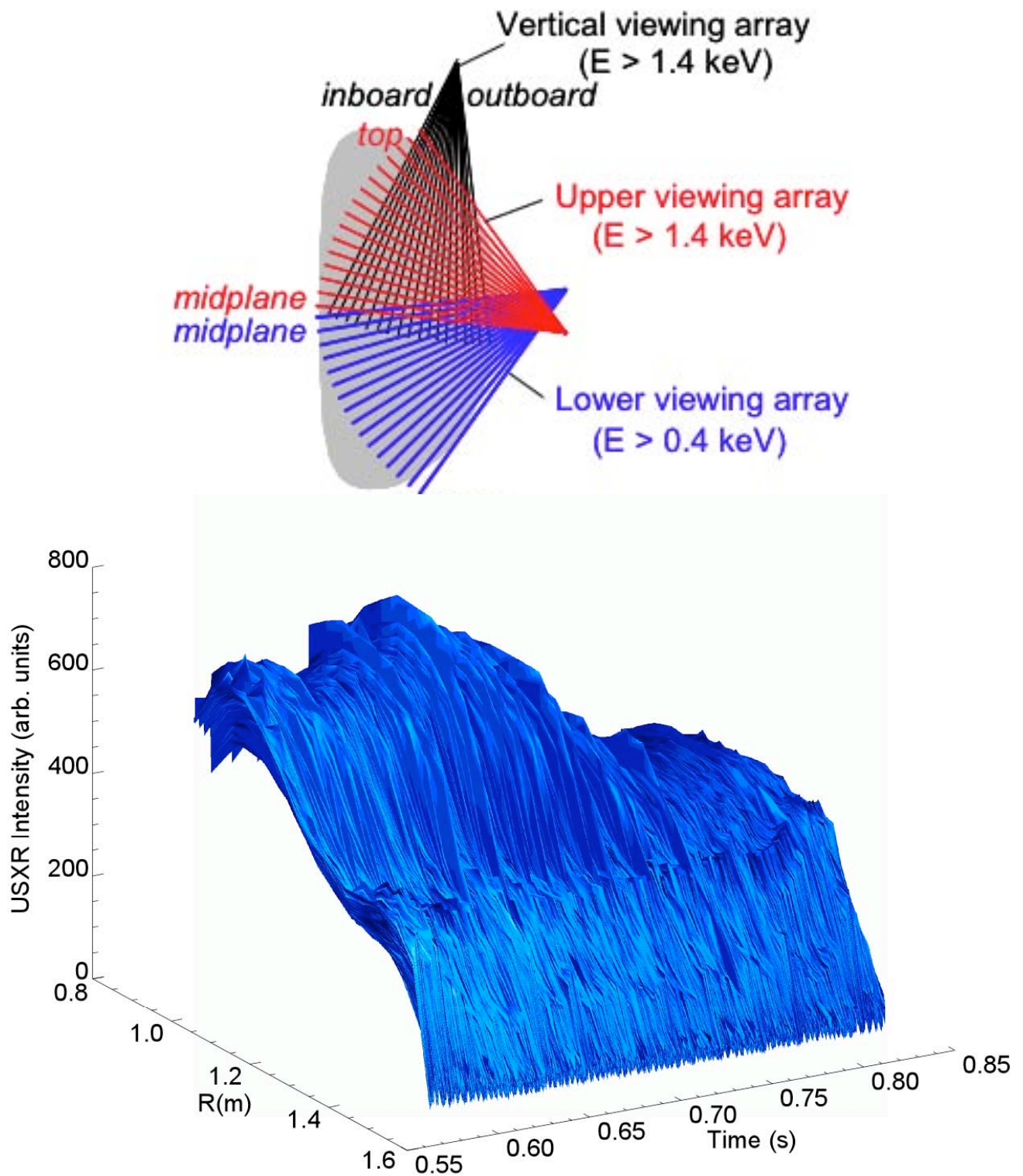


Fig. 19. Illustration of the USXR diagnostic measurements used for guidance in defining the radial profile of the anomalous fast ion diffusion used in TRANSP. The roll-off of the USXR intensity at  $t \sim 0.7$  s is due to a collapse of the core  $Z_{\text{eff}}$  (the  $n_e$  and  $T_e$  profiles are virtually constant so thus do not contribute to the roll-off).

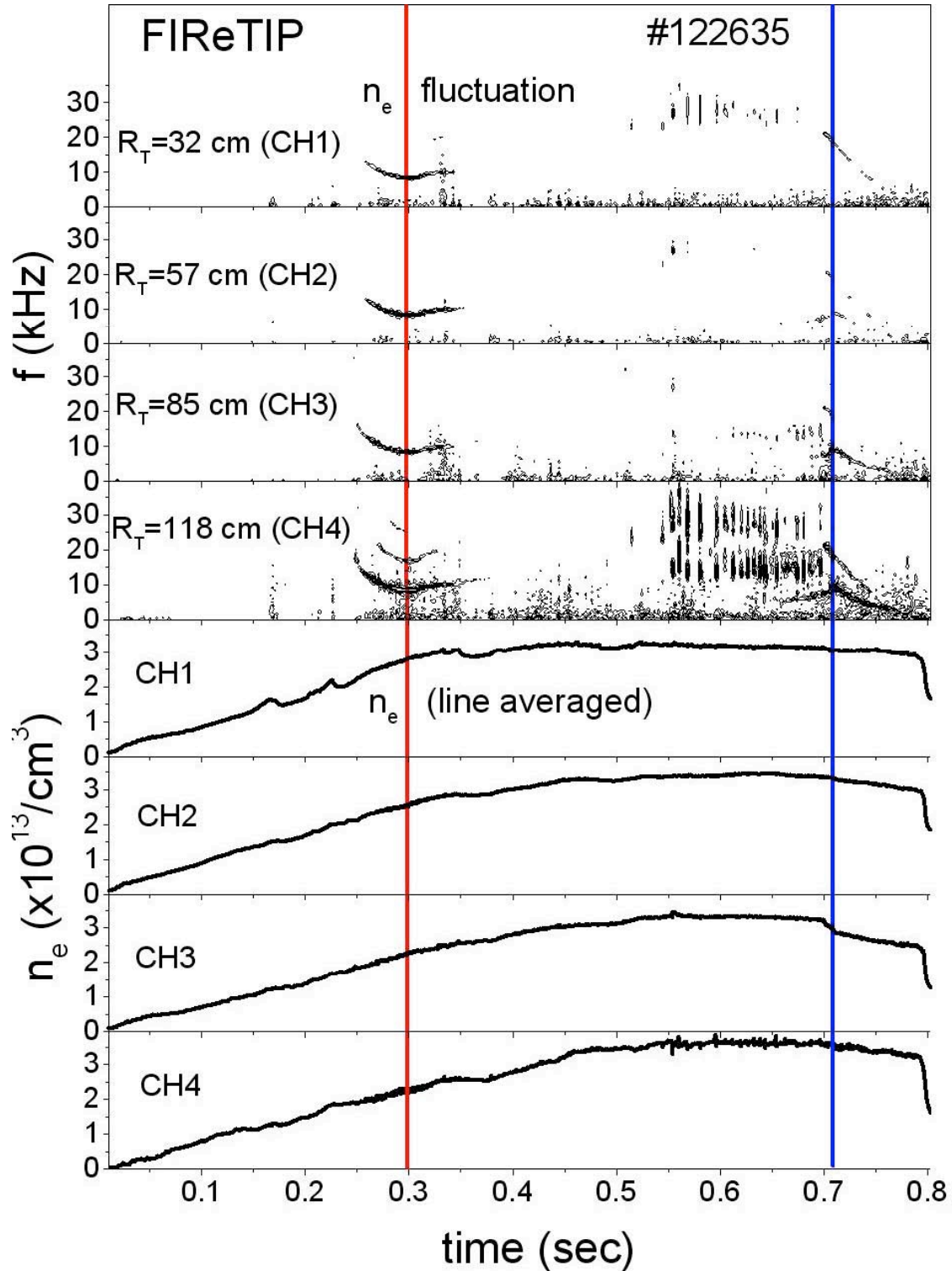


Fig. 20. Shown are FReTIP measurements of the line-averaged electron density (upper panels) and the density fluctuation spectra (lower panels). A comparison with Fig. 7 reveals that only certain classes of MHD activity generate significant density fluctuations (e.g. during the periods  $t \sim 0.25$ - $0.35$  s and  $t \sim 0.55$ - $0.8$  s).

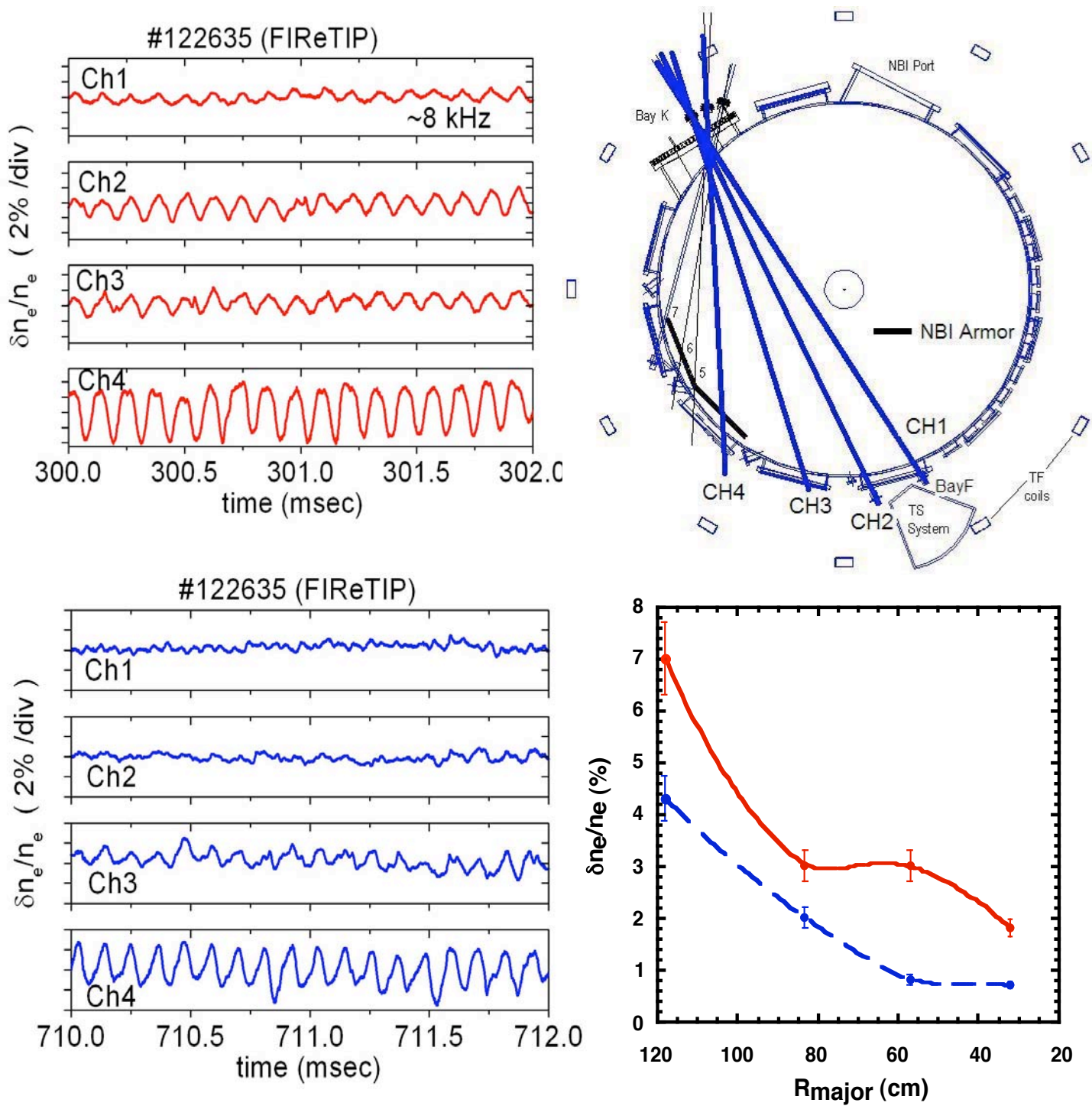


Fig. 21. FReTIP measurements show that the electron density fluctuations are core localized in agreement with USXR data in Fig. 19.

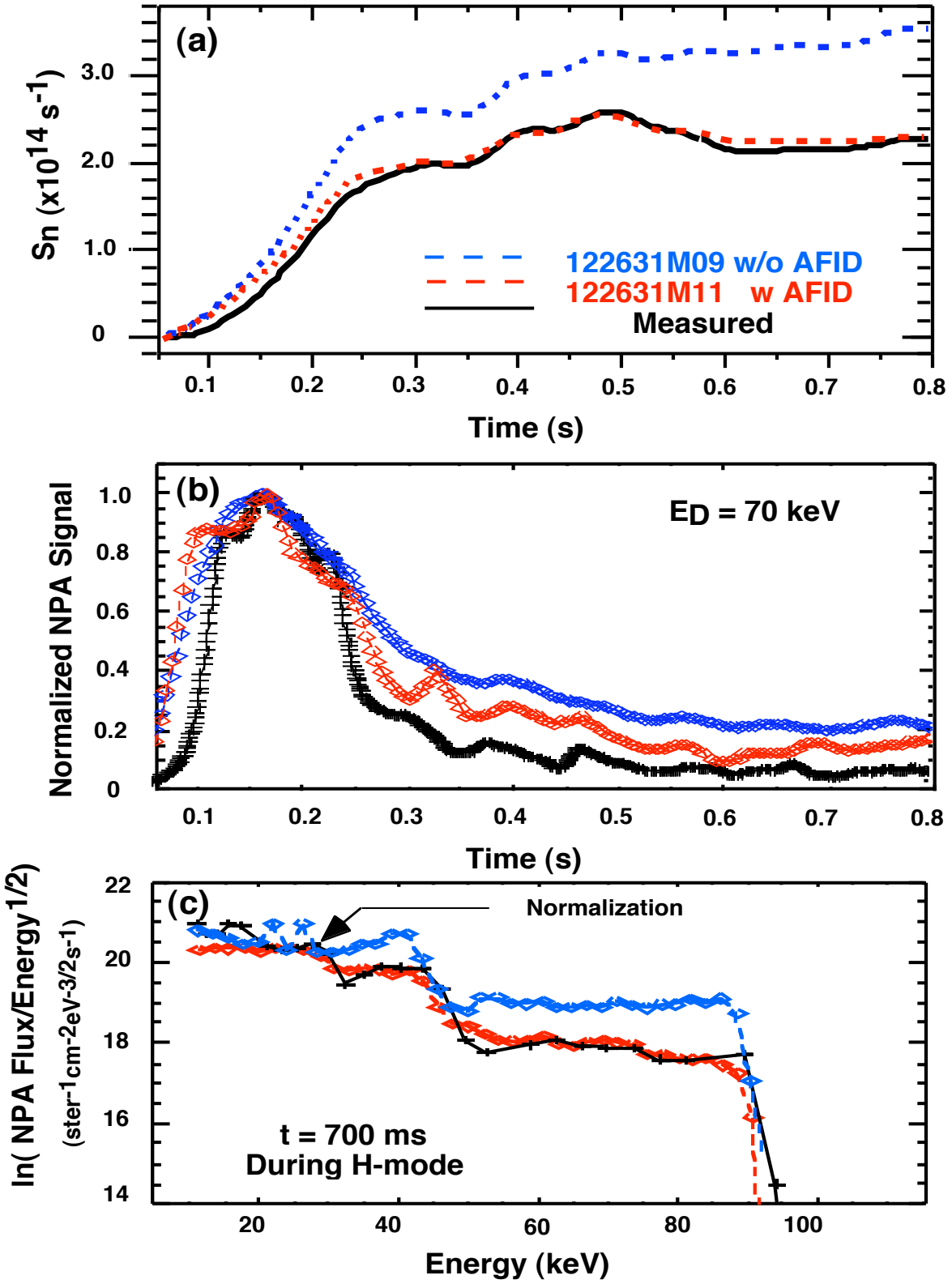


Fig. 22. Shown are results of TRANSP simulation using anomalous fast ion diffusion for discharge 122631. Black lines are measurements and red/blue lines are TRANSP simulations with/without anomalous fast ion diffusion. The time of interest is 0.7 s. Matching of the measurements with TRANSP AFID model are presented for: (a) neutron yield, (b) NPA signal evolution, and (c) NPA energetic ion spectra.

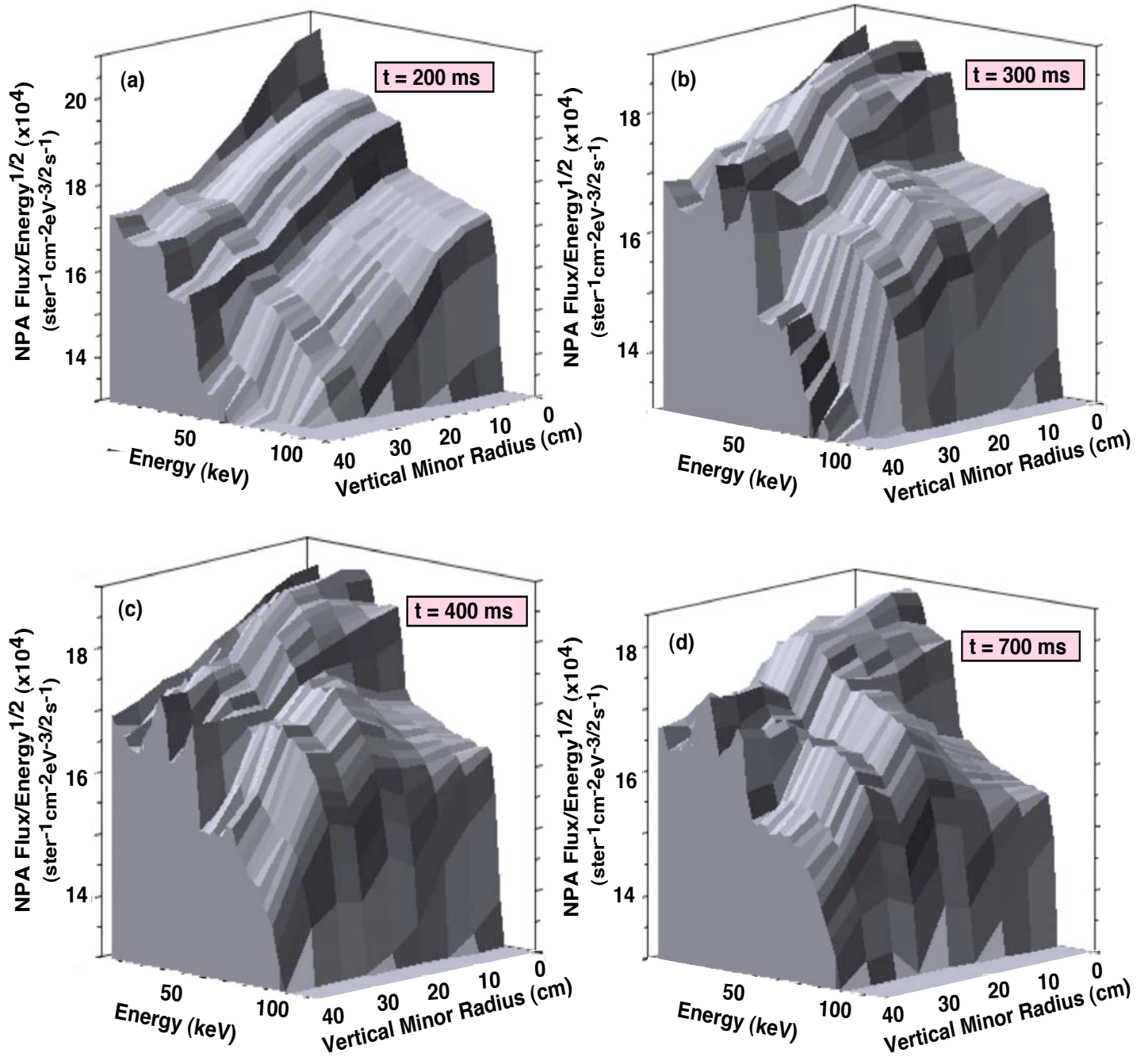


Fig. 23. TRANSP simulation of the NPA vertical scan using anomalous fast ion diffusion as shown in Fig. 12 to emulate MHD-induced energetic ion redistribution for the NPA horizontal tangency radius,  $R_{tan} = 70 \text{ cm}$  (122631M04).

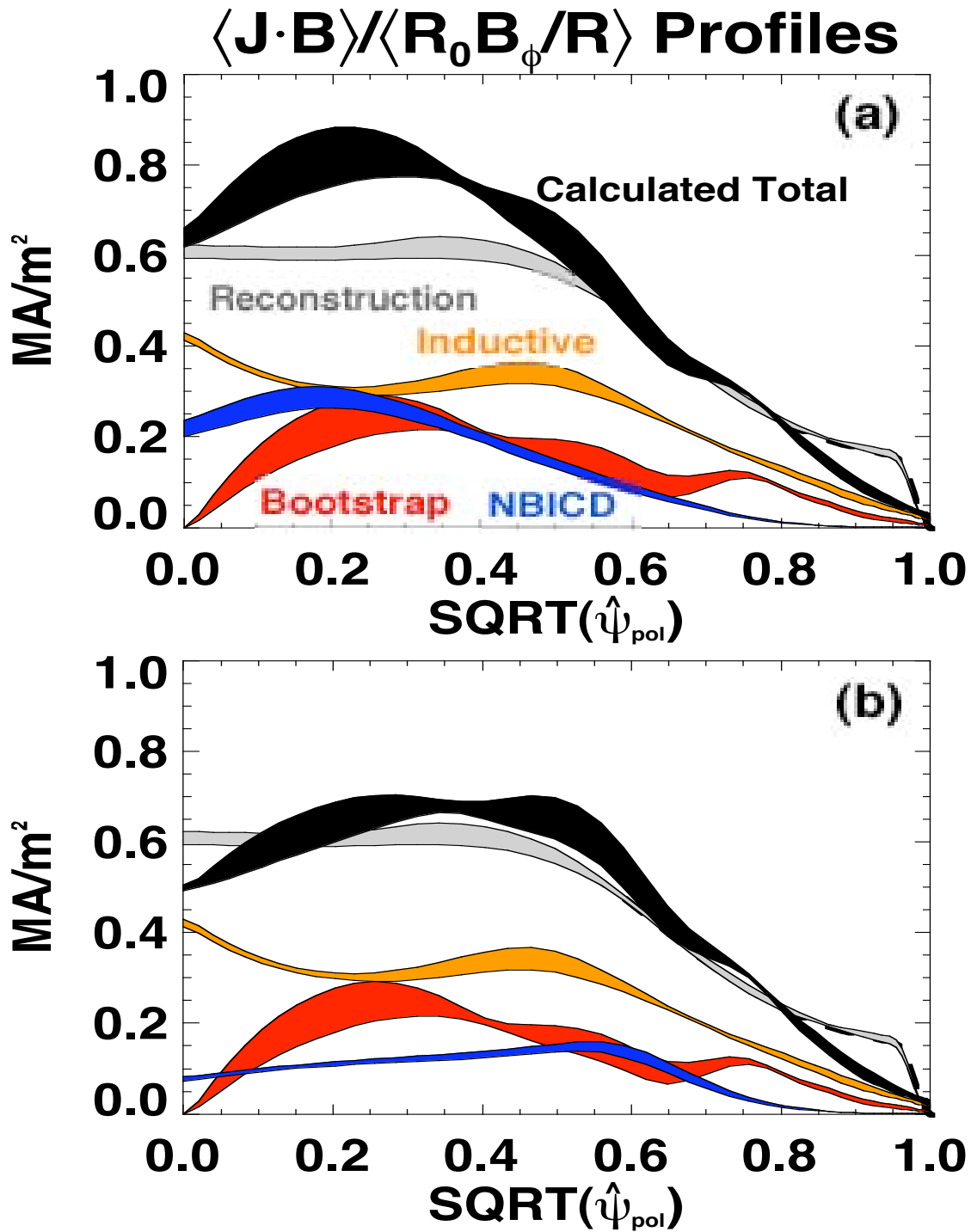


Fig. 24. Illustration of matching MSE-reconstructed and calculated current profiles using AFID in TRANSP for NBICD redistribution.

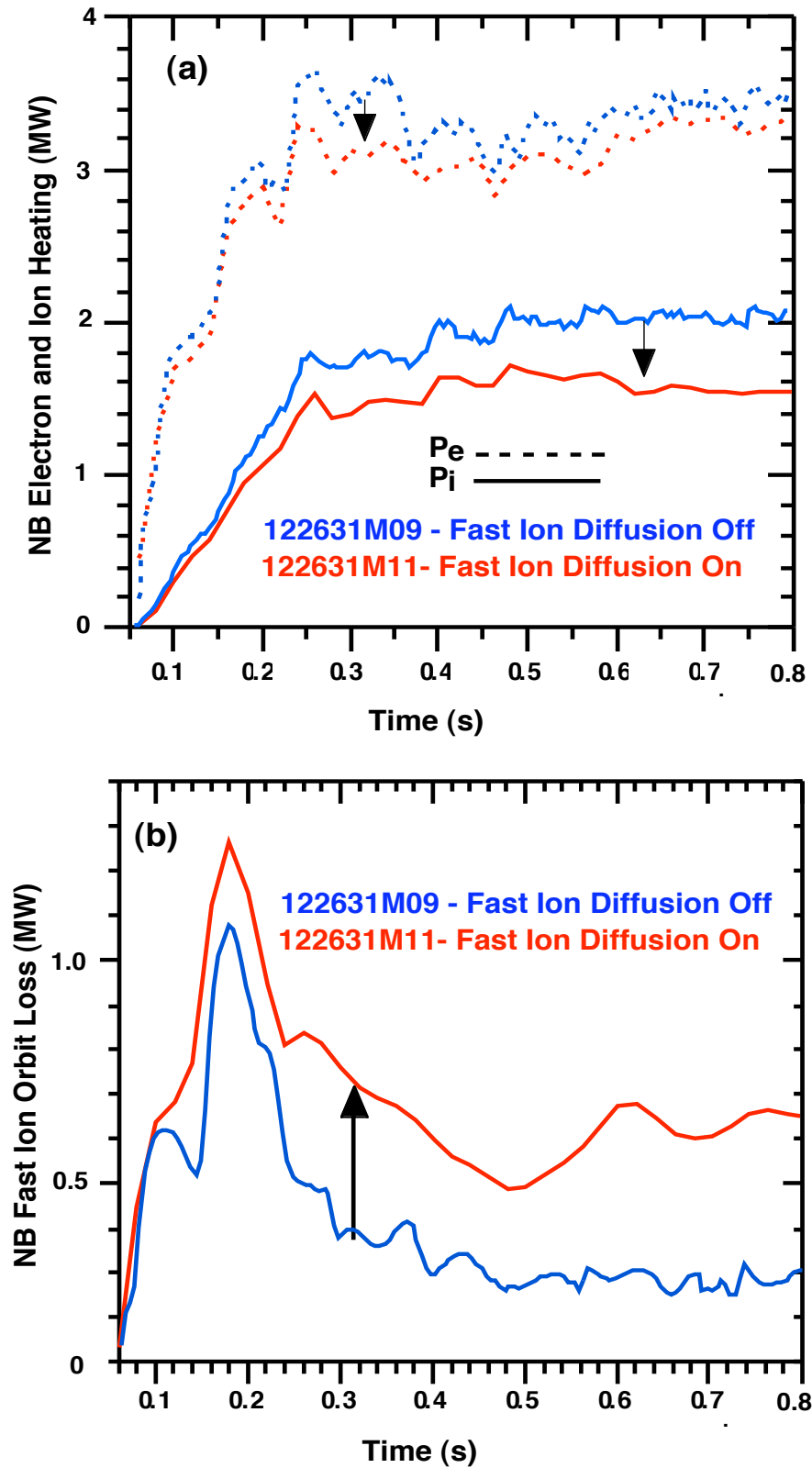


Fig. 25. TRANSP calculation of neutral beam power to electrons and ions (upper panel) for SN122631 without fast ion diffusion (blue curves) and with fast ion diffusion (red curves) and NB fast ion power loss (lower panel) are shown.

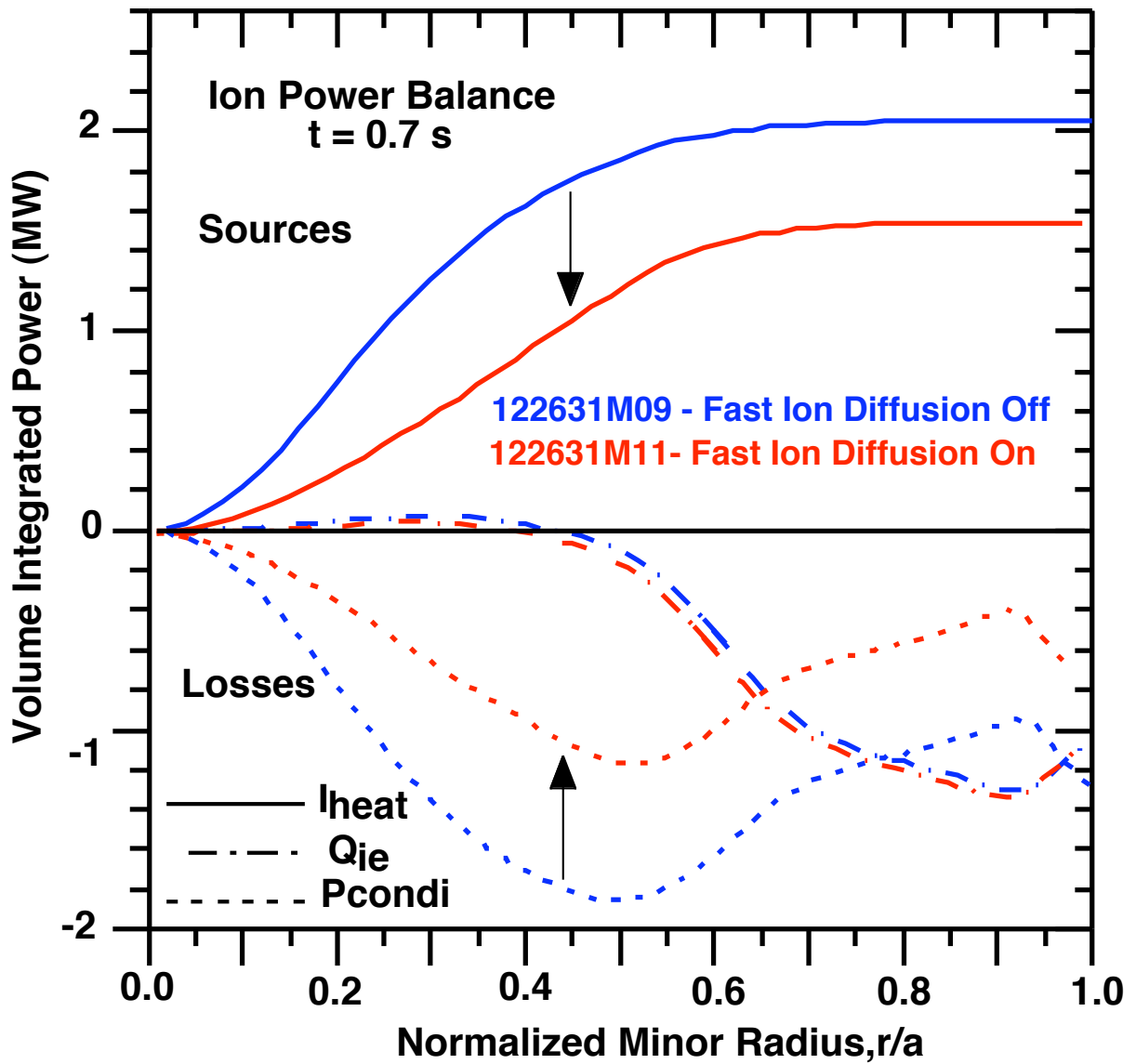


Fig. 26. TRANSP calculation of ion power balance at  $t = 700$  ms with and without fast ion diffusion for SN122631 is shown.  $I_{heat}$  is the total ion heating,  $Q_{ie}$  is the power transferred from ions to electrons (which is negative because  $T_i > T_e$ ) and  $P_{condi}$  is the ion conduction power loss.

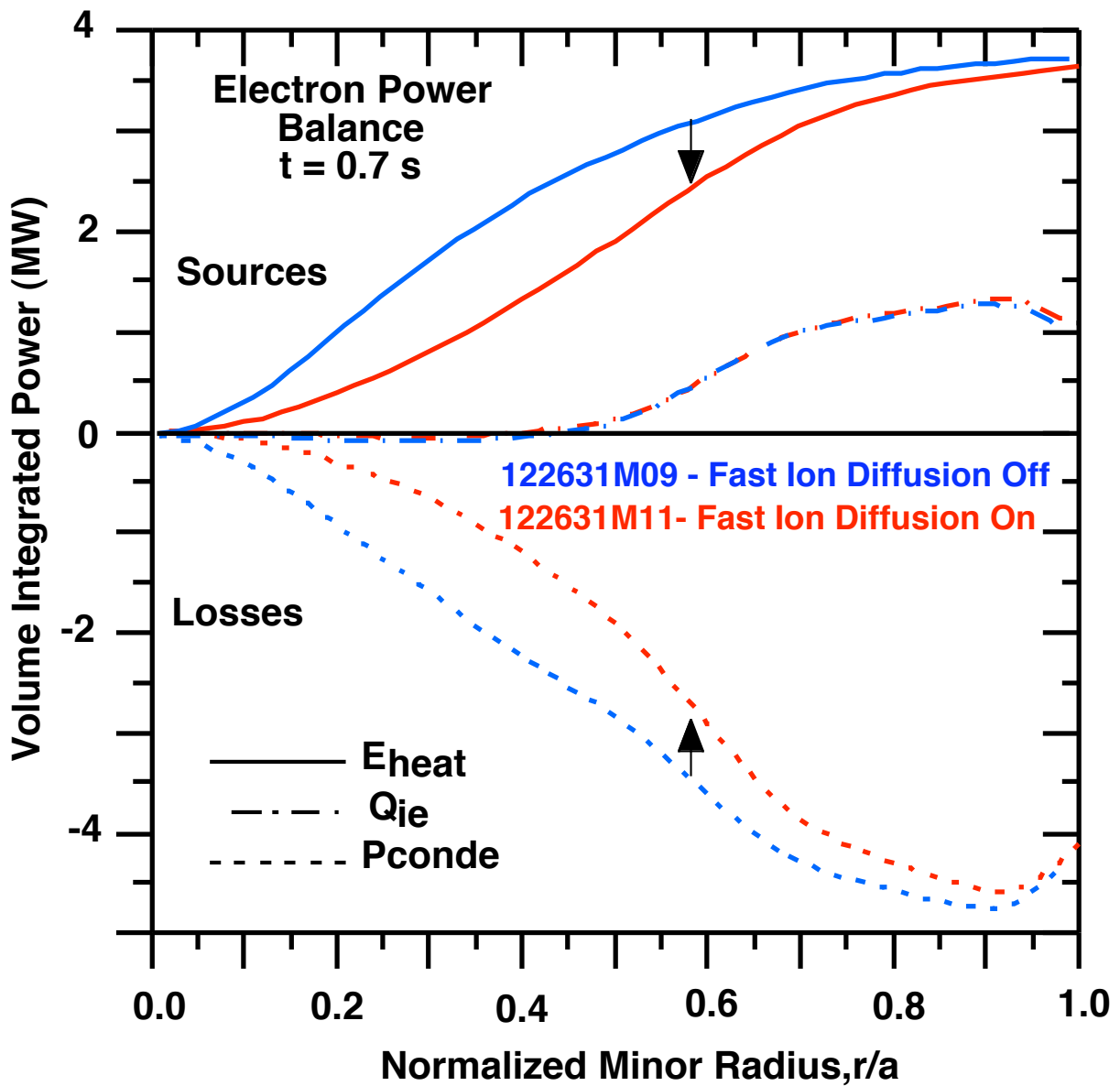


Fig. 27. TRANSP calculation of electron power balance at  $t = 700$  ms with and without fast ion diffusion for SN122631 is shown.  $E_{heat}$  is the total electron heating,  $Q_{ie}$  is the power transferred from ions to electrons (which is positive because  $T_i > T_e$ ) and  $P_{conde}$  is the electron conduction power loss.

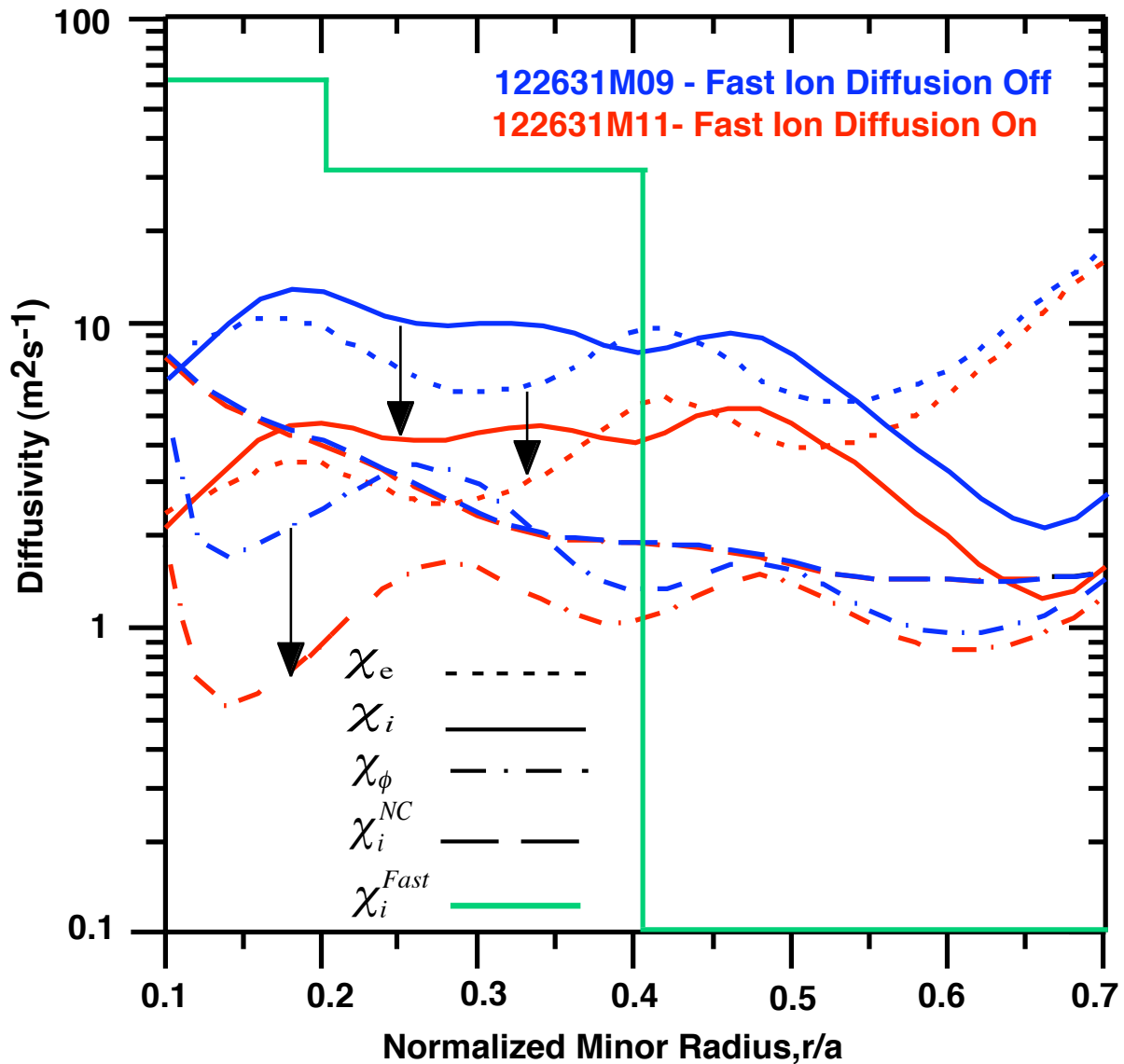


Fig. 28. TRANSP calculation of power balance diffusivities at  $t = 700$  ms with and without fast ion diffusion for SN122631 is shown. In the core region,  $\chi_{\perp} \ll \chi_i \ll \chi_e \ll \chi_i^{NC} \ll \chi_i^{Fast}$  with and without fast ion diffusion. Near the mid-radius region,  $\chi_{\perp} \ll \chi_i^{NC} \ll \chi_i \sim \chi_e \ll \chi_i^{Fast}$  both with and without the fast ion diffusion model. It can be seen that fast ion diffusion reduces  $\chi_e$ ,  $\chi_i$ , and  $\chi_{\perp}$ .

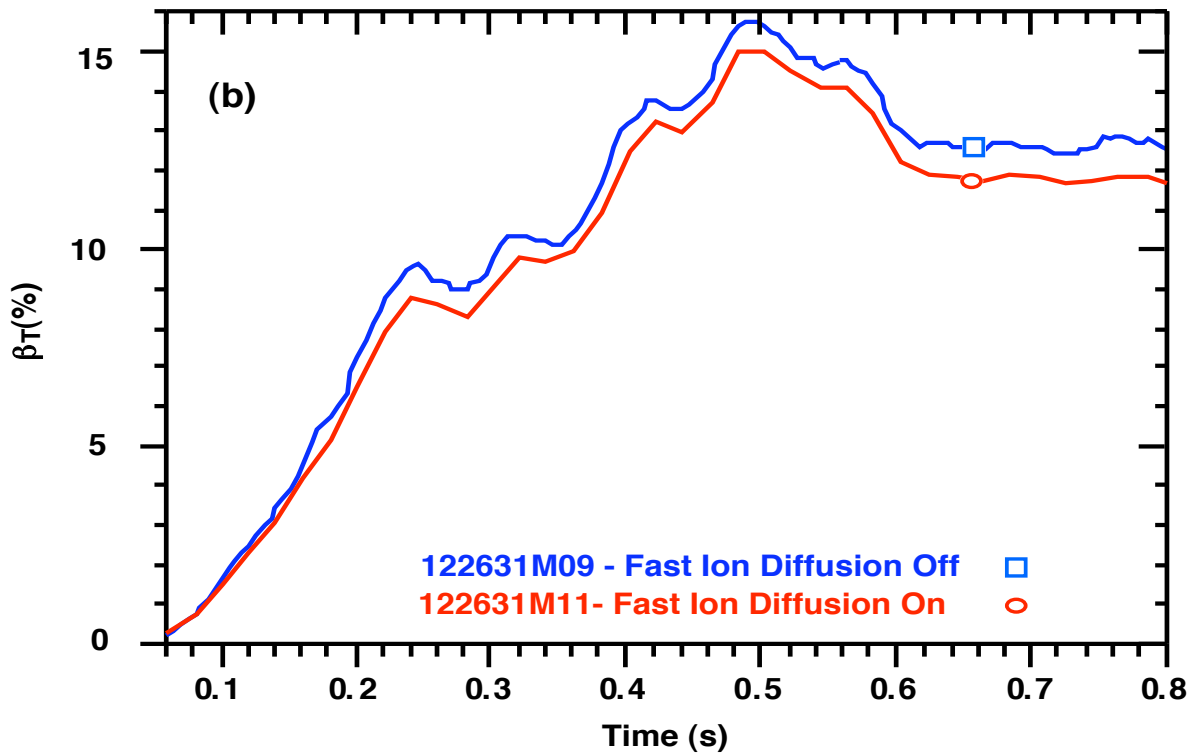
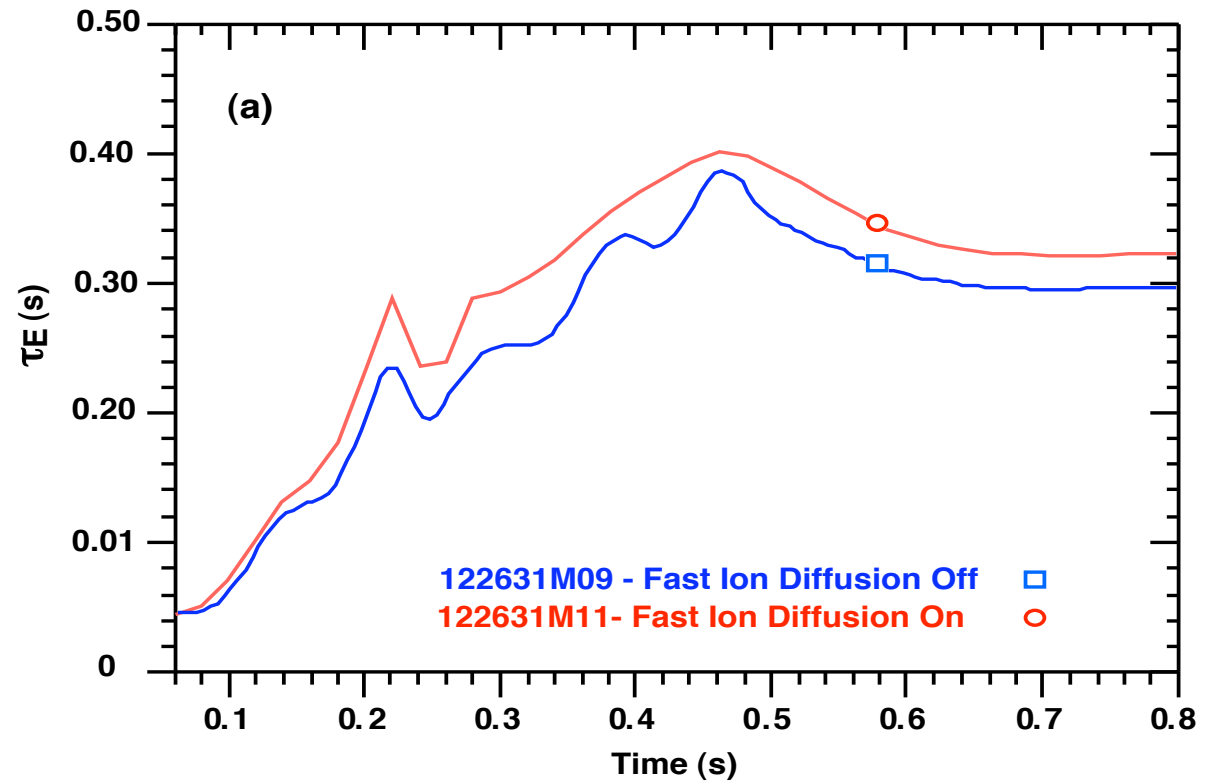


Fig. 29. TRANSP calculation of thermal energy confinement time (a) and toroidal beta (b) at  $t = 700$  ms with and without fast ion diffusion for SN122631 is shown. For this case, accounting for fast ion loss increased the thermal energy confinement ( $\bar{E}$ ) by  $\sim 7\%$  and reduced the toroidal beta ( $\bar{T}$ ) by  $\sim 8\%$ .

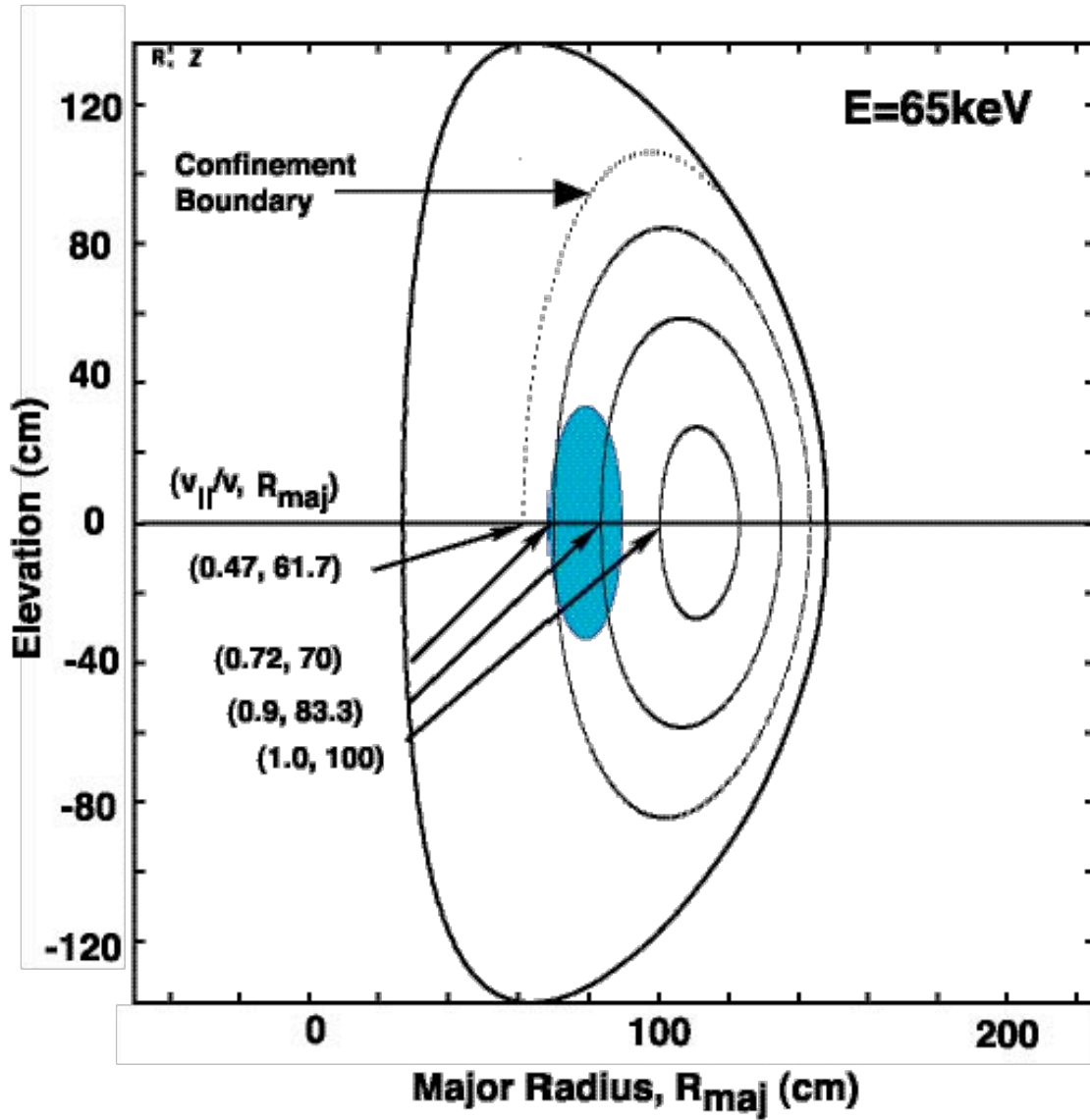
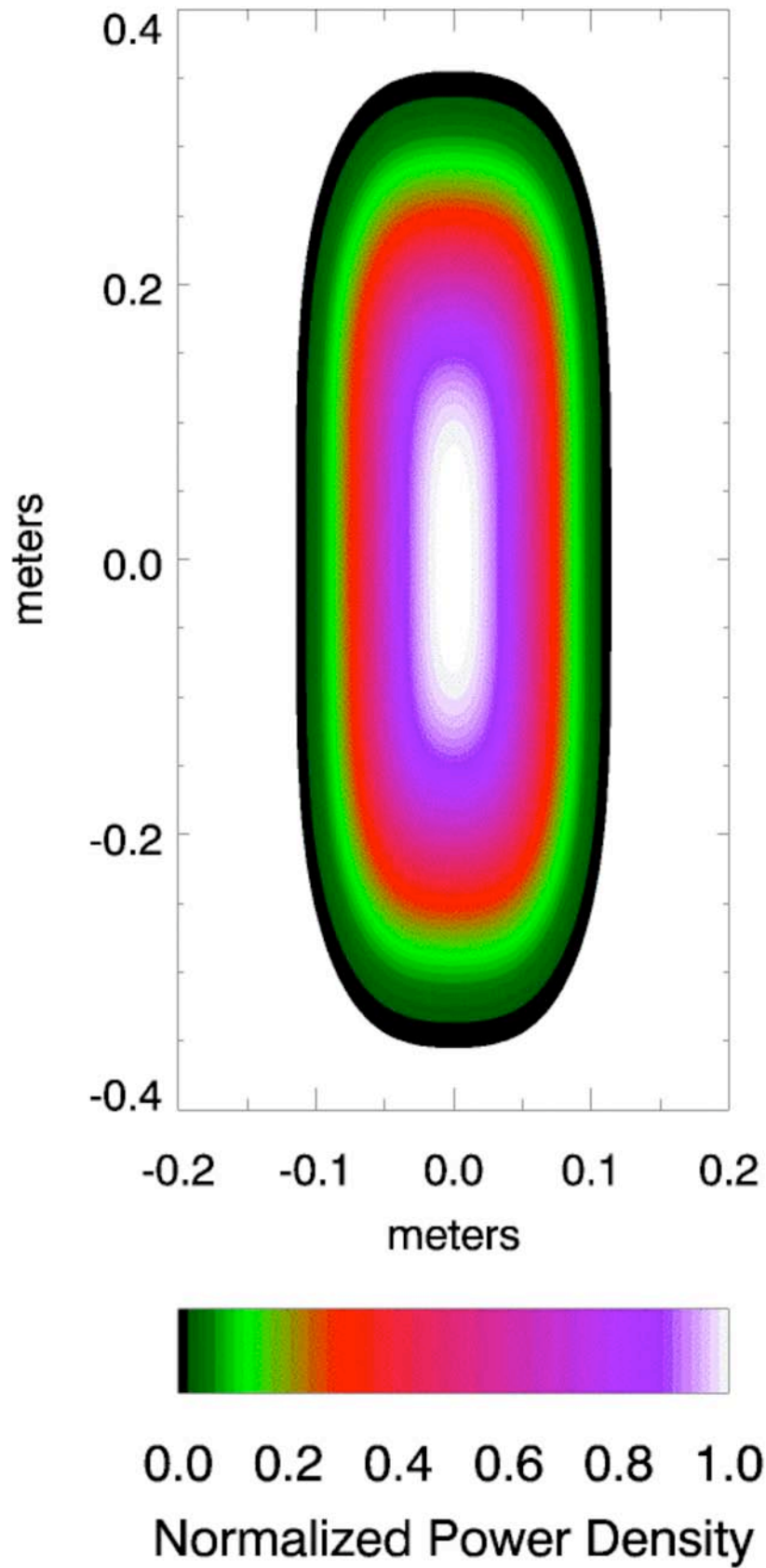


Fig. 30. ORBIT modeling of particle trajectories that are viewed by the NPA diagnostic during horizontal scanning measurements.



*Fig. 31. Contour plot of the primary neutral footprint for an NSTX heating beam.*

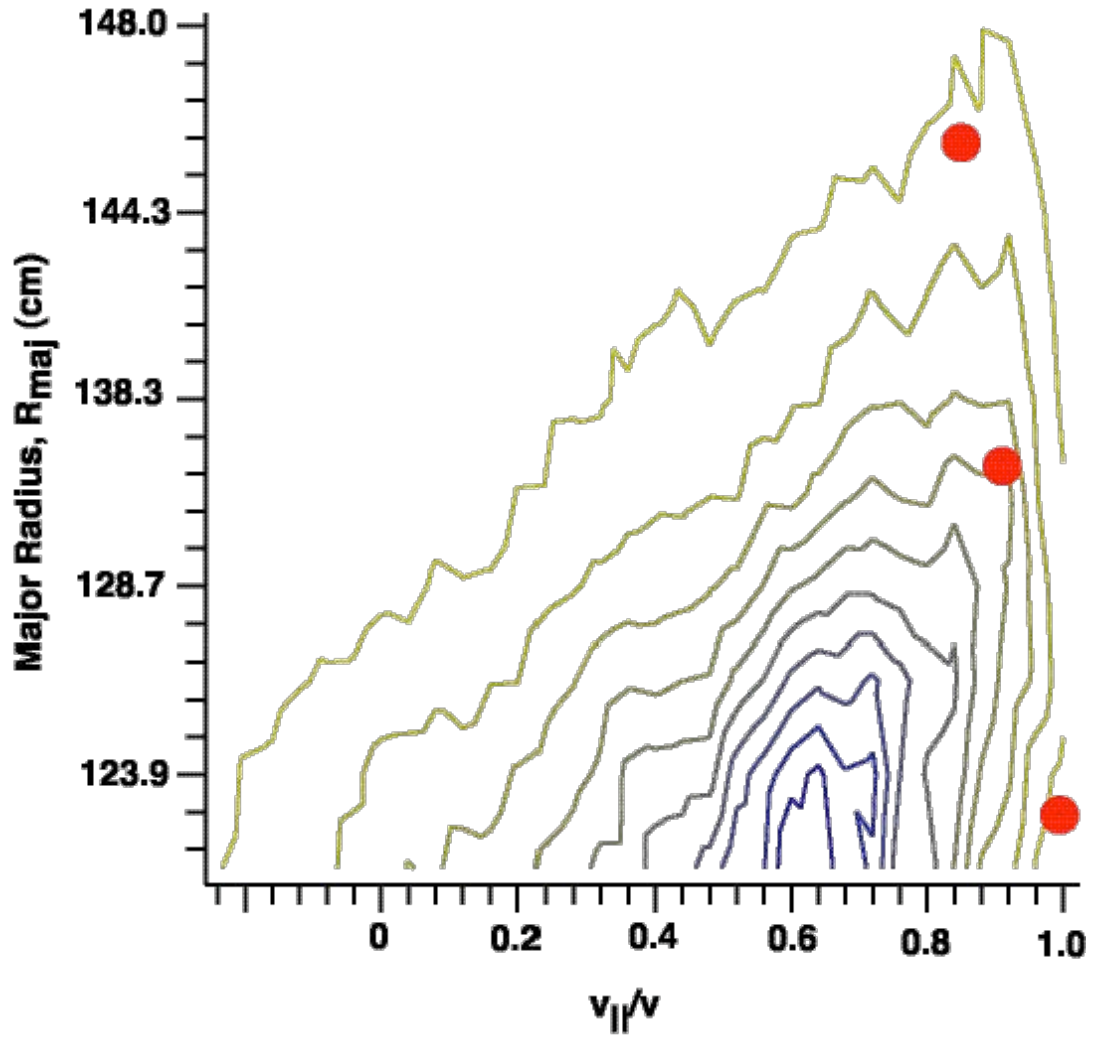


Fig. 32. Contour plot of the beam ion distribution at  $E = 65$  keV showing a sample (red circles) of the pitch angles ( $v_{\perp}/v$ ) that are viewed by the NPA during horizontal scanning.

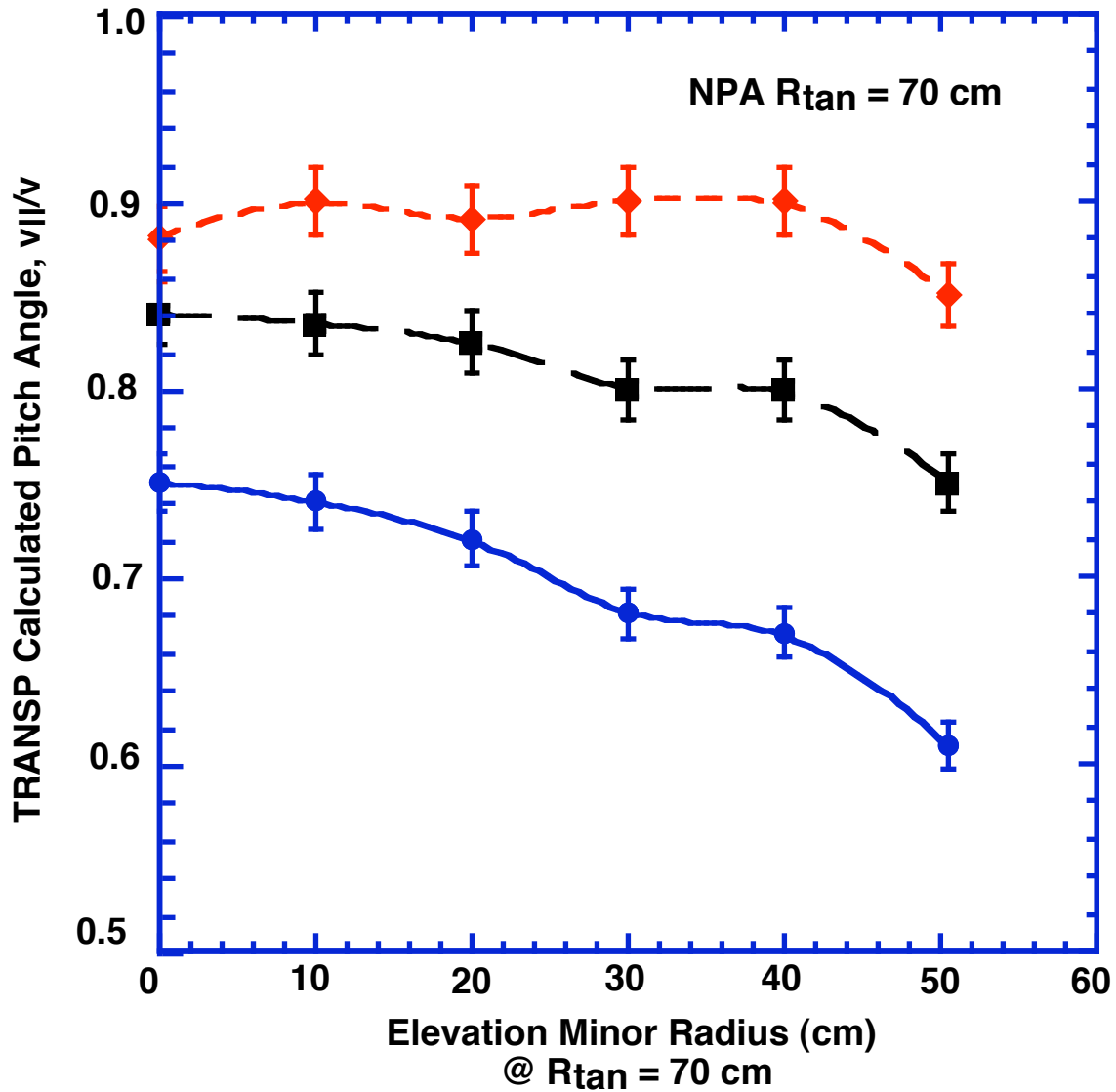


Fig. 33. TRANSF calculated pitch angle,  $v_i/v$ , versus elevation minor radius centered on the NB footprint. The black curve is the pitch angle at the peak of the change exchange emissivity measured along the NPA sightline. The red (blue) curves are the maximum (minimum) pitch determined by the width of the emissivity profile that in effect is determined by the horizontal width of the beam primary neutral profile. Beyond the elevation minor radius of 50 cm the NPA sightline misses the NB footprint.

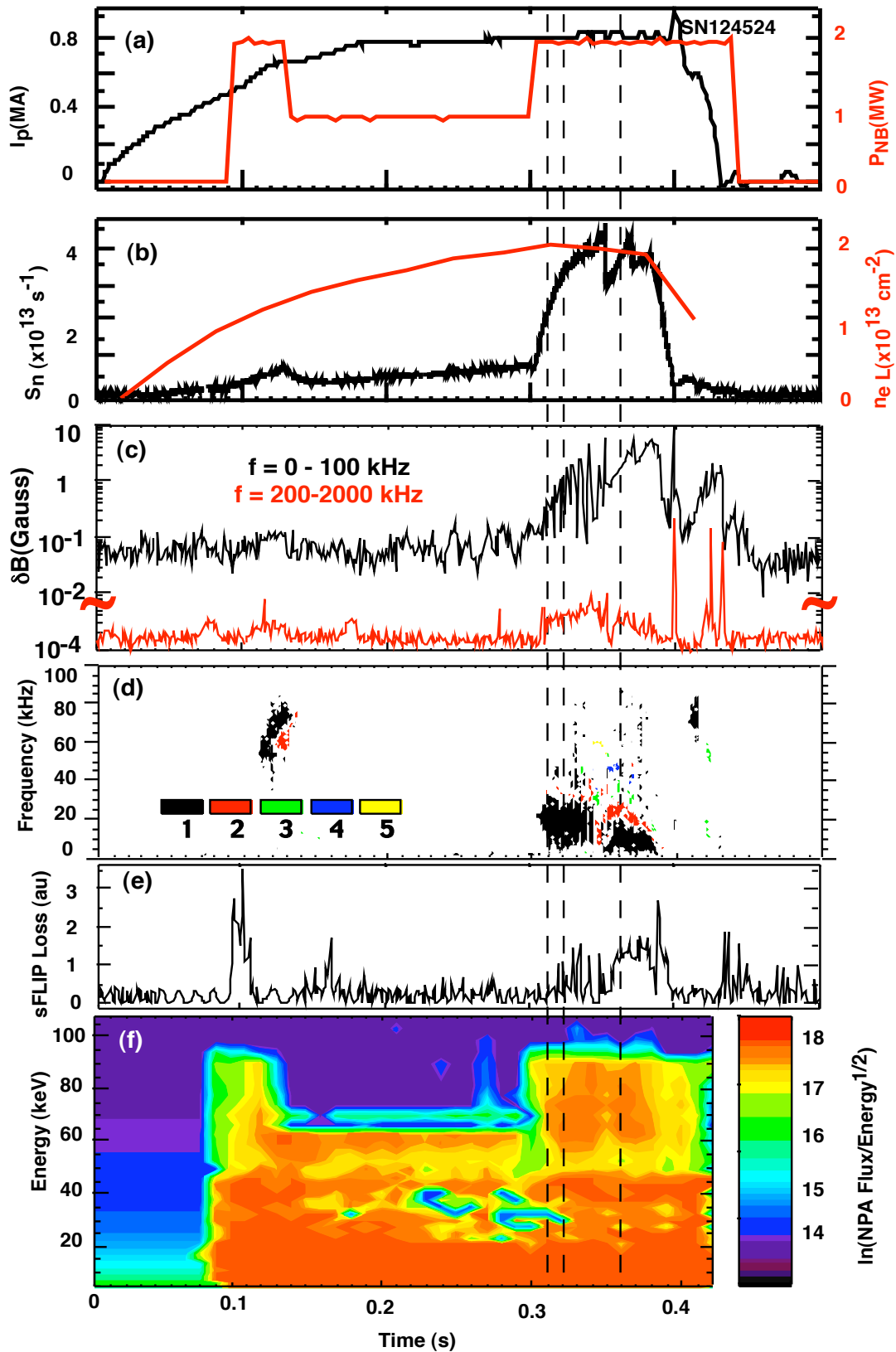


Fig. 34. Discharge characteristic for NPA vertical scan measurements during L-mode in a neutral beam heated Helium plasma.

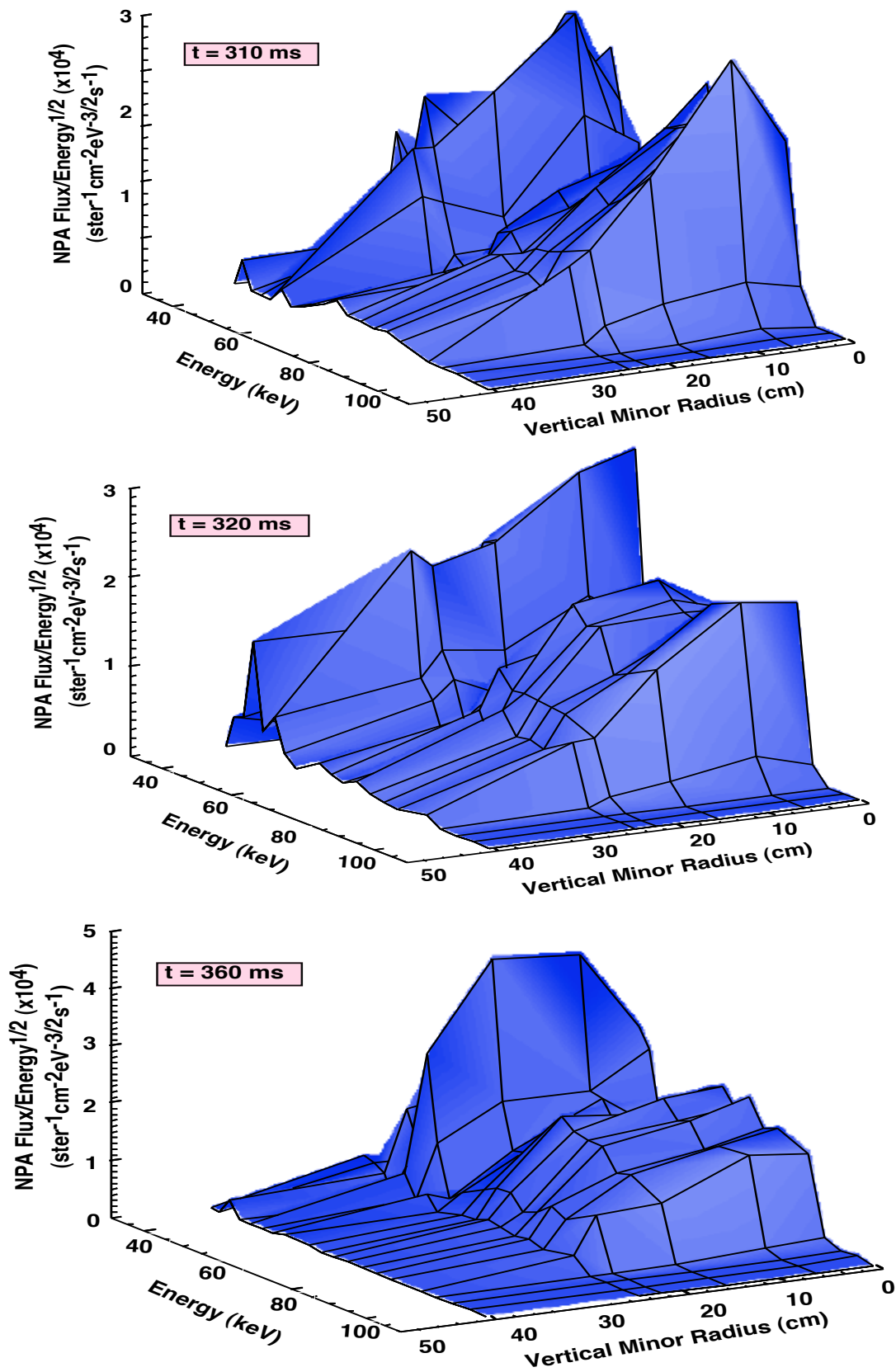


Fig. 35. NPA vertical scan measurements during L-mode in a neutral beam heated Helium plasma. The NPA horizontal tangency radius was  $R_{\text{tan}} = 70$  cm.

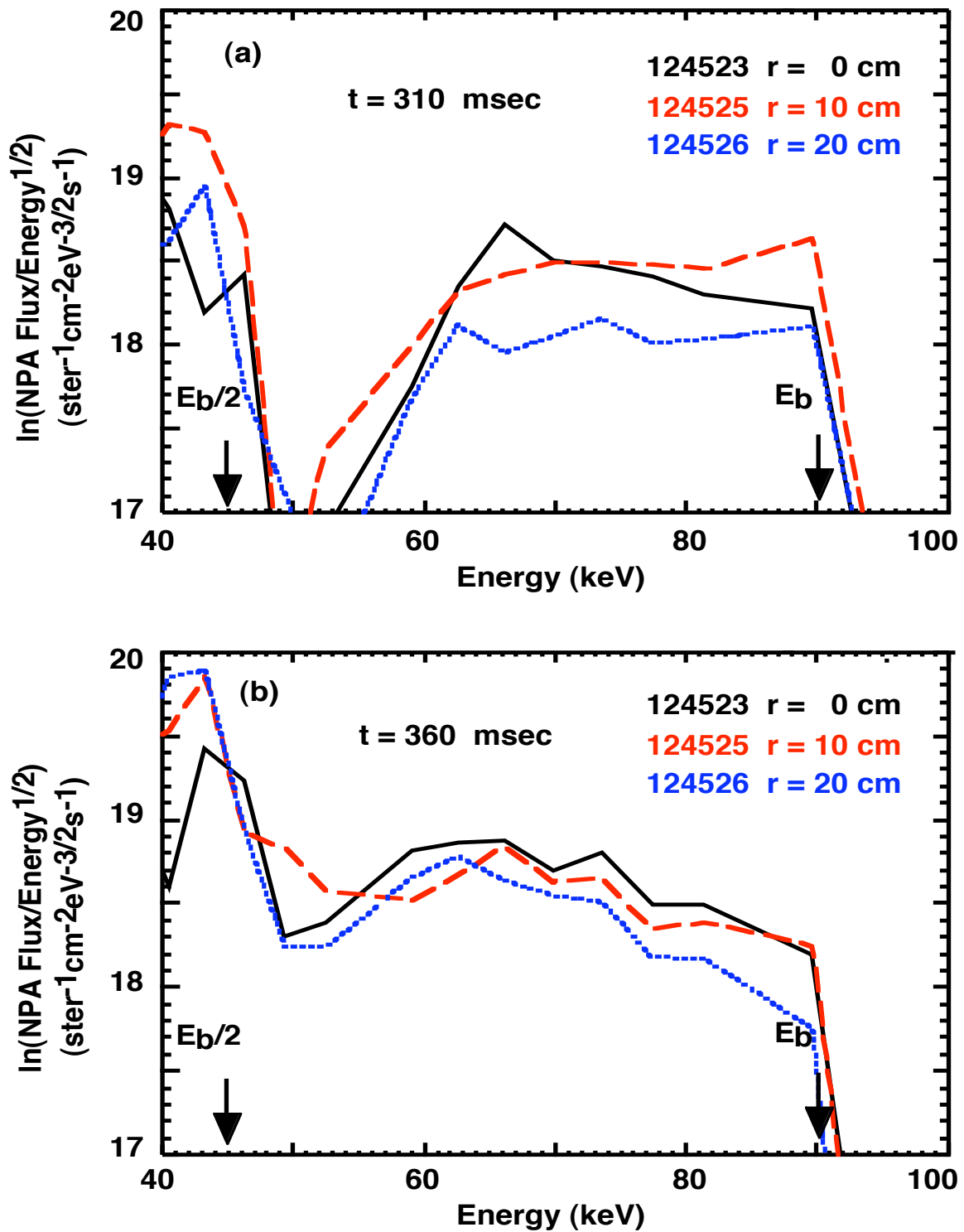


Fig. 36. The energy spectra on a natural logarithmic flux scale for  $t = 310$  and  $t = 360$  ms are displayed in triplets corresponding to vertical minor radii of approximately 0, 10, and 20 cm. The energetic ion redistribution with increasing time is evident.

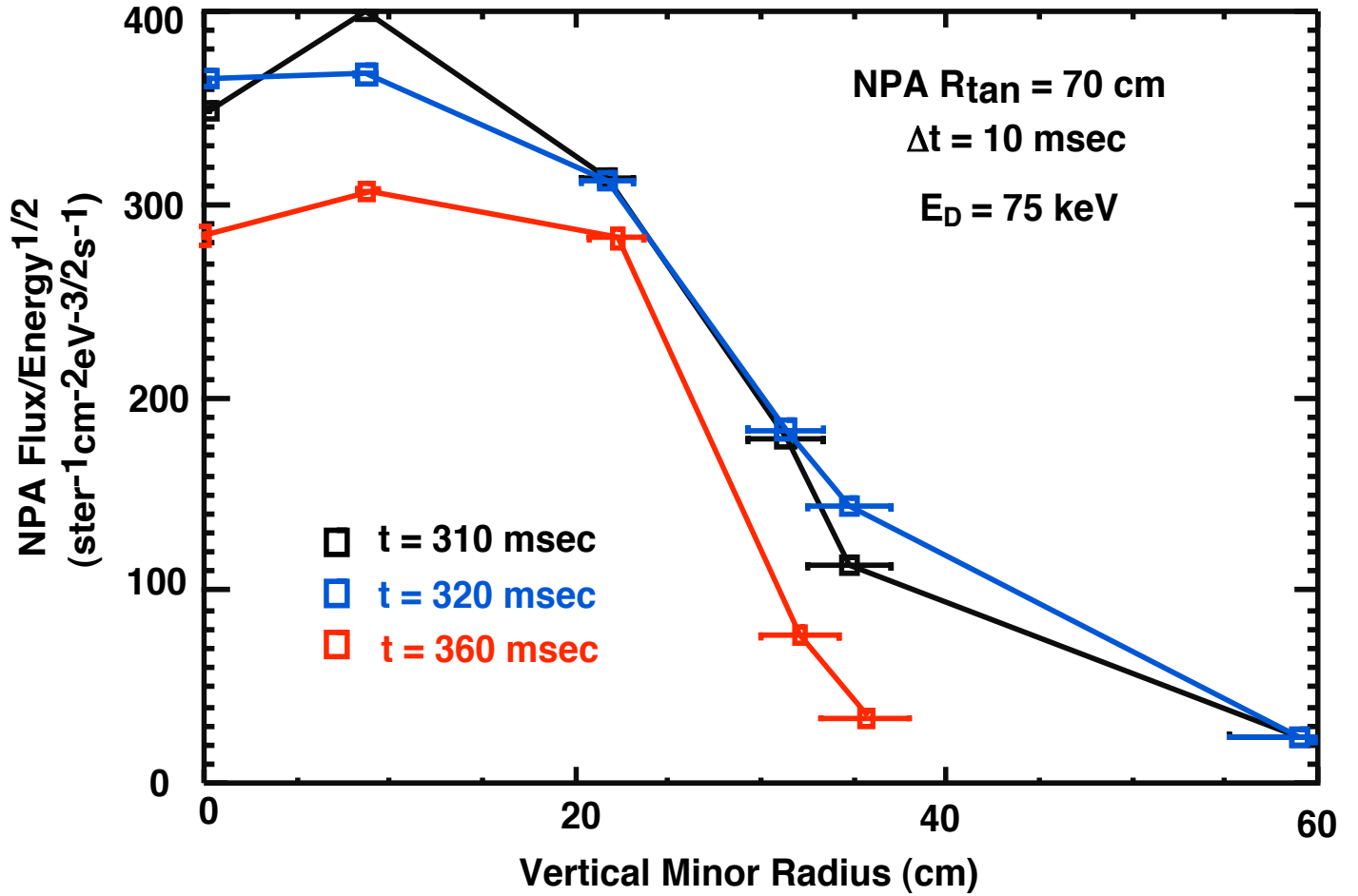


Fig. 37. The energetic ion distributions versus vertical minor radius are plotted at times  $t = 310, 320$  and  $360$  ms for an energy of  $E_D = 75$  keV. The flattening in the core of the energetic ion profile is clearly evident.

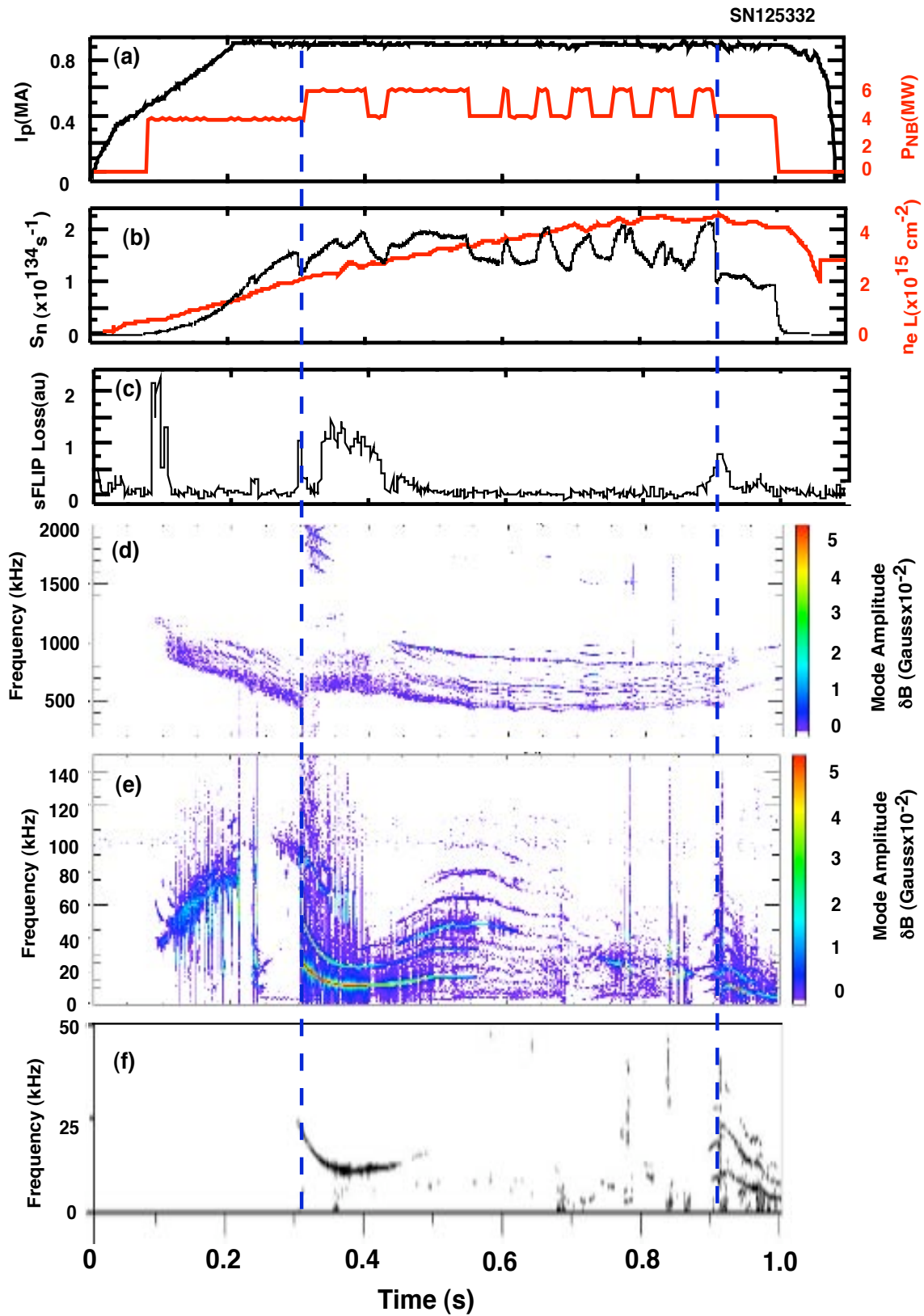


Fig. 38. Discharge showing correlation of FIREtIP electron density fluctuations and sFLIP energetic ion loss with certain types of MHD activity.

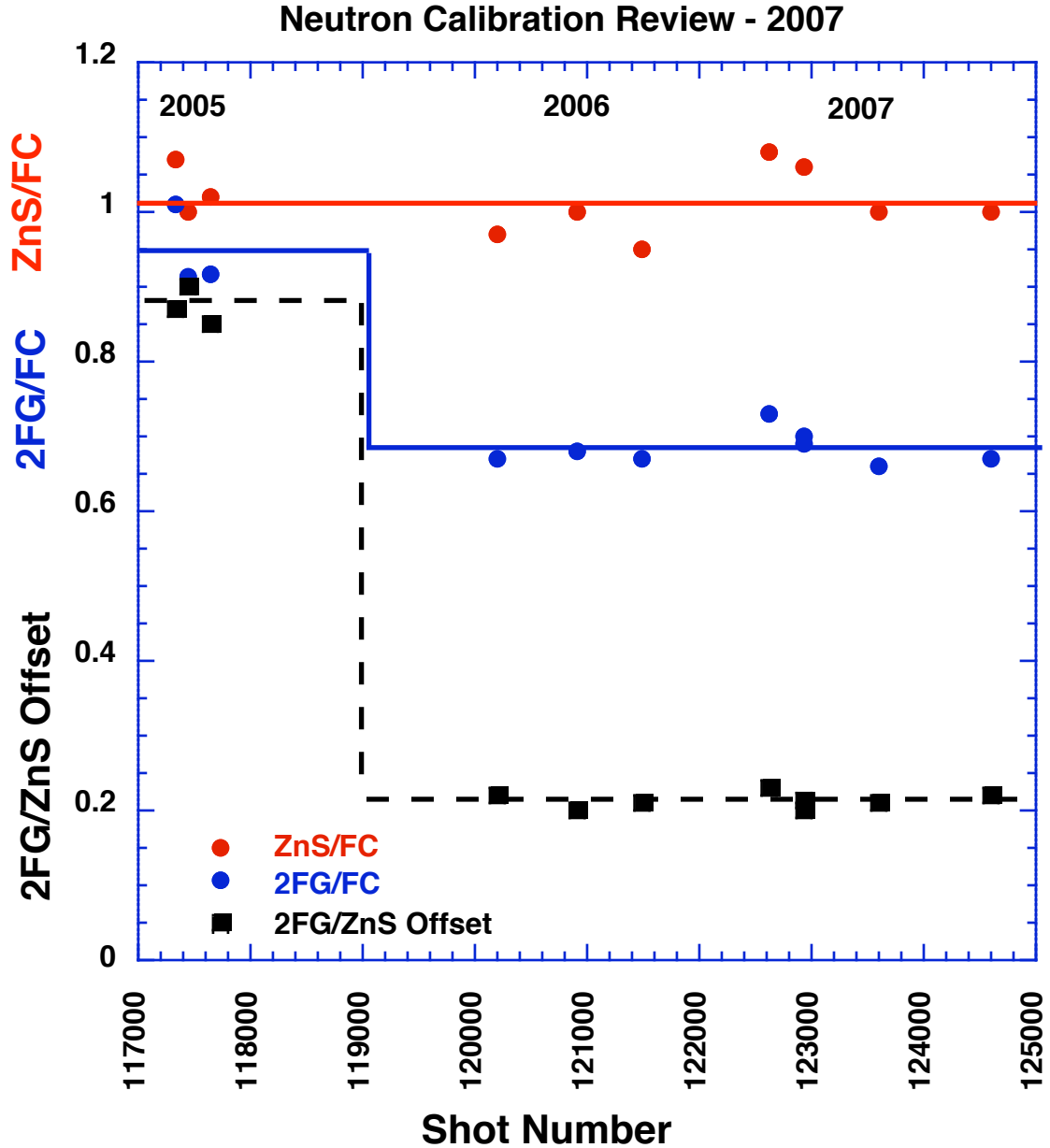


Fig. 39. A check in 2007 of the NSTX neutron diagnostics revealed that the responses of the fission chamber (FC) and ZnS detectors were constant over the period 2005-2007, but the response of the 2FG scintillator detector dropped by a factor of  $\sim 2/3$  and the correction for the raw signal voltage offset decreased by a factor of four. This does not affect the results of this report since the highly stable fission detector was used throughout for the neutron measurements.

The Princeton Plasma Physics Laboratory is operated  
by Princeton University under contract  
with the U.S. Department of Energy.

Information Services  
Princeton Plasma Physics Laboratory  
P.O. Box 451  
Princeton, NJ 08543

Phone: 609-243-2750  
Fax: 609-243-2751  
e-mail: [pppl\\_info@pppl.gov](mailto:pppl_info@pppl.gov)  
Internet Address: <http://www.pppl.gov>